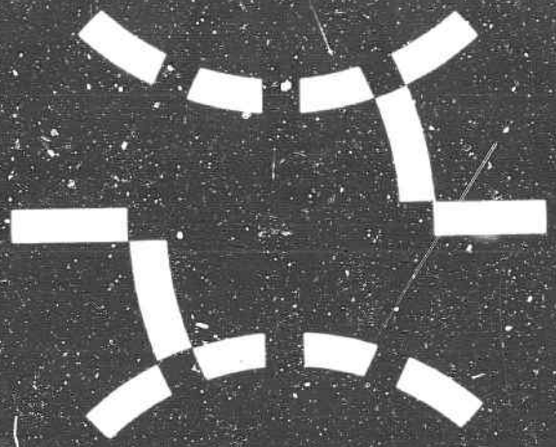

SERVICES, INC.

A SUBSIDIARY OF GLOBAL MAR

OCEANOGRAPHIC SERVICES, INC.

OSI#102-2
10 December 1968
Santa Barbara, California

Prepared For

OFFICE OF NAVAL RESEARCH
Field Projects Programs
Washington, D. C. 20301

Sponsored By

DEFENSE ATOMIC SUPPORT AGENCY
Washington, D. C. 20301

Submitted By

OCEANOGRAPHIC SERVICES, INC.

Authors

N. R. Wallace and C. W. Baird

EXPLOSION-GENERATED WAVES

1965 MONO LAKE TEST SERIES

Contract Nonr 4904(00) -- NR 087-159

Richard Kent

Approved: Richard Kent, President

Abstract

In the summer of 1965, 10 spherical TNT charges, each weighing about 9,200 pounds were detonated in Mono Lake, California. This report treats the analysis and comparison of wave data collected during the tests. Generation, propagation, and runup of the explosion-generated waves are discussed and the results are examined in relation to current methods of predicting these properties.

Table of Contents

List of Figures

List of Tables

EXPLOSION-GENERATED WAVES
1965 MONO LAKE TEST SERIES

Section I

INTRODUCTION

In the summer of 1965, 10 spherical TNT charges, each weighing about 9,200 pounds, were detonated off the southern shoreline of Mono Lake, California. This test program conducted by the Army Corps of Engineers, Waterways Experiment Station, was to provide experimental information on the generation, propagation, and shoreline runup of explosion waves with special interest attached to the relationship of absolute runup to the offshore wave heights and periods.

Most of the data collected in these experiments have been published. The main topic of this report is comparison of the data with current methods of prediction and analysis of the results.

Description of the Test

The location of the test site on the south shore of the lake has several features desirable for the purposes of the experiment.

The shoreline in the test region is fairly straight and the nearshore bathymetry is geometrically similar to a typical continental slope. The deep portion of the lake, with a depth of about 130 feet, is within 5,000 feet of the shoreline, and this is just enough depth to permit deep-water generation from 9,200 pounds of TNT detonated near the free surface.

The first nine shots were fired in the same location, Surface Zero #1, shown in Figure 1. Shot 10 was detonated closer to shore at Surface Zero #2.

A total of 48 surface-piercing wave sensors of the parallel resistance-wire type were arranged radially along four lines extending from Surface Zero #1. Three of these instrumented radials extended to the shoreline but the sensors on the fourth radial were all in deep water. The water depth at each sensor and the distance of the sensor from Surface Zero #1 are given in Table 1. The tabulated water depths do not correspond consistently to the approximate depth contours appearing in Figure 1. The tabulated values are to be preferred and have been used throughout this report.

Two plywood ramps were specially constructed on the beach at the shoreward terminations of Radials 1 and 2. The ramp on

Radial 1 was 100 feet long by 16 feet wide with a slope of 1 in 50. The end of this ramp was about 4 feet from the water. Continuous connection was made to the water by a steeper section of ramp whose slope varied, as a result of wave action, between 1 in 16 and 1 in 11.6 during the course of the test series.

The primary ramp on radial 2 had a slope of 1 in 30, and the steeper ramp connecting it to the water varied in slope between 1 in 10.5 and 1 in 7.1.

These two ramps simplified the determination of vertical runup. The horizontal encroachment of water on the ramp can easily be transformed to vertical runup since the slopes are known.

Motion picture cameras were positioned near these ramps to film the water motion both on the ramps and in the nearshore breaker zone. To facilitate the estimation of runup distances from the film records, pylons were placed at intervals of five feet on Ramp 1 and at intervals of three feet on Ramp 2. In addition, poles were driven into the lake bottom at intervals of 10 feet in the nearshore zone of Radial 1. These, too, had camera coverage and proved to be essential to the later determination of the bore and breaker heights.

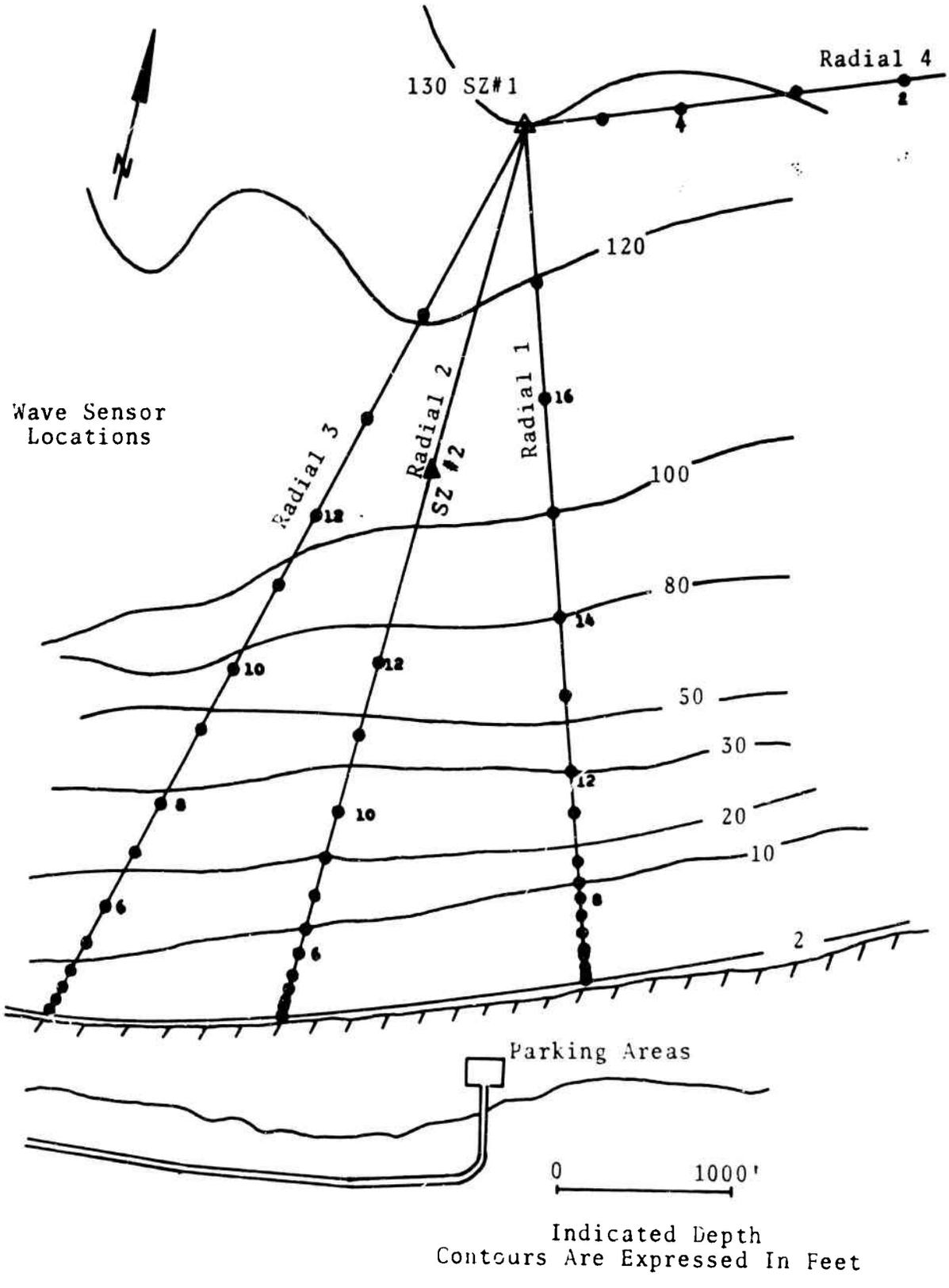

Figure 1 Shot Locations and Instrument Radials

Table 1

Water Depths and Distances from Surface Zero #1*

	Radial 1		Radial 2		Radial 3		Radial 4	
Sensor	Sensor Depth	Dist. S.Z.	Sensor Depth	Dist. S.Z.	Sensor Depth	Dist. S.Z.	Sensor Depth	Dist. S.Z.
Shore-line	0.0	4820	0.0	5160	0.0	5660		
1	0.9	4780	0.8	5140	0.5	5631	117.3	3226
2	1.0	4762	1.0	5110	1.0	5612	124.5	2164
3	1.5	4714	1.5	5048	1.5	5570	126.9	1422
4	2.3	4664	3.2	4970	6.0	5452	127.2	866
5	4.0	4596	5.6	4895	7.4	5352	128 **	461
6	5.2	4479	7.0	4757	9.1	5123		
7	6.1	4365	8.1	4616	12.1	4925		
8	7.1	4279	11.2	4415	20.3	4552		
9	8.3	4194	18.7	4216	26.6	4265		
10	11.2	4074	22.4	3928	85.0	3200		
11	21.4	3808	36.0	3484	96.5	2830		
12	26.3	3578	69.3	3065	100.7	2438		
13	58.3	3149			108.8	1826		
14	76.8	2716			116.5	1169		
15	97.4	2136						
16	107.6	1506						
17	118.3	849						

* Depths and distances in feet
** Estimated

To supplement the data obtained from cameras and wave sensors, visual information was gathered visually by personnel of the Waterways Experiment Station (WES). This included observations of wave arrival times, distance from the shoreline at which wave breaking occurred, and extent of runup on the ramps for each wave. Observations were made also of the maximum runup at 32 beach stations spaced 100 feet apart between the terminations of Radials 1 and 3.

All of the available data on runup gathered in the 1965 test series in Mono Lake have been published (Reference 1). It is recommended that this reference be consulted not only for the complete listing of runup per wave but also for details of the shore instruments and ramp structures. All of the available wave sensor data have been published also. These are presented as amplitude-time traces for the first 400 seconds after shot time (Reference 2). These two reports constitute the source of much of the data upon which this analysis report is based. Frequent referral will be made to them.

Scope of this Report

All four phases of explosion-wave phenomena, generation, propagation, shoaling and runup, are treated in this report with emphasis on intercomparison among shots and direct comparison with prediction methods.

With the exception of the Kranzer and Keller theory for wave propagation in water of constant depth, methods of predicting the properties of explosion-generated waves are themselves derived from previous experimental work. In some respects, these results from the 1965 Mono Lake test series merely add to the body of information already in existence. This, by itself, is important, since these charges were the largest ever fired for the purpose of gathering detailed information on all aspects of the resulting wave motion and runup. Where agreement occurs between the results of this test series and results from earlier tests with smaller charges, the scalability of that property is supported. Where agreement does not occur, the situation receives special attention and an opinion as to whether the problem is inherent in the data or in the phenomenon.

In the following sections, results of the analysis are presented in topical order from generation through runup. Observations made there are summarized in Section 5, Conclusions.

Section 2

GENERATION AND PROPAGATION

General Description of the Shot Sequence

Table 2 lists the actual charge weights and depths of burst for all 10 shots of the test series. Virtually no data was collected on Shot 1, but the same depth-of-burst was duplicated in Shot 6.

It was reported by WES (Reference 1) that the lake was calm for all shots but numbers 6 and 10. It was estimated for the former that a 10 mph wind was blowing from the northwest. Paoha and Negit Islands, located in the middle of the lake, usually shield the south shore from the direct effects of a northwest wind. However, packets of approximately 2 second waves approaching from the northwest were visible on both the film and the sensor traces. The instrumented portion of the lake was otherwise calm prior to the shot.

The 5 mph wind reported for Shot 10 had no appreciable influence on the wave patterns.

Table 2

Shot Data

Shot	Charge Weight (pounds)	Depth of Burst (feet)	Time	Date
1	9213	0.00	0955	13 Aug 65
2	9210	0.67	1055	17 Aug 65
3	9163	1.40	1155	23 Aug 65
4	9212	1.04	1235	24 Aug 65
5	9213	8.20	1245	26 Aug 65
6	9223	0.00	1828	26 Aug 65
7	9233	41.00	1207	27 Aug 65
8	9228	51.50	1315	30 Aug 65
9	9250	21.00	1615	7 Sep 65
10	9190	1.04	1146	8 Sep 65

The Deep Water Wave Systems

It is known from the linear theory of Kranzer and Keller (Reference 3) that the product of wave amplitude at the envelope crest η_{max} and the radial distance from the burst r should be constant. It is only necessary that the water depth be constant and large enough compared to the diameter of the explosion cavity that the Kranzer and Keller theory applies. The product $\eta_{max} r$ was formed for all the deep-water sensor traces presented in Reference 2 which had acceptable calibration curves. These products are given in Table 3. The missing entries in the table correspond to missing sensor data or to sensor traces whose calibration had to be estimated by one of several alternative methods discussed in Reference 2.

For the purposes of this table, deep-water was considered to be any depth greater than about 60 feet. The period of the envelope crests for the various shots corresponded to a period of less than or equal to 8 seconds. Modification of the crest amplitude through shoaling and refraction was deemed small for these periods so long as the water depth was no less than 60 feet.

As discussed in the previous report on reduction of the sensor data, a great deal of extraneous noise was superimposed on the traces of the wave motion. Much of it could not be separated

Table 3

Values of $\eta_{max} r$ at Deepwater Sensors

Radial-Sensor	Shot Number								
	2	3	4	5	6	7	8	9	10
1-17						726		858	
1-16	2033	1619		1009		633			1425
1-15		1121		1047		641	502	929	
1-14		1494		964	1412	516	516	1141	
1-13		1732		1023	1669	567	551	1417	1959
2-12	2375	1533	1456	1364	1548	521		920	1864
3-14	1157			848	1426	444	380	713	
3-13	1023							758	
3-12	829	1524	1158			341	317	670	
3-11	736	1585	1415	1047	1415	354	354	835	1351
3-10	944	1760	1952	1088	1600	464	656	864	1313
4-4						459	316	498	2116
4-3						512	469	704	2641
4-2								649	1840
4-1		1855	1823			694	597		
Averages	1300	1580	1560	1048	1510	530	465	840	1810
Standard Deviations	593	198	289	137	100	116	114	226	420

from the desired signal, and this circumstance is reflected in the large variances in $\eta_{max} r$ for all the shots. In general, Shot 10 appears to have produced the largest waves, somewhat higher even than those produced on Shot 4 which was fired at the same depth but in deeper water.

The average for each shot is plotted in Figure 2 as $\frac{\eta_{max}\, r}{W^{0.54}}$ versus $\frac{Z}{W^{0.3}}$. Z is the depth of burst. W is the charge weight.

The solid line is the average of data collected from previous experiments over a wide range of charge weights. It is the curve used for predicting maximum wave height from knowledge of the charge weight and depth of explosion in deep-water. This curve applies only when the water depth, h, satisfies the inequality $\frac{h}{W^{0.3}} \geq 6$. This condition is not satisfied for Shot 10, but the others just meet the requirement with an $\frac{h}{W^{0.3}}$ of about 6.1. All nine shots are plotted on the diagram. Also included are data from two of the three 9,200 pound charges fired in 130 feet of water during a similar experiment at Mono Lake in the summer of 1966 (Reference 4).

Near the upper critical depth, the near-surface maximum in the curve, the data points lie below the curve but within the range of all previous data (denoted by the dotted lines). The two

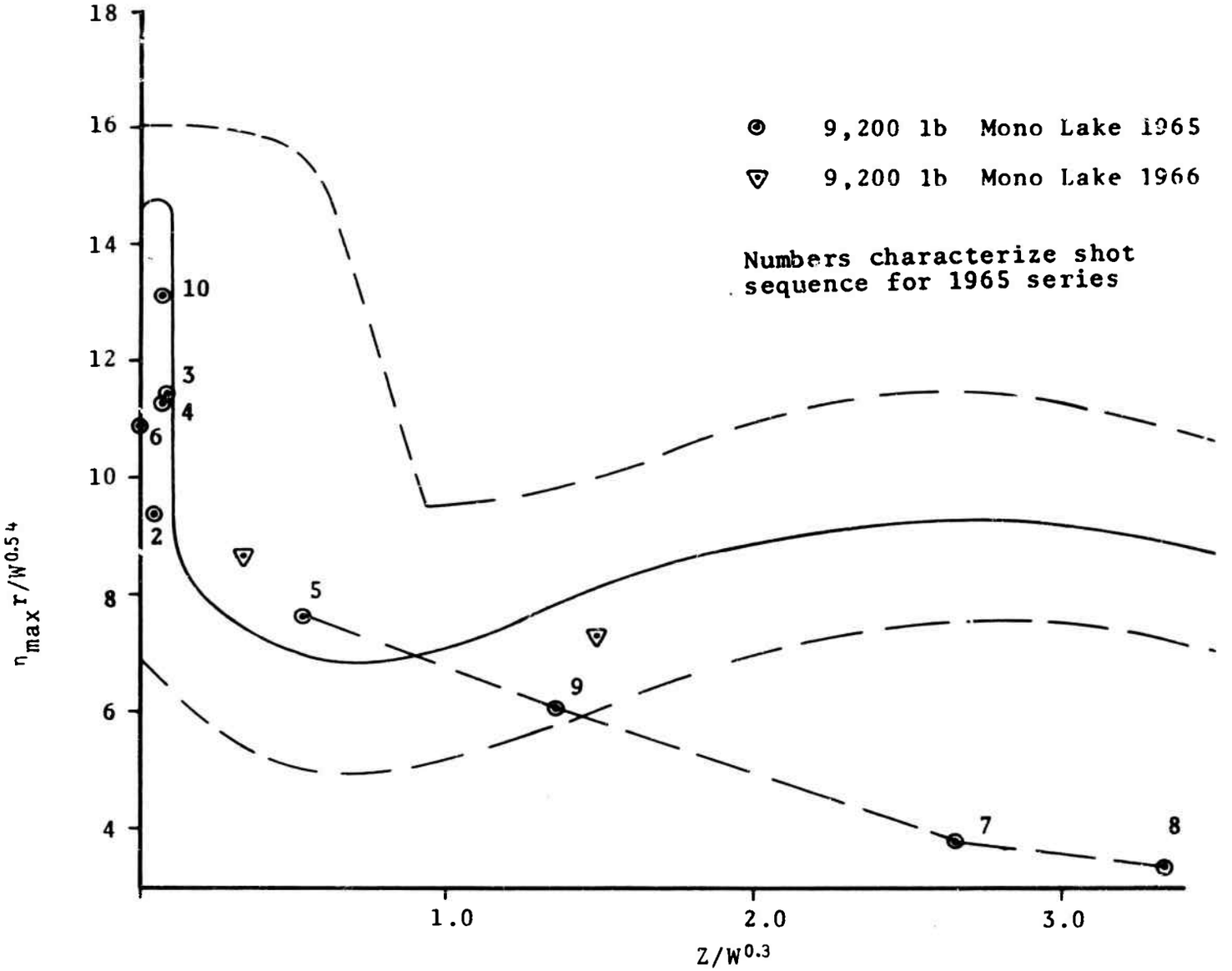

Figure 2 $\frac{\eta_{max}{}^{r}}{W^{0.54}}$ versus $\frac{Z}{W^{0.3}}$

deep shots, 7 and 8, were fired near the expected second maximum in the curve known as the lower critical depth. The data points for these shots fall well below the band of previous results. The reasons for this are unknown, and this pattern compares unfavorably with the results from the 9,200 pound charge detonated at a depth of 60 feet during the 1966 test series in Mono Lake. For that event, a value of $\frac{\eta_{max} r}{W^{0.54}}$ of 10.3 was achieved at reduced depth $\frac{Z}{W^{0.3}}$ of 3.87. This places a point at the upper edge of the data range but off the scale to the right in Figure 2. The water depth for this shot wa the same as for Shots 7 and 8 of the 1965 test series, viz. 130 feet. Since Shots 7 and 8 deviate so greatly from the band of previous data, the possibility exists that the charges were faulty or the sensor calibrations were not adequate.

However, another aspect of these deeper shots is consistent with the results and suggests that the lower critical depth may vanish for large charges. Figure 5 shows a comparison among smoothed envelope shapes for Shots 3 through 8 recorded at or normalized to sensor Station 16 on Radial 1. The near surface detonations, Shots 3, 4, and 6 display a first envelope shape typically produced by a parabolic cavity in the undisturbed surface. The period at the envelope crest for these shots of about 6 seconds or less corresponds to an initial cavity radius of about 70 feet.

This radius has been corroborated through high-speed photography of the plume (Reference 5). As the depth of burst increases through Shots 5, 7, and 8, the period at the envelope crest increases to almost 8 seconds and the amplitude at the crest of the envelope decreases. The general trend of increasing crest period coupled with decreasing crest amplitude indicates that the effective generating cavity obtains more the shape of a wide, shallow saucer as the depth of burst increases. If this comparison is continued to the 60 feet depth-of-burst shot in the 1966 Mono Lake series, it is found that the period for the crest of that envelope is 6.7 seconds — the same as a near surface shot. It appears that the explosion bubble from the deep shot of the 1966 series may have broken through the free surface at the first minimum of its oscillation cycle. However, none of the data from the nominal 9,200 pound shots from either the 1965 or the 1966 Mono Lake test programs show the presence of a lower critical depth.

The invariance of period with distance of travel for any point on a wave envelope is predicted by linear theory and is well-verified by the wave traces from these experiments. This property is such a consistent element of the sensor data that identification of a particular part of an envelope can often be made most accurately from the local wave period. Since period

invariance can be established for all wave envelopes from the same shot, differences in phase between waves from different shots are easy to identify.

The long-period waves (greater than 7 seconds) from all shots were in-phase with each other at the same sensor and at the same time after the shot. For those shots where the leading wave could be distinguished from background noise, it was a crest. It is a consequence of the Kranzer-Keller theory that a leading crest is produced when waves are generated by a cavity. Should generation be due to an impulse on the free surface, the leading wave is a trough. The identification of a leading crest for some shots and the sameness of phase for the long waves of all shots imply that all shots produced waves primarily by the mechanism of cavity formation.

The near surface shots, 2, 3, 4, and 6, showed complete agreement in phase. However, when the near surface shot was compared with the deeper shots, phase shifts in the period range less than 7 seconds were evident. This is shown in Figure 4. When waves of a given deep shot advance in phase relative to the waves of a near-surface shot, the phase angle is taken to be positive in the figure.

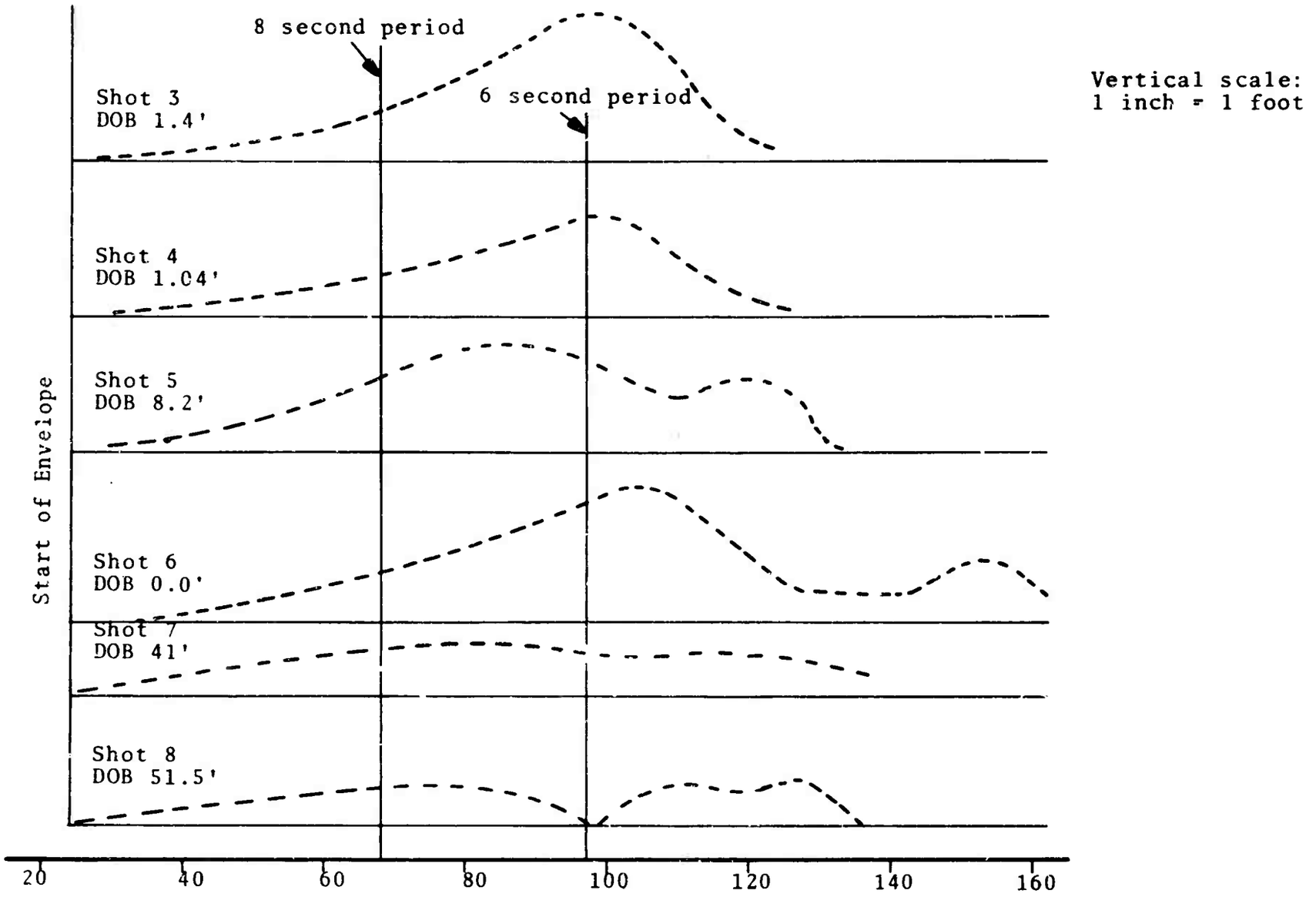

Figure 3 Wave Envelope Comparisons from Station 16 Radial 1

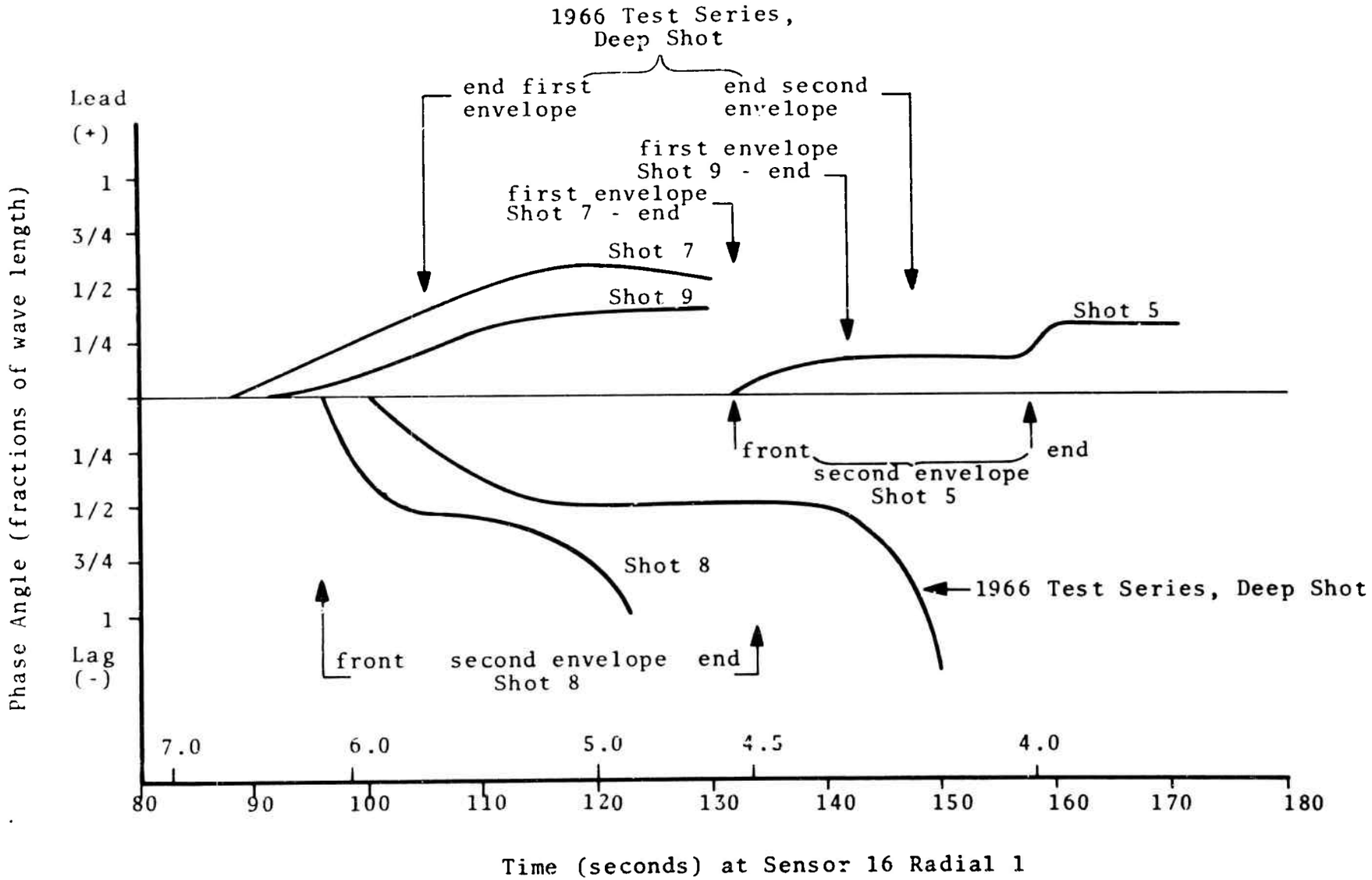

Figure 4 Phase Shifts Between Deep Shots and Near Surface Shots

Shot 5, fired at a depth of 8.2 feet, exhibited no deviation from the phase of a near-surface shot until the period had decreased to about 4.5 seconds, but the deeper shots showed marked phase changes as early as the 7 second point in the envelope. Between the burst depth of 41 feet for Shot 7 and 51.5 feet for Shot 8, the phase shift changed from an advance to a lag. This phase-lag behavior continues to act at a depth of 60 feet as illustrated by the deep shot from the 1966 Mono Lake series.*

The wave system of Shot 8 is especially interesting from the standpoint of phase changes. The change from the state of being in-phase to a half wavelength phase lag, as compared to the wave system of a near-surface shot, occurs very rapidly at the end of the first envelope. The lag increase of another half wavelength occurs almost as rapidly at the end of the second envelope. Note, too, that the first envelope of Shot 8 (Figure 3) ends at a period of 6 seconds which corresponds to a period value associated with the crest in the near-surface shots. This behavior of the Shot 8 wave system together with the progression of phase changes with shot depth shown in

*The phase comparison for this shot was made with the shot fired closest to the surface in the 1966 series. The depth of burst for that near-surface shot was 5.2 feet.

Figure 4 suggests that the changeover from phase advance to phase lag occurred near the burst depth of Shot 8.

Together, these results indicate that the largest waves are associated with the smallest crest period, and that the small crest periods may recur periodically with increasing depth of burst. The cycle appears to be related to the period of the bubble oscillation and, of course, to the migration of the bubble. Between the optimum depths of burst, the effective cavity produced at the free surface is too shallow to generate high waves, and this was the case for charges fired at the lower critical depth as scaled from experiments with smaller charges.

The conclusions are tentative — being based on only two shots. Further experimental work is recommended to clarify the situation, perferably with charges larger than 9,200 pounds, and in water depths greater than 130 feet.

These considerations are further compromised by the water depth of 130 feet at the site of the burst for Shots 7 and 8. In this depth, the wave period at the envelope crests of about 8 seconds is in a range where the waves "feel bottom." The shoaling coefficient is less than 1.0. The crest amplitude is expected to be somewhat reduced but not by the amount exhibited in the data.

Propagation into Shallow Water

As the explosion-wave envelopes propagate from deep to shoaling water, the complete description of the linear wave system given by Kranzer and Keller no longer applies. However, the preservation of period remains until the water depth becomes so shallow that nonlinear effects dominate the water motion. Period preservation continues through the breaking zone provided the measure of period is referred to the primary waves of the systems as distinguished from the secondary waves.

On the motion picture film, separate wave crests were seen to form out of and to follow behind the original wave. The separation appeared to take place when the original or primary wave neared its breaking point. This is a phenomenon of wave instability and not of dispersion since all dispersion in the usual sense had ceased. These newly-generated waves were always smaller than the primary wave, and their number per primary wave varied from one to about three. From other evidence obtained for solitary waves propagating over a slope into shallower water (Reference 6), it would appear that still more secondary waves can be produced from the same primary wave. Naturally, this generation process is stopped when the primary wave breaks or runs up on the shore.

The secondary waves were observed to have some influence on the fine structure of the runup patterns, but no significant effects in wave propagation or runup could be attributed to them. In the remainder of this discussion, all reference to waves within or beyond the nearshore zone is intended to mean the primary waves.

It is well known that explosion-wave systems are made up of all wave periods with the longest periods at the front of the expanding disturbance and with a monotonic decrease in period in a direction towards the origin of the disturbance. With a nominal charge weight of 9,200 pounds of TNT, the maximum amplitude of the first envelope lies in the period range of 6 to 8 seconds as was discussed earlier. The water depth of 130 feet at surface zero is not great enough to be deep water for this range of periods because waves of periods greater than about 7 seconds "feel bottom" in this depth. This means the part of the first envelope between the front and the crest for shots fired at Surface Zero #1 is slightly distorted from the shape expected for an explosion in very deep water. Recorded as a function of time in a given location, distortion should increase as the wave system approaches shore because the longer waves have the larger shoaling coefficients. The possibility exists that the application of linear shoaling theory (based on the conservation of energy flux) to an explosion-wave system

might be in error because of selective reflection of wave energy by the sloping bottom. In his pre-test predictions, LeMehaute (Reference 7) discounted this possibility for these wave periods and for the shallow bottom slopes on Radials 1 through 3. Therefore, it would be expected that each element of the wave envelope would undergo linear shoaling and refraction as determined by the period associated with that element, and this assumption will be made. The large number of sensors on each shoreward radial (see Figure 1) provides enough amplitude-time measurements to follow each wave system through all stages of shoaling and to allow comparison with the predictions from linear shoaling and refraction methods.

As the wave envelope approaches shore, the wave heights are modified by refraction, shoaling, and dispersion. The refraction coefficient K_R accounts for the spread of energy laterally along the wave front and the consequent change in wave height. If b_i is the length of an element of wavefront contained between two refraction orthogonals and located at a distance r_i from surface zero, and if b_j is the length of an element of wavefront between the same two orthogonals at a distance r_j from surface zero, then

$$K_R = \sqrt{\frac{b_i}{b_j}}$$

The change in waveheight through refraction alone is given by

$$\frac{H_j}{H_i} = K_R \ .$$

In water of constant depth,

$$b_i = \theta r_i$$
$$b_j = \theta r_j$$

since the refraction orthogonals are radial lines from surface zero. Then the refraction coefficient becomes

$$K_R' = \sqrt{\frac{r_i}{r_j}} \ .$$

The dispersion coefficient K_D accounts for the decrease in amplitude of the wave envelope caused by dispersive spreading of the envelope with distance of travel.

$$K_D = \sqrt{\frac{r_i}{r_j}} \ .$$

Note that in water of constant depth,

$$\frac{H_j}{H_i} = K_R' K_D = \frac{r_i}{r_j} \ .$$

That is, the wave height is inversely proportional to the distance of propagation in agreement with the results of Kranzer and Keller.

When it is assumed that energy flux is conserved in a periodic wave train passing from deep water into a region of gradually decreasing depth, the wave height at first decreases and then increases steadily until the wave breaks. The ratio of the wave height in water of depth d to the wave height in infinitely deep water is the shoaling coefficient K_s. This coefficient is derived for linear waves and is tabulated as a function of wavelength in the appendix to Reference 8.

Tables 4 through 6 present tabulations of the three coefficients for all shoreward radials and for wave periods of 6 and 8 seconds. The coefficients were determined on the basis of water depths measured at the sensors and which are listed in the tables. These were preferred over the water depths taken from bathymetric maps of Mono Lake because the sensor depths were obtained at the time of the test series while the maps were prepared earlier.

It will be noted that the coefficients are referenced to a particular sensor on each radial so that the product of the tabulated coefficients gives the ratio of wave height at the indicated sensor to the wave height at the reference sensor. For example, on Radial 1, the wave height expected at any sensor, i, is obtained from:

Table 4

Refraction, Shoaling, and Dispersion Coefficients
for Surface Zero #1, Radial 1 Normalized to Sensor 16

Sensor Number	Water Depth (feet)	6 Second Period		8 Second Period		
		K_R	K_S	K_R	K_S	K_D
1	0.95	0.56	1.68	0.60	1.99	0.56
2	1.0	0.56	1.66	0.62	1.96	0.56
3	1.5	0.56	1.50	0.62	1.78	0.57
4	2.3	0.56	1.36	0.62	1.61	0.57
5	4.0	0.58	1.20	0.62	1.41	0.58
6	5.2	0.58	1.14	0.62	1.32	0.58
7	6.1	0.59	1.10	0.63	1.29	0.59
8	7.1	0.59	1.07	0.63	1.25	0.59
9	8.3	0.59	1.04	0.64	1.20	0.60
10	11.2	0.60	0.99	0.64	1.13	0.61
11	21.4	0.63	0.92	0.67	1.01	0.63
12	36.3	0.64	0.92	0.69	0.96	0.65
13	58.3	0.69	0.95	0.74	0.94	0.69
14	76.8	0.75	0.98	0.80	0.96	0.75
15	97.4	0.85	0.99	0.92	0.98	0.84
16	108.0	1.00	1.00	1.00	0.99	1.00
17	118.0	1.34	1.00	1.43	1.00	1.33

$$K_R = \sqrt{\frac{b_{\text{sensor 16}}}{b_{\text{sensor j}}}} \quad , \quad K_D = \sqrt{\frac{r_{\text{sensor 16}}}{r_{\text{sensor j}}}}$$

K_S is normalized to 1.0 at Sensor 16

Table 5

Refraction, Shoaling, and Dispersion Coefficients
for Surface Zero #1, Radial 2 Normalized to Sensor 12

Sensor Number	Water Depth (feet)	6 Second Period		8 Second Period		
		K_R	K_S	K_R	K_S	K_D
1	---	0.86	----	.89	----	.77
2	1.0	0.86	1.71	.89	2.04	.78
3	1.5	0.86	1.55	.89	1.88	.78
4	5.2	0.86	1.16	.89	1.40	.79
5	5.6	0.86	1.15	.89	1.38	.79
6	7.0	0.86	1.11	.89	1.32	.80
7	8.1	0.85	1.08	.89	1.27	.81
8	11.2	0.85	1.02	.89	1.20	.83
9	18.7	0.86	0.96	.89	1.09	.85
10	22.4	0.89	0.95	.89	1.05	.88
11	36.0	0.94	0.95	.95	1.01	.94
12	69.3	1.00	1.00	1.00	1.00	1.00

$$K_R = \sqrt{\frac{b_{\text{sensor 12}}}{b_{\text{sensor j}}}} \qquad K_D = \sqrt{\frac{r_{\text{sensor 12}}}{r_{\text{sensor j}}}}$$

K_S is normalized to 1.0 at Sensor 12

Table 6

Refraction, Shoaling, and Dispersion Coefficients
for Surface Zero #1, Radial 3 Normalized to Sensor 14

Sensor Number	Water Depth (feet)	6 Second Period		8 Second Period		
		K_R	K_S	K_R	K_S	K_D
1		0.48		0.45		0.46
2	1.0	0.48	1.66	0.45	1.97	0.46
3	1.5	0.48	1.51	0.46	1.78	0.46
4	6.0	0.48	1.11	0.46	1.29	0.46
5	7.4	0.48	1.06	0.46	1.23	0.47
6	9.1	0.48	1.03	0.47	1.17	0.48
7	12.1	0.49	0.98	0.48	1.11	0.49
8	20.3	0.49	0.93	0.49	1.02	0.51
9	26.6	0.50	0.91	0.51	0.98	0.52
10	85.0	0.60	0.99	0.60	0.97	0.60
11	96.5	0.64	0.99	0.61	0.98	0.64
12	101.0	0.69	0.99	0.69	0.98	0.69
13	109.0	0.80	1.00	0.80	0.99	0.80
14	117.0	1.00	1.00	1.00	1.00	1.00

$$K_R = \sqrt{\frac{b_{\text{sensor 14}}}{B_{\text{sensor j}}}} \qquad K_D = \sqrt{\frac{r_{\text{sensor 14}}}{r_{\text{sensor j}}}}$$

K_S is normalized to 1.0 at Sensor 14

$$\frac{H_i}{H_{16}} = K_R K_S K_D \qquad 1)$$

This function, as adjusted to the proper reference sensor, is plotted for 6 and 8 second waves for Radials 1, 2, and 3, and for Shots 2 through 9 in Appendix A. For Shot 10, only Radial 2 for 6 and 8 second waves is presented. Radials 1 and 3 for Surface Zero #1 do not extend radially from the Surface Zero #2 of Shot 10.

In the calculation of the expected wave height ratio, the dispersion coefficient, K_D, was retained in the above function all the way from deep water to the shoreline even though dispersion gradually ceases with decreasing water depth.

There is no wave dispersion when the phase velocity of the waves is effectively the same as the group velocity of the wave envelope, and this occurs when the wavelength is approximately ten times the water depth. Consequently, cessation of dispersion will occur at the front of an explosion-wave system and will spread back into the shorter wavelengths as the wave system shoals. For a fully dispersive wave system in deep water, the time between the arrival of any two points on the envelope (or any two periods) increases linearly with distance of travel. When dispersion has stopped for all periods contained between two points

on the envelope, the time between arrivals of these points is essentially independent of distance from the source. It is easy to distinguish these two regimes of dispersive behavior on time-of-arrival curves as calculated for various periods between the shot point and the shore (Figures 5 through 7). The transition from the deep water to the shallow water regime is gradual, but dispersion appears to have stopped for most wave periods of interest at the 20 feet water depth contour. If K_D were maintained constant at its value for a water depth of 20 feet from this point shoreward instead of continuing the dispersion, it would make negligible difference in the wave height decay curves.

Wave heights were read from the sensor traces given in Reference 2 and divided by the wave height measured at the reference sensor. These ratios are presented as data points with the computed height decay curves in Appendix A. Since the curves are calculated for 6 and 8 second waves only, it was necessary to take the height of the envelope as the wave height at times on the trace corresponding to the arrival time of 6 second and 8 second waves. These arrival times were taken from the curves of Figures 5 through 7 which were computed by numerical integration of the expression:

$$\text{Time of Arrival at } X = \int_0^X \frac{dx}{c}$$

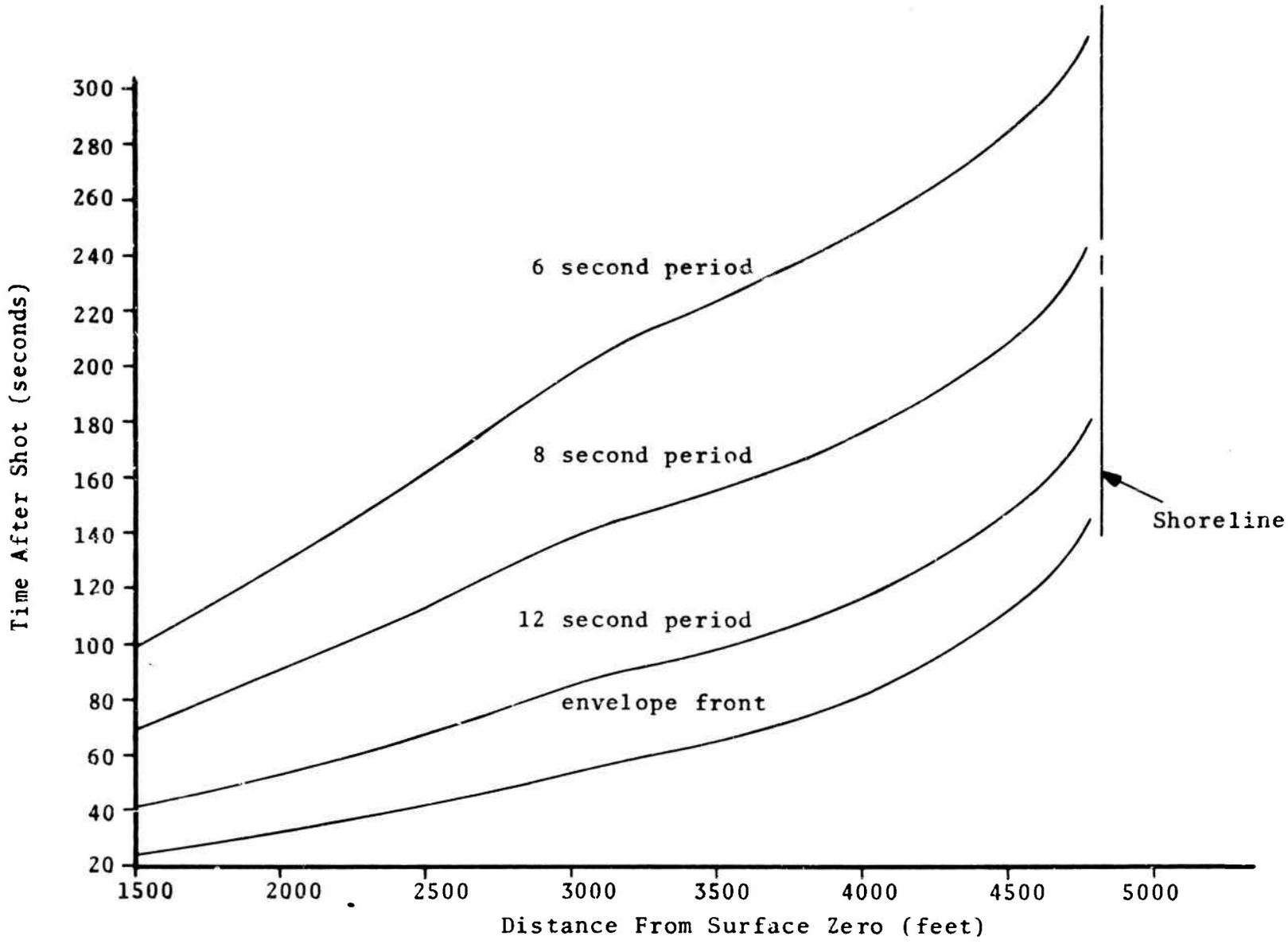

Figure 5 Times of Arrival of Wave Periods at Sensors on Radial 1

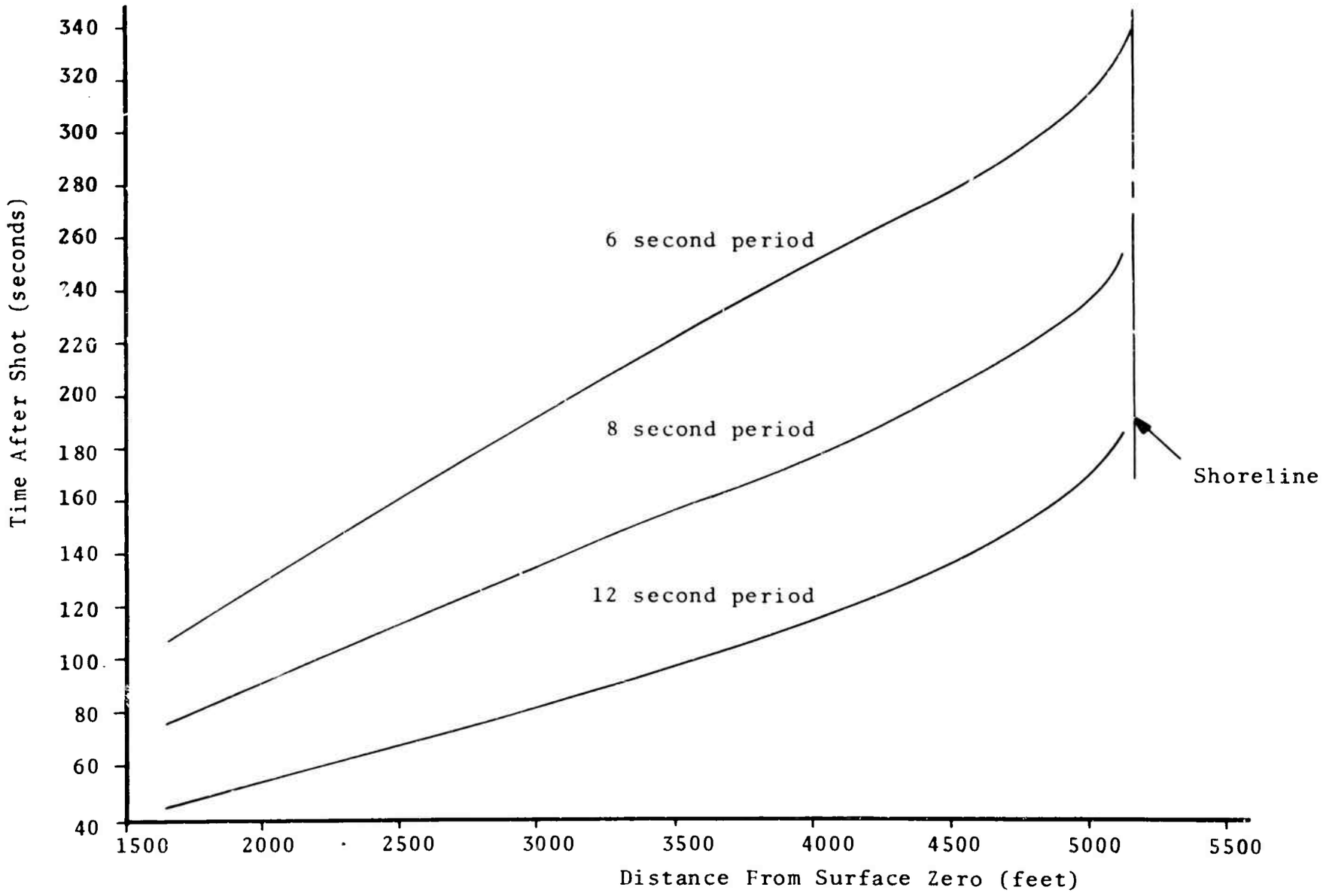

Figure 6 Times of Arrival of Wave Periods at Sensors on Radial 2

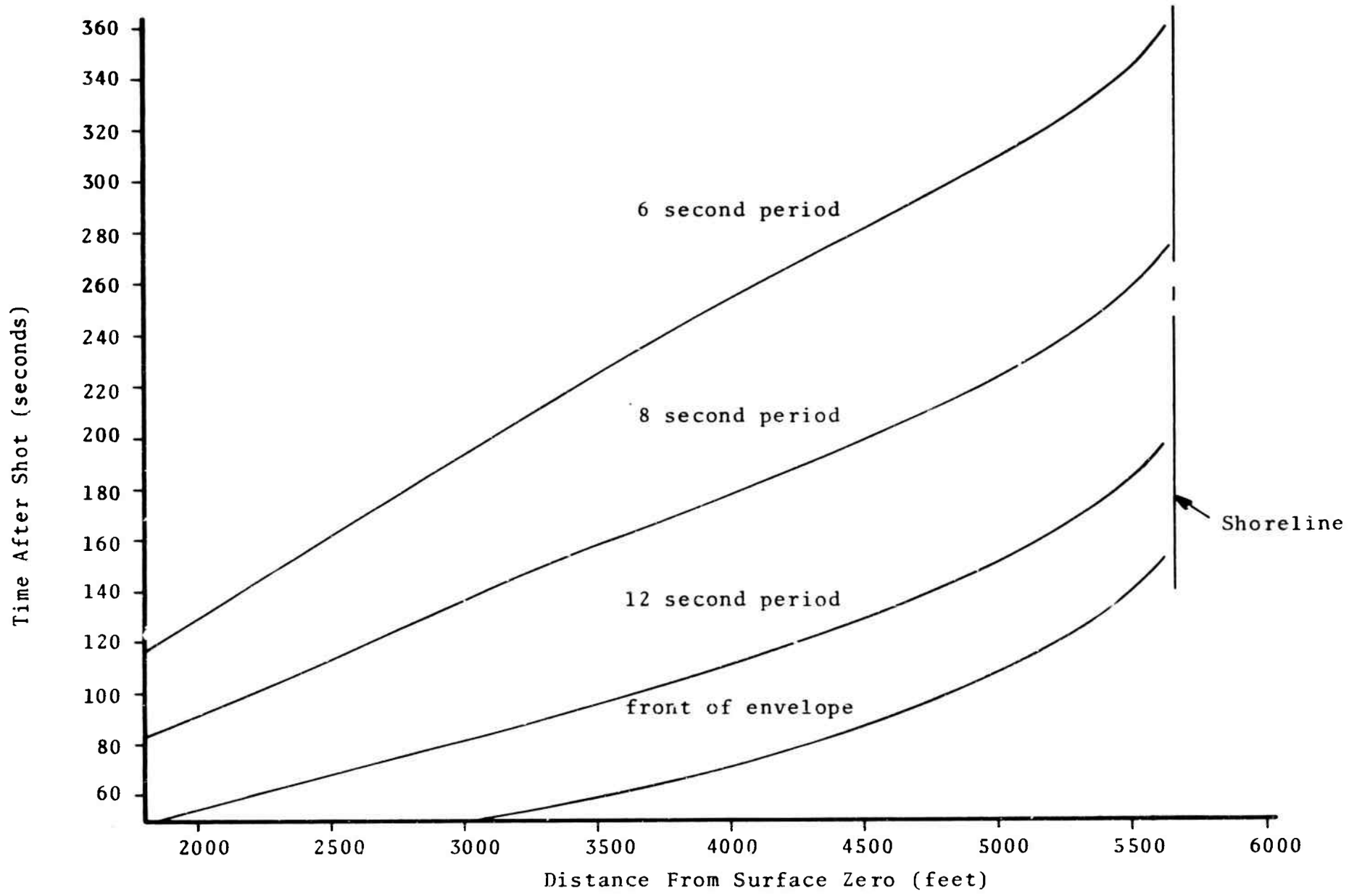

Figure 7 Times of Arrival of Wave Periods at Sensors on Radial 3

Here c is the average group velocity over the distance interval, dx. These calculated values are compared in Figure 8 with periods determined from the crest to crest time differences for the waves on the sensor traces of Reference 2. Considering that the crest to crest time differences from the waves are only approximate measures of the local wave period, it can be seen that the agreement is good.

The envelopes of the wave sensor traces given in Reference 2 are generally irregular not only from shot to shot but even from sensor to sensor. This is most marked in the traces for Shot 9 which show additional modulation beyond that ascribable to the multiplicity of envelopes. The 6 second period point of the envelope will occur at the envelope crest for one sensor trace and at a depression between two crests for the next sensor trace on the same radial. These variations produce significant spread in the measured envelope heights, especially when the measurements are made for specific, pre-selected arrival times on each sensor trace. Therefore, the envelope heights corresponding to each period selected were taken from a smoothed estimate of the local envelope shape, normalized to reference sensor envelope heights and presented along with the expected heights in Appendix A. Only sensor traces from Reference 2 which had complete calibrations were used for this

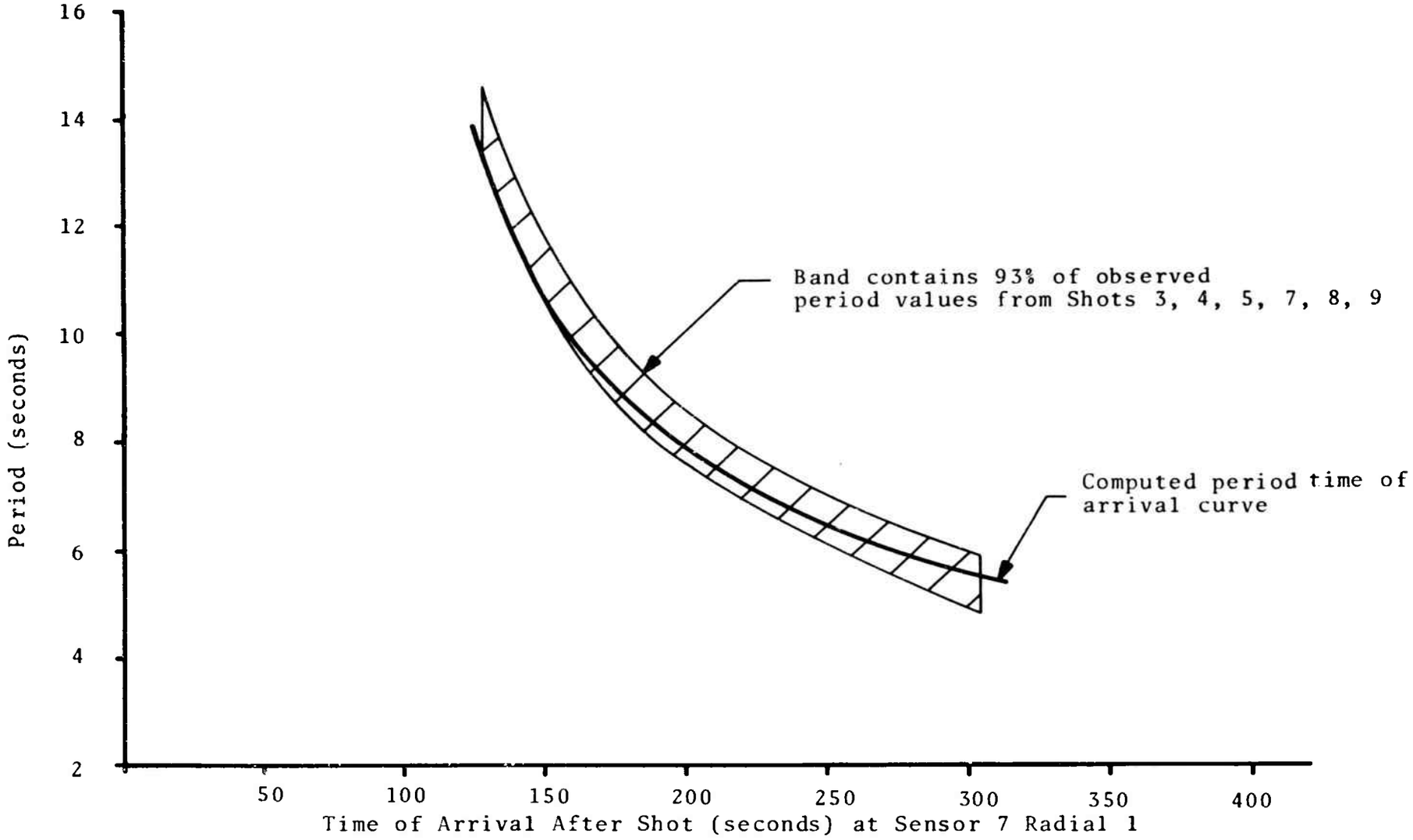

Figure 8 Comparison Between Observed and Computed Times of Arrival for Wave Periods Sensor 7 Radial 1

comparison, and those with conditional calibrations (numbered from 1 to 8 in Reference 2) were rejected.

Wave-height variation along the instrumented radials as predicted by linear methods (Eq. 1) is in reasonably good agreement with the sensor data from Radials 1 and 3. Agreement between predicted and observedwave heights for Radial 2 is less satisfactory, possibly because of noise transients communicated to Radial 2 from the surrounding Radials 1 and 3.

It will be observed that the nearshore sensors, as, for example, Sensors 7, 8, and 9 on Radial 1 record consistently below the predicted value for both 6 and 8 second waves. Still closer to shore, the observed values are larger than predicted, yet none of the data shown were obtained near the breaking zone where nonlinear effects might modify the predictions. The very low values of the data cannot be attributed to real fluid effects such as bottom friction, since the amplitude decrease is too great over the short distance of propagation from those sensors which are in good agreement with the predicted curve. It is most likely that those sensors which consistently record too high or too low are suspect even though their calibrations were considered acceptable in Reference 2.

In general, the wave heights from the sensor data in the offshore zone were in satisfactory agreement with the wave heights expected from shoaling of the deep water wave systems.

Section 3

THE BREAKING ZONE AND RUNUP

Breakers

Electronic wave sensors were located in the surf zone as close as 20 feet to the shoreline. However, none of the sensors in the surf zone had acceptable amplitude calibrations, and noise on the sensor traces, produced by the breaking waves and bores, generated large spikes at the crest of each wave. Thus, wave height magnitudes could not be obtained from the surf-zone sensor traces, but wave periods and times of arrival could be read from them. Breaker heights had to be determined from the shore-based motion picture coverage. Only on Radial 1 were there cameras directed out into the lake, and, for this reason, most of the following discussion will be based on results obtained for Radial 1.

Vertical poles were driven into the bottom at intervals of 10 feet along Radial 1 directly out from the runup ramp. These had 1 foot interval markings and were in the field of view of a camera out to 120 feet from shore. The sensors were arrayed parallel to this line of staffs at a distance of about 30 feet from them. With this arrangement it was possible to estimate the

breaking points and heights at breaking of all waves on Radial 1, to correlate these breakers with a wave period from the sensor data and to relate the breaker heights to wave heights far offshore. Again, the offshore wave height would be taken as the smoothed envelope height which corresponds at a given sensor to the same wave period. Sensor 2 on Radial 1 was taken as the nearshore sensor for the association of period with each observed wave. Waveheights for the corresponding periods were identified from a deep water sensor trace whose amplitudes agreed well with the curves of predicted waveheights as given in Appendix A. These wave height values will be identified as H_i where i is the number of the sensor at which this height occurred. From this, one can determine the wave height in deep water of the normally-incident, plane-fronted, wave train which will have the same height and period in the nearshore zone. This equivalent wave height will be called H'_o in keeping with current terminology (see, for example, Reference 8). H'_o is the wave height of a plane-fronted wave system corrected for refraction to the shoreline but not corrected for shoaling. To derive H'_o from H_i, the refraction correction for propagation from the reference sensor to shore must be made. In addition, the correction for dispersion must also be included.

The water depth at the reference sensor was shallow enough usually that a further correction for de-shoaling was required to obtain H'_o.

$$H'_o = \frac{H_i}{K'_S} \cdot \frac{K_R(\text{sensor 1})}{K_R(\text{sensor i})} \cdot \frac{K_D(\text{sensor 1})}{K_D(\text{sensor i})} \qquad 2)$$

The coefficients K_R and K_D are given for 6 and 8 second periods in Table 4. K'_S is the shoaling coefficient from deep water to the water depth at the reference sensor i. This is obtained for the periods of the H_i from tables of the shoaling coefficient (Reference 8).

Representative waves from Shots 3 through 10 are listed in Tables 7 and 8 in the order of the wave count at the shoreline. Also given are their effective periods, wave heights at the selected reference sensor, and the equivalent heights of plane waves in deep water as calculated from Eq. 2. Knowledge of H'_o is required in order to use current methods of predicting wave breaking and the runup of breaking waves. Comparison between prediction and the results of observation will draw upon the values of H'_o listed.

For each of the waves, presented in Tables 7 and 8, the bore heights were measured from the motion picture film using the 1 foot marks on the nearshore poles as reference lengths.

Table 7

Deep-Water Waveheight Equivalents for
Waves Observed in the Surf Zone, Radial 1, Shots 3 through 6

	Number of Wave Arriving at the Shoreline	Period (seconds)	H_i (feet)	H'_o (feet)
	n	T	H_{13}	H'_o
Shot 3	3	13.2	0.10	.069
	4	11.3	0.15	.11
	9	8.4	0.31	.23
	19	6.3	0.99	.70
	n	T	H_{16}	H'_o
Shot 4	3	13.2	0.28	0.099
	5	10.4	0.45	0.17
	8	8.7	0.70	0.25
	12	7.6	1.25	0.42
	16	6.8	1.80	0.58
	20	6.2	2.08	0.65
	n	T	H_{13}	H'_o
Shot 5	2	16.7	0.10	0.084
	6	9.8	0.27	0.20
	8	8.7	0.34	0.25
	10	8.1	0.40	0.29
	14	7.2	0.58	0.41
	18	6.4	0.52	0.36
	22	6.0	0.45	0.31
	n	T	H_{13}	H'_o
Shot 6	3	13.2	0.10	0.068
	5	10.4	0.13	0.093
	7	9.1	0.23	0.16
	11	7.8	0.34	0.24
	15	7.0	0.60	0.42
	19	6.3	0.70	0.49
	23	5.9	0.90	0.62

Table 8

Deep-Water Waveheight Equivalents for
Waves Observed in the Surf Zone, Radial 1, Shots 7 through 10

	Number of Wave Arriving at the Shoreline	Period (seconds)	H_i (feet)	H'_o (feet)
	n	T	H_{16}	H'_o
Shot 7	2	16.7	0.15	0.051
	4	11.3	0.31	0.11
	6	9.8	0.50	0.18
	8	8.7	0.66	0.22
	12	7.6	0.83	0.27
	16	6.8	0.82	0.26
	20	6.2	0.65	0.20
	n	T	H_{13}	H'_o
Shot 8	4	11.3	0.12	0.086
	7	9.1	0.17	0.13
	12	7.6	0.23	0.16
	n	T	H_{13}	H'_o
Shot 9	2	16.7	0.04	0.022
	5	10.4	0.28	0.20
	9	8.4	0.32	0.23
	13	7.4	0.42	0.30
	17	6.6	0.45	0.31
	21	6.1	0.38	0.26
	n	T	H_{10}	H'_o
Shot 10	2	9.9	0.24	0.17
	3	9.0	0.34	0.25
	9	6.3	1.22	1.01

Decay of the bore heights from the point of breaking of the wave to the reference pole 6 feet offshore is shown in Figures 9 through 17. Most of the bores reformed into smooth waves just before reaching the toe of the runup ramp and then broke again on the toe of the ramp. This reformation into a wave was most probably caused by the nonuniformity of the nearshore bottom slope. It will be seen in Table 1 or Table 4 that the water depth is the same for both Sensors 1 and 2, and other evidence indicates that a deepening of the water occurred just offshore of the ramp. This situation can cause a bore to become a nonbreaking wave; for it has been observed that even for single slopes gentler than 1 in 50, breakers will reform into waves before reaching the shoreline (Reference 9).

In the particular case of Shot 6, the bores reformed at 30 feet offshore into very steep waves breaking slightly at the crests. Shot 6 differs from the others in only one significant regard. As discussed earlier, packets of short period waves were superimposed on the explsion-wave system, and the directions of travel of these two wave systems were almost the same in the nearshore zone. It is believed that this additional wave system was responsible for the unusual behavior of the Shot 6 bores, but the correlation has not been investigated.

In all shots, only the first and second waves arrived at the beach without having broken at least once. The following waves broke further and further from shore since their deep-water wave height increased up to the crest of the first envelope. Thereafter, the offshore wave heights decreased to the node between the first and second envelopes, and the breaking points moved back towards shore. Even though the point of breaking and the height of breaking varied considerably for waves in the first envelope, the bore heights near the shoreline H_s did not. The higher the wave, the further offshore it breaks and the further it has to decay in height. This feature of breaking waves has great influence on the eventual runup and will be discussed at greater length in that connection.

The height of breaking H_b, referred to the undisturbed water level is given by

$$H_b = \left(\frac{H_o' T}{2.66} \right)^{2/3} \qquad 3)$$

(see Reference 8). H_o' and T are taken from Tables 7 and 8. The breaker heights predicted from this equation are shown in Figures 9 through 17 in company with the observed values. All the measured breaker-height values and Eq. 3 are shown again in Figure 18 as a function of $\frac{H_o'}{T^2}$. Allowing for the usual scatter of data from measurements made in the surf zone, the agreement can be considered good.

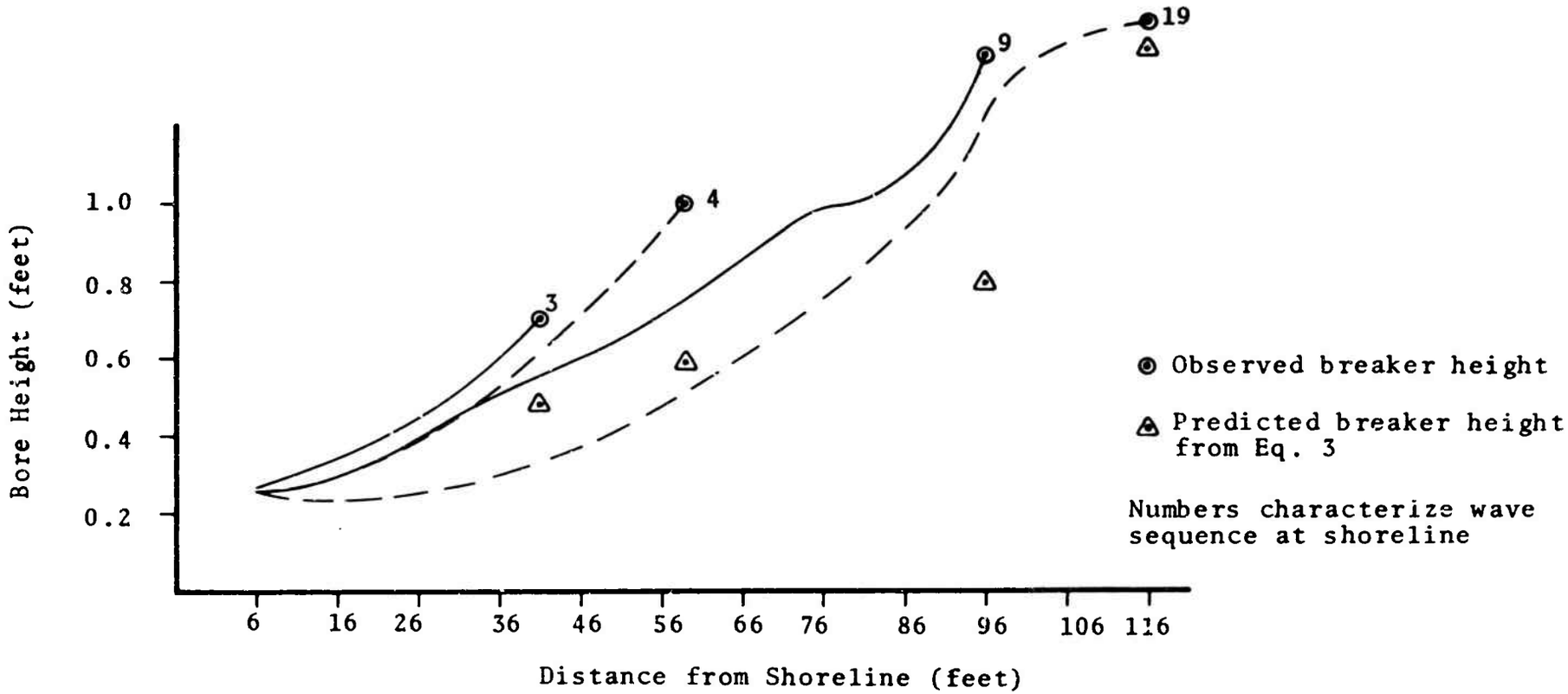

Figure 9 Bore Decay Shot 3 Radial 1

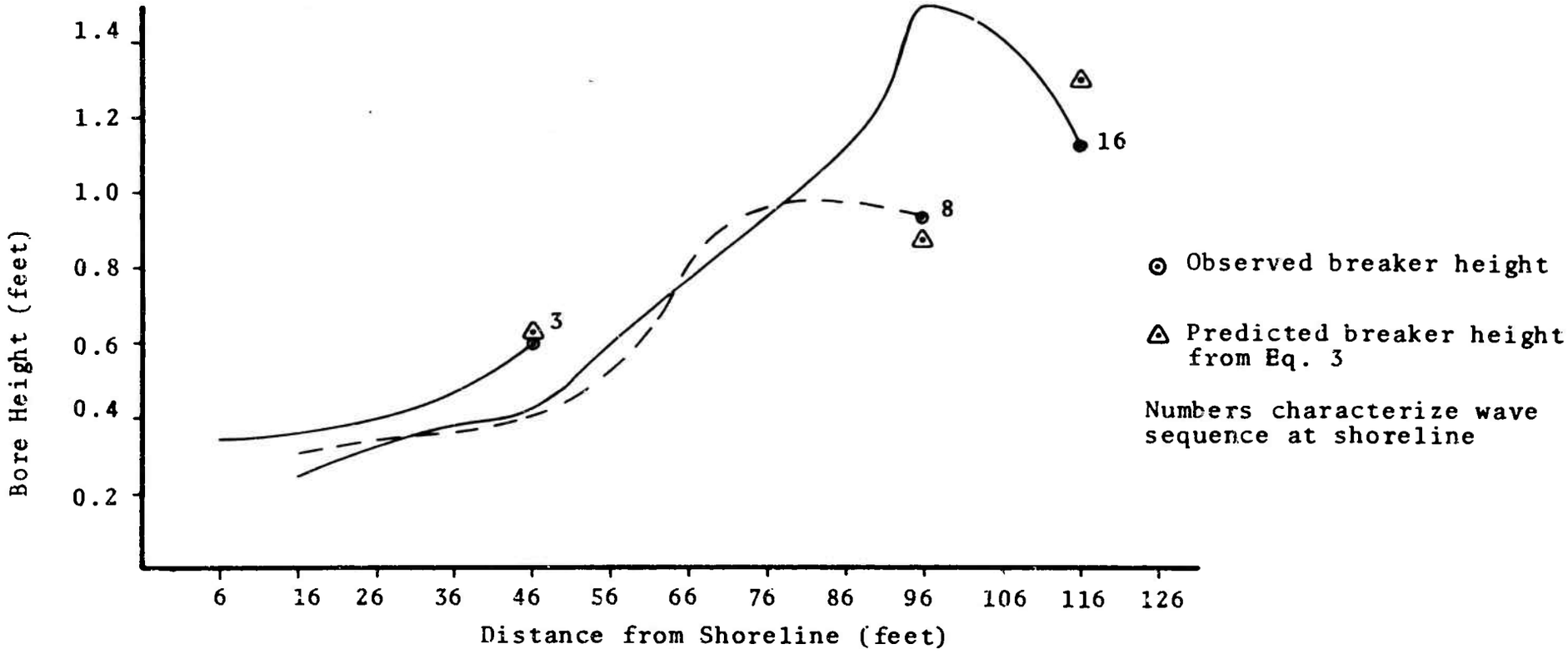

Figure 10 Bore Decay Shot 4 Radial 1
Waves 3, 8, and 16

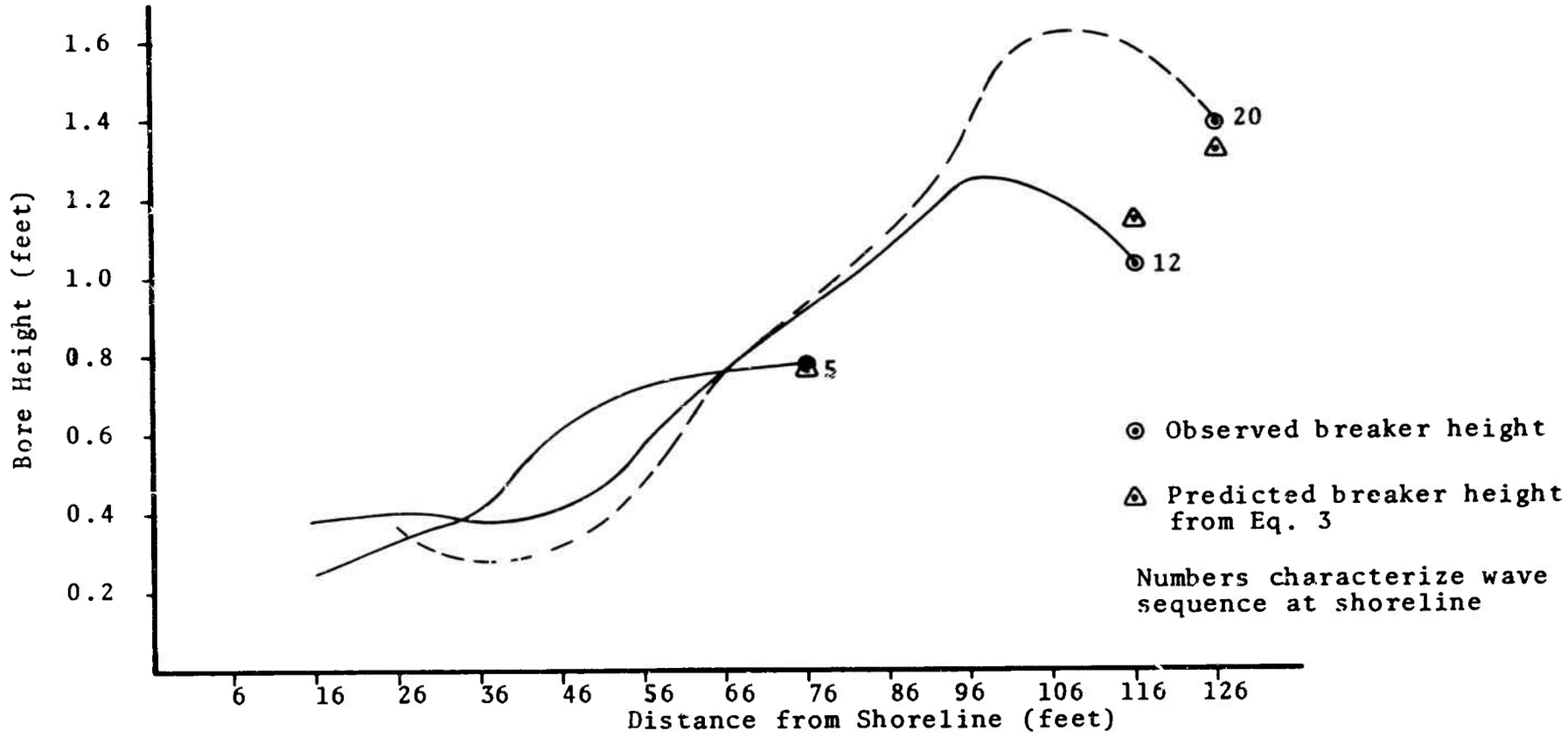

Figure 11 Bore Decay Shot 4 Radial 1
Waves 5, 12, and 20

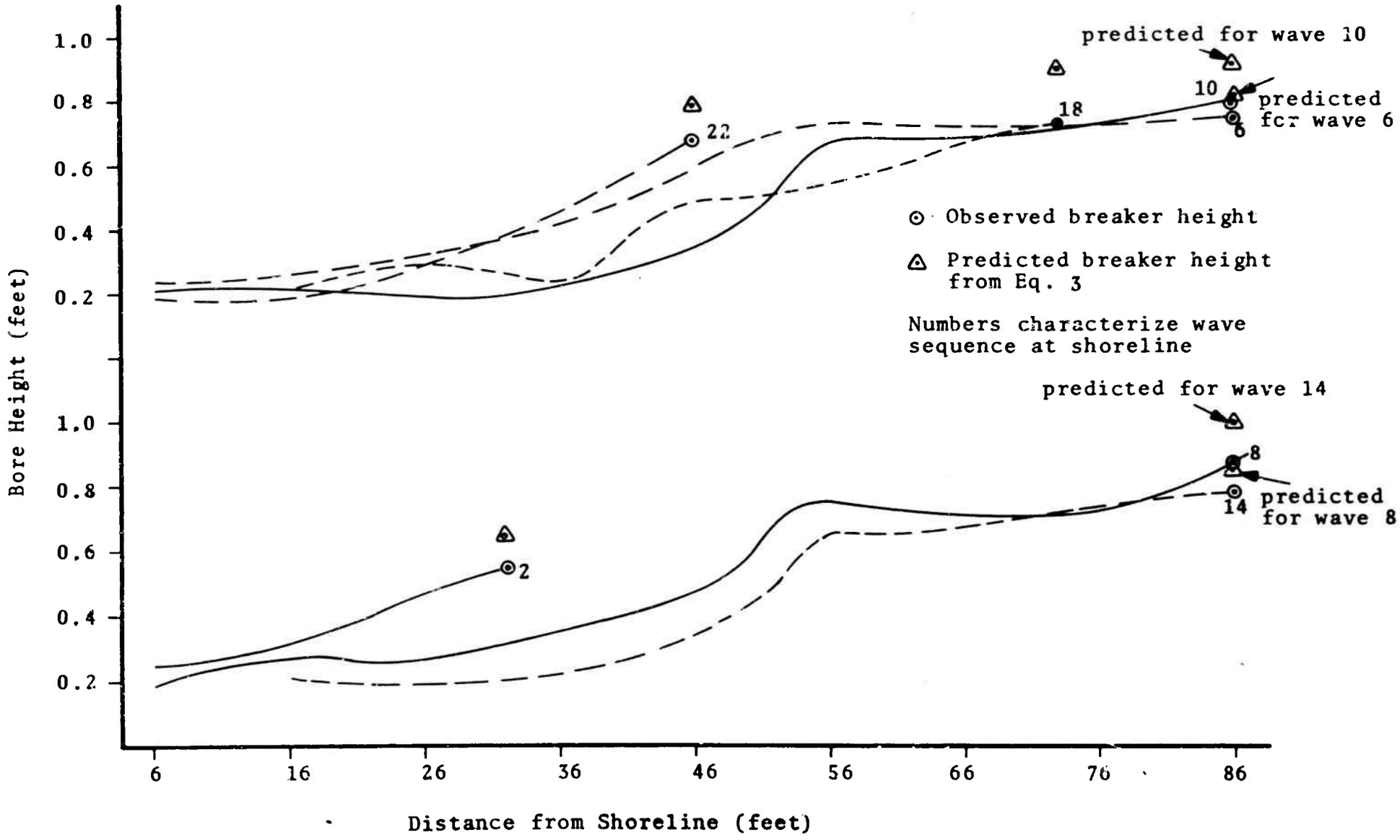

Figure 12 Bore Decay Shot 5 Radial 1

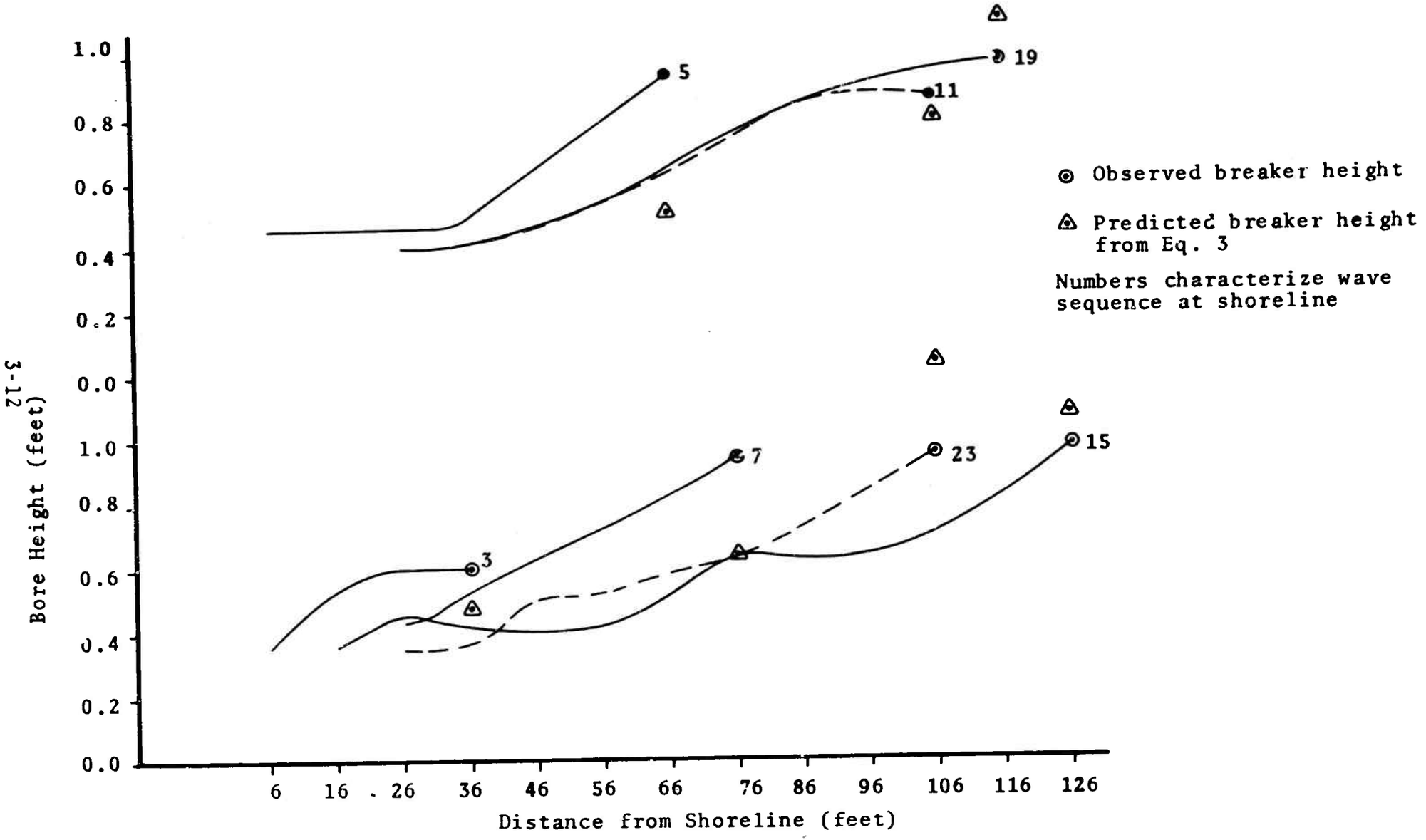

Figure 13 Bore Decay Shot 6 Radial 1

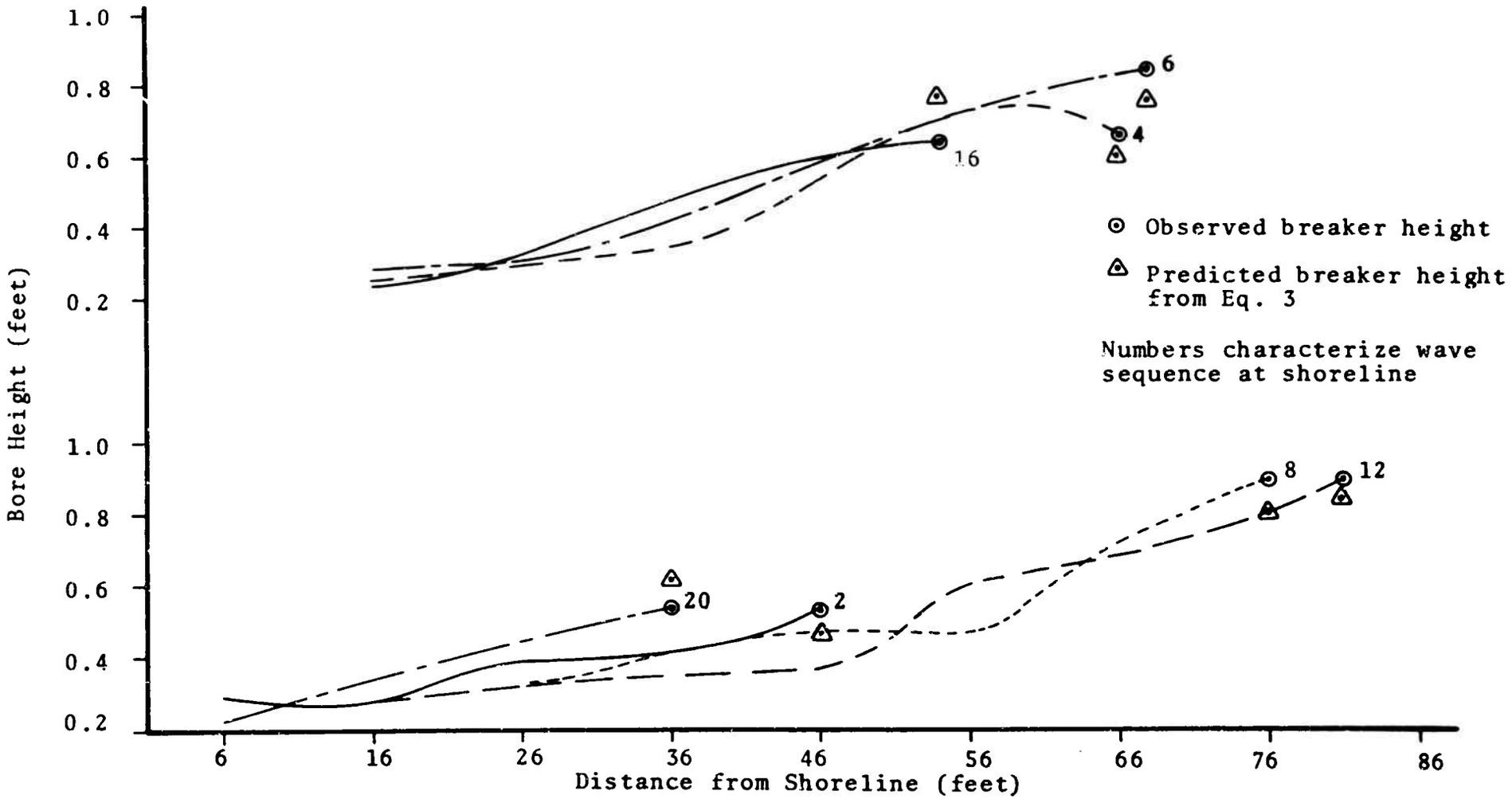

Figure 14 Bore Decay Shot 7 Radial 1

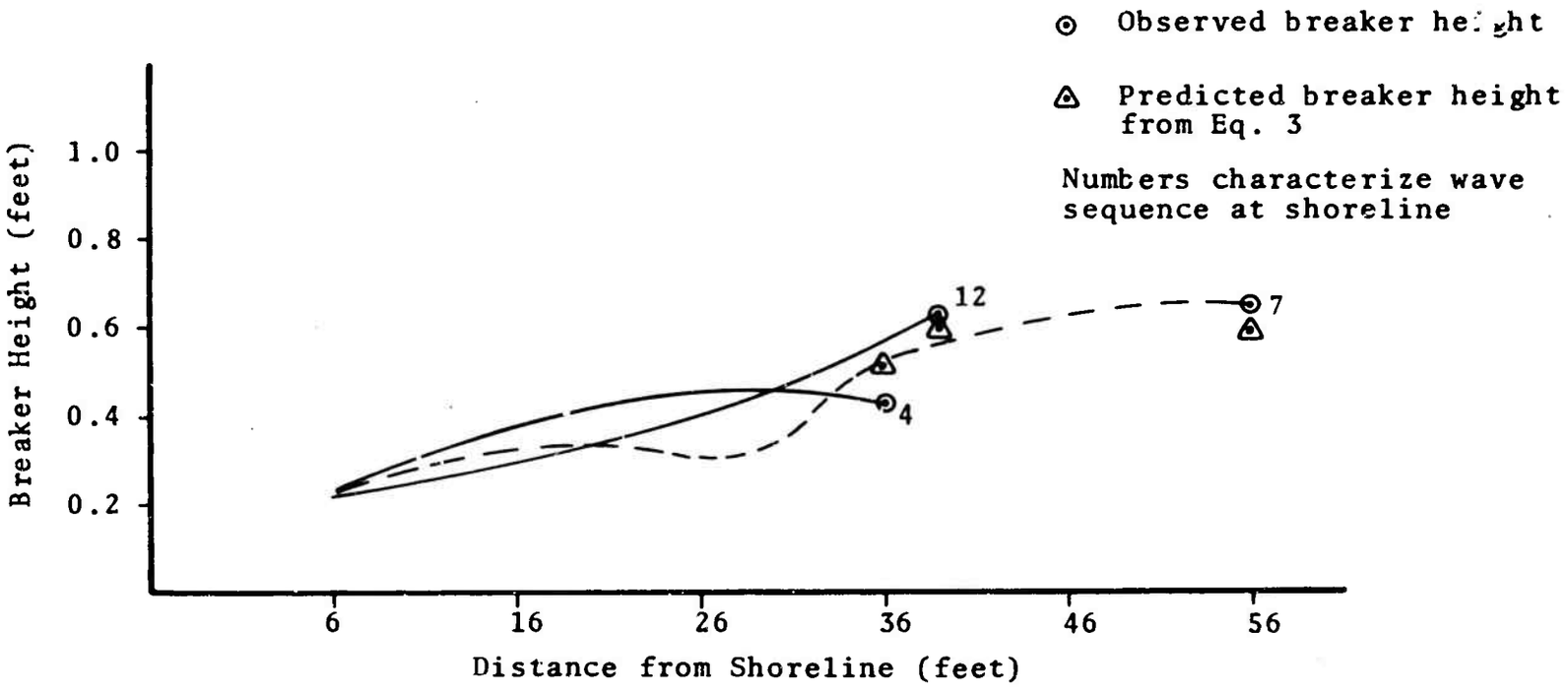

Figure 15 Bore Decay Shot 8 Radial 1

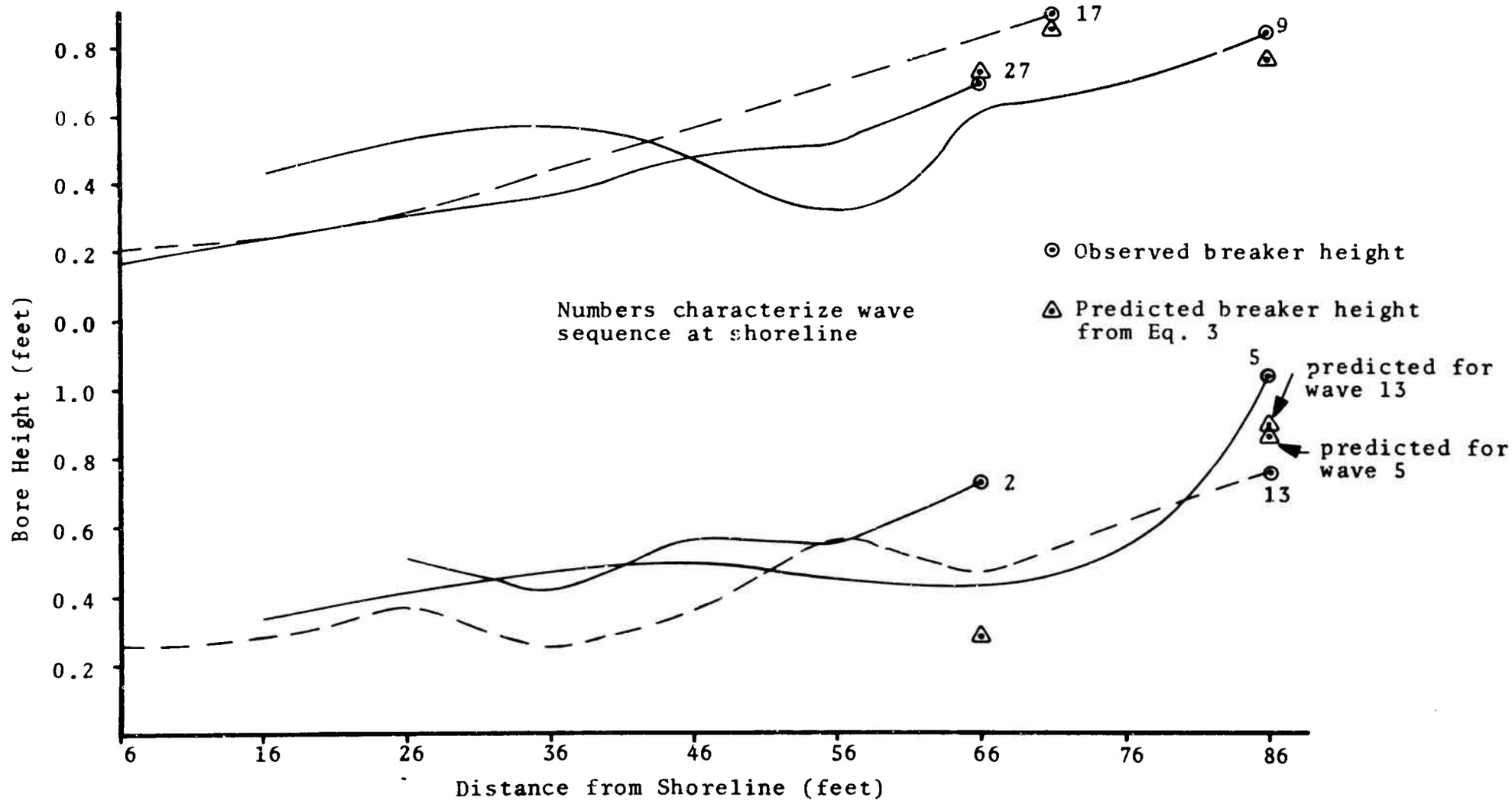

Figure 16 Bore Decay Shot 9 Radial 1

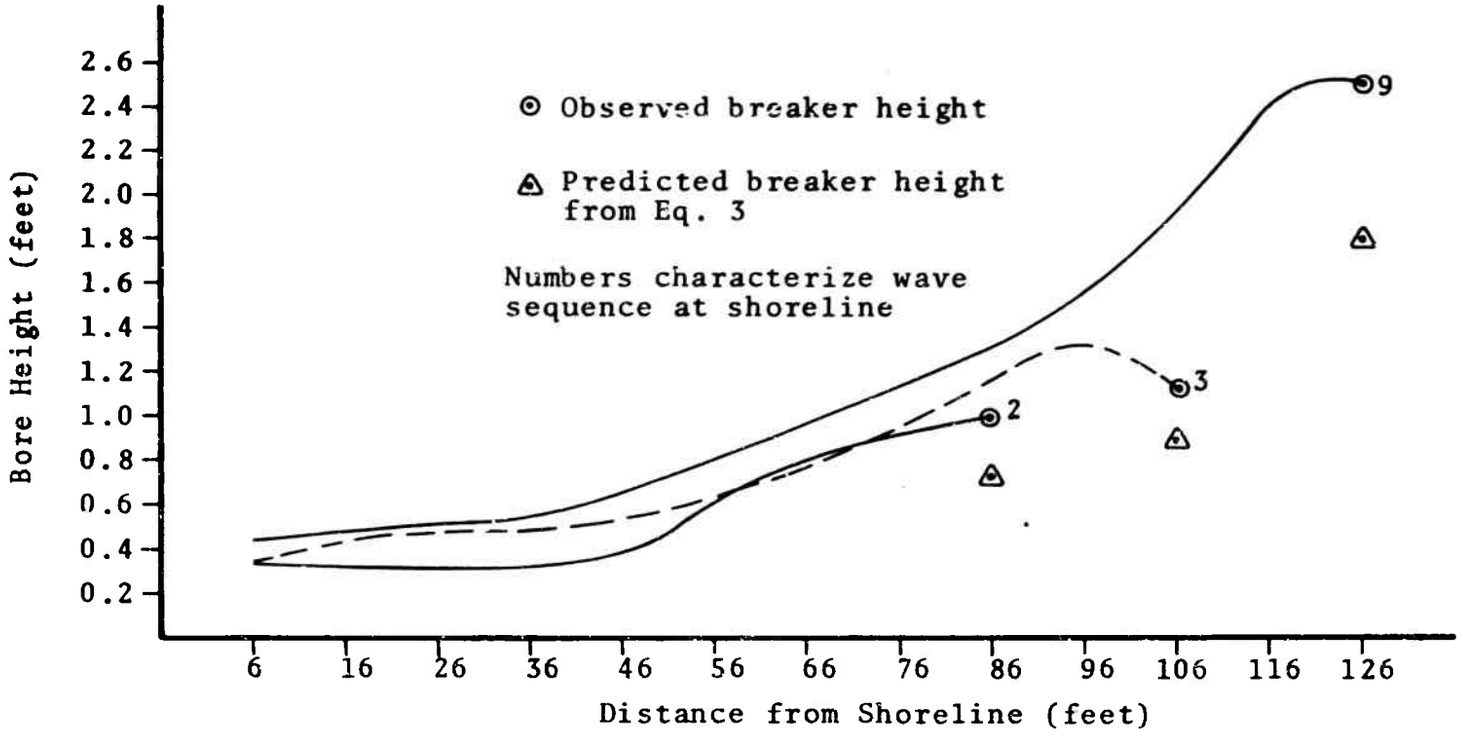

Figure 17 Bore Decay Shot 10 Radial 1

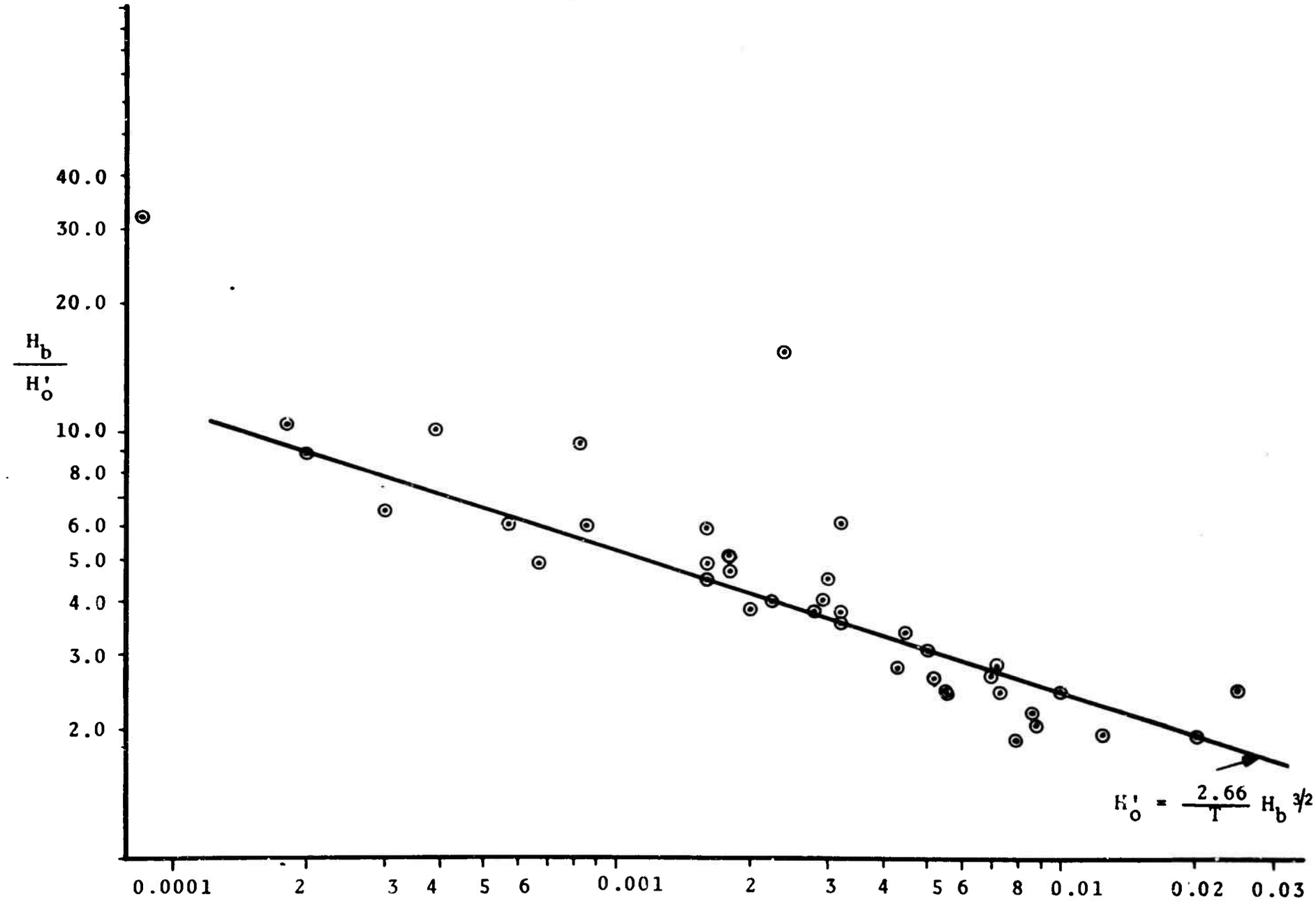

Figure 1[illegible] Breaker Heights

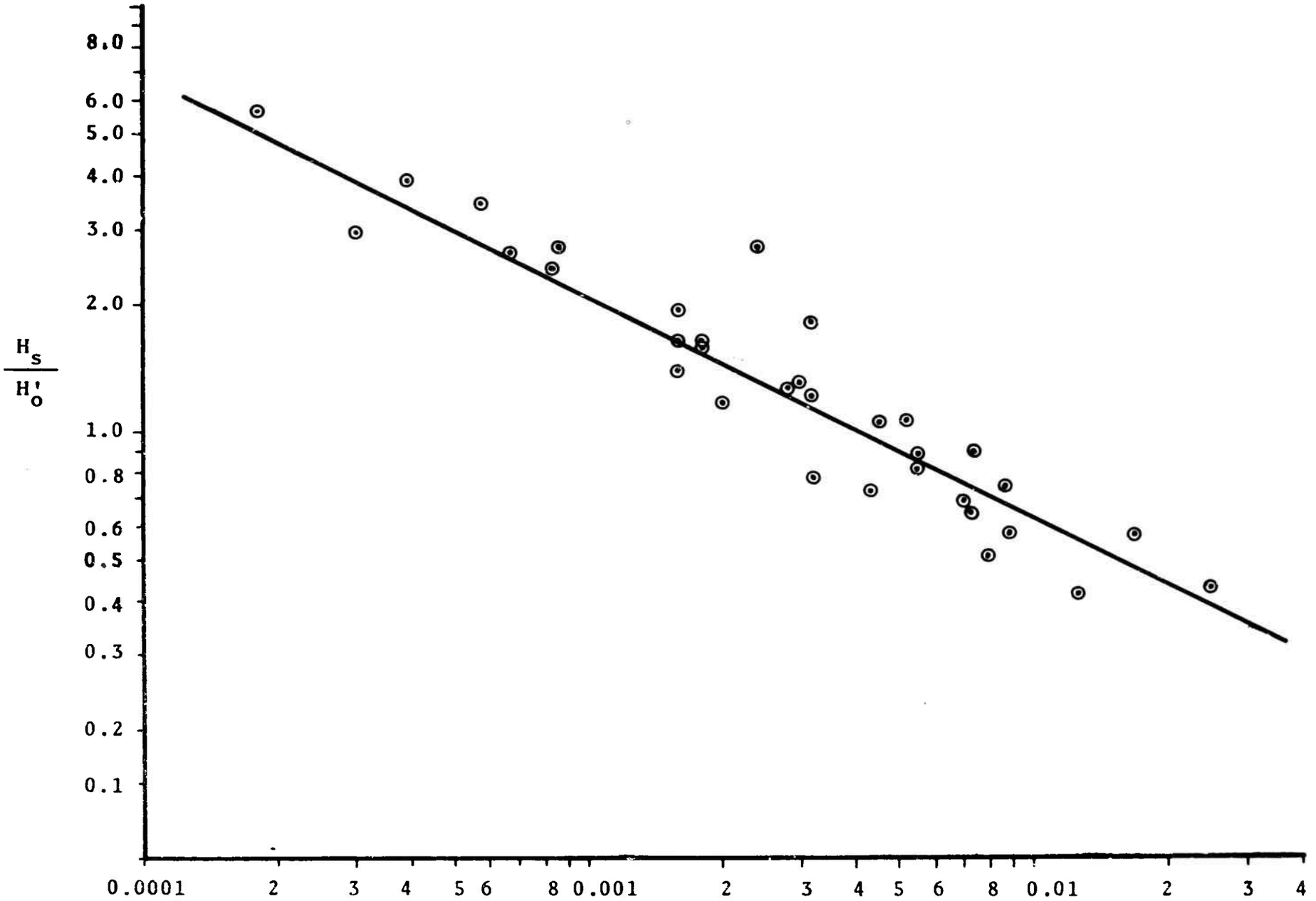

Figure 19 Nearshore Bore Heights

In similar way, the ratios of the nearshore bore heights to the deep-water wave height equivalents are shown in Figure 19 as a function of $\frac{H'_o}{T^2}$. A straight line has been fitted to the data by eye. It will be noted that this curve has a steeper slope than that for $\frac{H_b}{H'_o}$, showing a greater tendency for H_s to increase with decreasing wave steepness than does H_b.

Runup

Vertical runup per incident wave for all shots from 2 through 10 was reported by WES (Reference 1) for runup Ramps 1 and 2. Runup per wave on the beach was also recorded at the termination of Radial 3 for Shots 6 through 10 and listed in the referenced report. Some comparisons of runup and the deep-water wave height will be made for runup Ramp 2 and for Radial 3; but, mostly, attention will be directed towards Ramp 1 where correlation can be made with the offshore breakers.

The vertical runup of the waves on Ramps 1 and 2 as tabulated in Reference 1 was derived by multiplying the horizontal encroachment of the water by the known slope of the ramp. That this procedure was used has been verified from the motion picture film of the runup on two ramps. However, the vertical runup referred to the undisturbed water level was, in fact, larger, because the water level lay below the intersection of the main ramp with the toe ramp.

The geometry of the main Ramps 1 and 2 and the toe ramps relative to the water level was illustrated in Reference 1 for each shot except for Shots 3 and 4. The geometry varied slightly from shot to shot because of a gradual decline of the water in the lake and because of changes in slope of the toe ramp due to wave action. The vertical distance from the still water level to the extension of the main ramp must be added to all ramp runup values reported in Reference 1. This additional distance is illustrated in the diagram of Table 9, and the correction terms for each shot and ramp number are listed. In the sequel, all runup values attributed to Reference 1 contain the appropriate correction term. In those few cases where the horizontal incursion of water was less than 4 feet, the vertical runup was calculated by multiplying this value by the slope of the toe structure.

Considerable data have been collected on the runup of breaking periodic waves on two-dimensional, impermeable shore structures. These data have been compiled into a set of prediction curves giving $\frac{R}{H'_o}$, as a function of bottom slope for a range of wave steepnesses, $\frac{H'_o}{T^2}$ (Reference 8, Figures 3-1 and 3-2). These are frequently referred to as the Saville curves. Predictions from these curves have been found to give good agreement with observation when the offshore slopes and wave steepnesses fall within their range of application (Reference 4). However, these curves only

Table 9

Runup Correction Terms

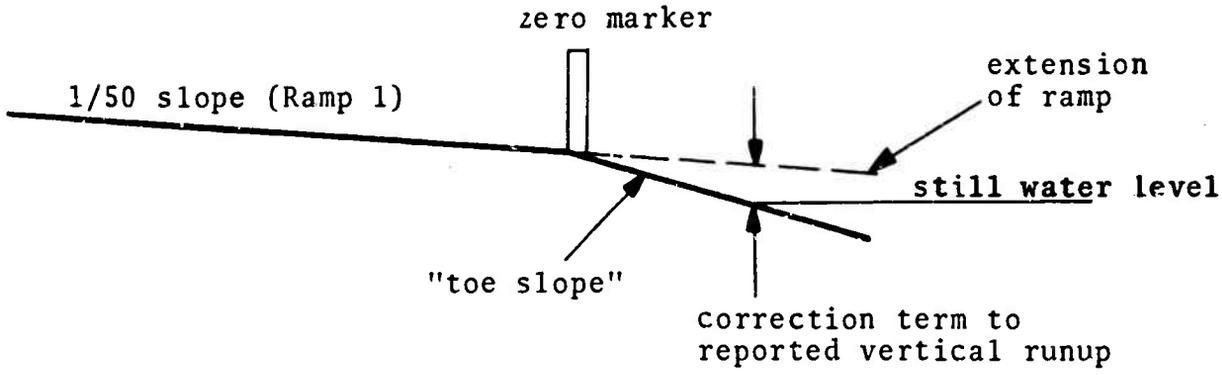

Shot	Runup Ramp 1	Runup Ramp 2
2	0.14 ft.	0.15 ft.
3	0.18 ft.	0.18 ft.
4	0.20 ft.	0.20 ft.
5	0.22 ft.	0.23 ft.
6	0.22 ft.	0.24 ft.
7	0.22 ft.	0.25 ft.
8	0.24 ft.	0.26 ft.
9	0.26 ft.	0.25 ft.
10	0.27 ft.	0.27 ft.

extend to wave steepnesses of $\frac{H'_o}{T^2}$ >.01 and to slopes steeper than 1 in 30. Explosion waves generally have a steepness less than .01 in $\frac{H'_o}{T^2}$ and, in the particular case of this test series in Mono Lake, the offshore slopes were less than 1 in 50 in the nearshore zone for all three radials. As mentioned before, the bottom very close to shore was flat enough to permit the bores to become smooth waves again. If the Saville curves are extended to smaller slopes by straight-line extrapolation, the predicted runup is too small by factors of from 2 to 4 even on the presumption that the effective offshore slopes were 1 in 50.

An alternative method of predicting runup on very shallow, irregular slopes will be described and compared with the measured runup. In this method, the runup is attributed to the dynamics of the nearshore bores through Bernoulli's equation

$$R = \frac{u^2}{2g} . \qquad 4)$$

R is the absolute runup, u is the particle velocity in the bore, and g is the acceleration of gravity. This relation has been derived by various authors who used the linear, shallow water equations in the treatment of runup on a dry bed. On a simpler basis, this equation is merely the statement that the dynamic head of a fluid can be transformed into static head. The water will be assumed frictionless in its runup on the ramp. Note

that the onshore slope does not influence the runup according to Eq. 4, but the particle velocity of the bore used in the equation is determined by the bore height which is itself a function of the offshore slope.

The data from this test series apply, of course, only to very shallow slopes, and the bore heights close to shore on steeper slopes have not been reported in the literature.

It is generally considered that the bore particle velocity becomes equal to the bore velocity near the water's edge. The two are certainly equal on the sub-aerial slope where the motion of the front edge of the water is produced by the water particle motion, but where equality occurs offshore is not known. It will be assumed that the bore velocity and the particle velocity are equal in the nearshore zone where the bore height has its minimum, H_s.

The bore velocity can be determined from the bore height and still-water depth h using the equation of the stationary hydraulic jump:

$$\frac{h+H_s}{h} = \frac{1}{2}\left(\sqrt{1+8\,\frac{u^2}{gh}} - 1\right) \qquad 5)$$

and the continuity equation

$$u_1 h = u_2 \ (h+H_s). \qquad 6)$$

(See for example, Reference 10, p. 698). Here, u_1 is the flow velocity in water of depth h entering the stationary jump and u_2 is the velocity leaving it in the new water depth $h+H_s$. Transforming this to a coordinate system in which the water ahead of the jump is at rest gives

$$u = \text{bore velocity}$$
$$= u_1 - u_2$$

and

$$u_1 = \frac{h+H_s}{H} \ u$$

Substitute this into Eq. 5) to get

$$\frac{u^2}{2g} = \frac{(h+H_s)(2h+H_s)}{4h} \ . \qquad 7)$$

This would be the absolute runup if h were chosen at the point where the particle velocity is equal to the bore velocity. It appears from the motion picture film that the bore height reaches a minimum value at some distance offshore and remains essentially constant at this value during the remainder of its travel to shore. In many cases, the bore reformed into a smooth wave

after obtaining this minimum and broke again on the ramp, but this final bore will be assumed to have the same height H_s.

Now u^2 in Eq. 7 is large for H and decreases to a minimum as h decreases for fixed H_s. As h continues to decrease towards zero, $\frac{u^2}{2g}$, approaches infinity since the stationary hydraulic jump, from which Eq. 7) was derived, is not defined on a dry bed. It will be assumed, therefore, that the bore velocity and the particle velocity approach equality close enough for the purposes of this discussion when Eq. 7) is a minimum with respect to h for fixed H_s.

Differentiating Eq. 7) with respect to h and setting it equal to zero gives:

$$h = \frac{1}{\sqrt{2}} H_s$$

The predicted runup is simply

$$R = \text{Min} \frac{u^2}{2g} = 1.45\ H_s \qquad 8)$$

In Table 10 observed runup on Ramp 1 is compared with the prediction obtained by substituting the observed values of H_s for each wave into Eq. 8). Agreement between observed and predicted runup is quite good although the runup values for Shot 6

Table 10

Comparison Between
Observed and Predicted Runup - Ramp 1

	Number of Wave	Predicted Runup (feet) Eq. 8	Observed Runup (feet)
Shot 3	3	0.39	0.44
	4	0.37	0.38
	9	0.37	0.38
	19	0.37	0.34
Shot 4	3	0.48	0.46
	5	0.34	0.42
	8	0.43	0.40
	12	0.54	0.40
	16	0.34	0.40
	20	0.51	0.40
Shot 5	6	0.33	0.40
	8	0.27	0.40
	10	0.30	0.40
	14	0.30	0.42
	18	0.30	0.40
	22	0.27	0.38
Shot 6	3	0.51	0.38
	5	0.66	0.40
	7	0.64	0.40
	11	0.58	0.40
	15	0.51	0.42
	19	0.58	0.40
	23	0.51	0.40
Shot 7	4	0.35	0.40
	6	0.40	0.38
	8	0.40	0.40
	12	0.40	0.40
	16	0.33	0.40
	20	0.31	0.40
Shot 8	4	0.31	0.40
	7	0.31	0.42
	12	0.30	0.42
Shot 9	5	0.47	0.46
	9	0.60	0.44
	13	0.37	0.44
	17	0.29	0.44
	21	0.23	0.44
Shot 10	2	0.45	0.49
	3	0.45	0.51
	9	0.63	0.65

are consistently smaller than the predicted. In the unusual case of Shot 6 discussed earlier, the minimum bore height H_s may not have been achieved before the bores reformed into waves.

Tables 11 and 12 give a comparison between the observed runup and the runup estimated from Eq. 8). The value of H_s was determined from Figure 19 by first establishing H_o' through the method used for Radial 1.

The agreement is not so good for Ramp 2 as it is for Ramp 1, but the nearshore bore heights were not observed on Radial 2. Even on Radial 3, for which there was no ramp, the prediction is mostly within a factor of 2 of the observed runup.

The influence of bottom slope on the height of the nearshore bore, H_s, is not known. The effective slope on Radial 1 is less than 1:50 by any method of estimation, but the slope is irregular. This circumstance may be responsible for the irregularity in the curves of bore decay from the breaking point to the shoreline. It has been observed in tank studies (Reference 11) that bore decay is virtually independent of slope on a uniform slope more gentle than about 1 in 50, and it is this concept which makes plausible the extrapolation of runup prediction to Radials 2 and 3 in the absence of observed bore

Table 11

Comparison Between
Observed and Predicted Runup - Ramp 2

	Number of Wave	H'_o (feet)	T (seconds)	Predicted Runup (feet) Eq. 8	Observed Runup (feet)
Shot 3	6	0.14	9.5	0.32	0.58
	12	0.26	7.5	0.35	0.61
	18	0.65	6.5	0.48	0.41
Shot 4	6	0.16	9.5	0.36	0.53
	12	0.24	7.5	0.35	0.57
	18	0.59	6.5	0.45	0.57
Shot 5	6	0.28	9.5	0.48	0.60
	12	0.31	7.5	0.38	0.56
	18	0.50	6.5	0.41	0.50
Shot 6	6	0.13	9.5	0.33	0.51
	12	0.29	7.5	0.37	0.61
	18	0.64	6.5	0.47	0.47
Shot 7	6	0.14	9.5	0.34	0.52
	12	0.16	7.5	0.28	0.48
	18	0.22	6.5	0.28	0.52
Shot 8	6	0.099	9.5	0.30	0.66
	12	0.12	7.5	0.25	0.53
	18	0.15	6.5	0.24	0.43
Shot 9	6	0.20	9.5	0.40	0.62
	12	0.20	7.5	0.32	0.48
	18	0.35	6.5	0.35	0.48

Table 12

Comparison Between
Observed and Predicted Runup - Radial 3

	Number of Wave	H'_o (feet)	T (seconds)	Predicted Runup (feet) Eq. 8	Observed Runup (feet)
Shot 7	6	0.097	9.9	0.31	0.54
	12	0.099	7.8	0.24	0.54
	18	0.12	6.8	0.22	0.54
Shot 8	6	0.097	9.9	0.31	0.54
	12	0.13	7.8	0.27	0.54
	18	0.092	6.8	0.20	0.68
Shot 9	6	0.17	9.9	0.39	0.81
	12	0.19	7.8	0.32	0.81
	18	0.19	6.8	0.27	0.68

heights. The slope irregularities on those radials may compromise this extrapolation and cause the less satisfactory agreement shown between observed and predicted runup in Tables 11 and 12. From a qualitative viewpoint, the constancy of runup values on a gentle slope for an entire explosion wave system correlates well with the constancy of nearshore bore heights for the same waves. For this reason alone, it is advisable to associate the runup on gentle slopes with the bore heights rather than with the distant wave heights. Until additional data become available, it is recommended that H_s from the mean curve of Figure 19 be used in Eq. 8 for predicting runup on shallow slopes.

Section 4

CONCLUSIONS

It may be concluded generally that the 1965 series of explosion-wave tests in Mono Lake, California, provided a comprehensive comparison between experimental results and current prediction methods for explosion-wave generation, propagation, and runup on shallow slopes. Specific conclusions are as follows:

1. Generation. Deep-water heights at the crests of the first envelope were in satisfactory agreement with values predicted from the charge weights and depths of shot with the exception of the two deepest shots. These were fired in the region of the lower critical depth, but the crest heights were much smaller than was expected from results of previous studies. It is not certain whether these shots were faulty or whether the phenomenon is real and represents a scale effect for large charges. Evidence based on period changes at the envelope crests and phase shifts in the wave system suggests the effects are real.

2. Propagation. Comparison between wave heights measured at the wave sensors with the heights predicted from linear methods for shoaling, refracting, and dispersing waves showed acceptable agreement. There was enough scatter in the data that small deviations from the linear prediction would have been masked.

3. Breaking. The equivalent deep-water wave height is customarily related to the wave height at breaking through the empirical equation:

$$H_o' = \frac{2.66}{T} H_b^{3/2}$$

Results of the tests showed good agreement with this relation.

4. Runup. Observed runup was considerably higher than predicted by any reasonable extrapolation of the Saville curves to the shallow offshore slopes typical of the test site. However, good agreement was found between the observed runup and the nearshore breaker height H_s through the relation:

$$R = 1.45\ H_s$$

Section 5

REFERENCES

1. Rooke, A. D., Jr., L. K. Davis, and J. N. Strange, Mono Lake Explosion Test Series, 1965 Results of the Wave Runup Experiments. Mis. Paper #1-947. Conducted by the U. S. Army Engineers Waterways Experiment Station, Corps of Engineers for the Defense Atomic Support Agency. December 1967.

2. Whitehill, W. J., D. D. Pollard, and C. W. Baird, Wave Sensor Traces from the Mono Lake Water-Wave Experiments. OSI Report #102-1. Prepared for the Office of Naval Research by Oceanographic Services, Inc. May 1968.

3. Kranzer, H. C. and J. B. Keller, Water Waves Produced by Explosions. Jour. of Appl. Physics, March 1959, Vol. 30, No. 3, p. 398-403.

4. Wallace, N. R. and C. W. Baird, Runup on an Irregular Shoreline, Mono Lake Tests. OSI Report #NVO-297-2. Prepared for the U. S. Atomic Energy Commission by Oceanographic Services, Inc., Santa Barbara, California, May 1968.

5. Walter, D. Explosion-Generated Wave Tests Mono Lake, California, Ground and Aerial Photography. URS Report #654-2. Prepared for the Office of Naval Research by URS Corporation Burlingame, California. January 1966.

6. Street, R. L., S. J. Burges and P. W. Whitford, The Behavior of Solitary Waves on a Stepped Slope. Technical Report No. 93. Prepared for the Defense Atomic Support Agency and Field Projects Branch, Office of Naval Research by the Department of Civil Engineering, Stanford University, Stanford, California. August 1968.

7. LeMehaute, B., R. W. Whalin and L. M. Webb, Predictions of the Water Waves and Runup Generated by TNT Explosions in Mono Lake, Volume I. NESCO Report #S-256-2. Prepared for the Office of Naval Research by National Engineering Science Company, Pasadena, California. October 1965.

8. Coastal Engineering Research Center, Shore Protection Planning and Design. Technical Report No. 4. Third Edition, 1966.

9. Nakamura, M., H. Shiraishi, and Y. Sasaki, Wave Decaying Due to Breaking. Proceedings of the Tenth Conference on Coastal Engineering, Vol. 1, Chapter 16, ASCE New York, New York. September 1966 .

10. Wehausen, J. V. and E. V. Laitone, Surface Waves. Encyclopedia of Physics, Vol. 9. Springer-Verlag, Berlin. 1960.

11. Horikawa, K. and C. Kuo, A Study on Wave Transformation Inside Surf Zone. Proceedings of the Tenth Conference on Coastal Engineering, Vol. 1, Chapter 15, ASCE New York, New York. September 1966.

APPENDIX A

This appendix presents comparisons between observed and predicted wave heights at the 6 second, 8 second, and crest points of the explosion-wave envleopes. All data were taken from the amplitude-time traces presented in Reference 2. The solid line in each figure is the expected ratio of wave height at the given sensor to the wave height at a deep-water reference sensor as given by Eq. 1) in the main text The data points are the observed wave heights for the stated wave period at the sensor divided by the wave heights observed for the same wave period at the reference sensor. The wave height ratios for the first envelope crests are also shown. Since the period at the envelope crest is not necessarily 6 or 8 seconds, the envelope crest data are placed on the plot for the period closest to the period of the crest. Points for the envelope crests are shown as open circles to distinguish them from the 6 or 8 second points (shown solid).

The wave height in feet at any sensor can be regained by multiplying the ordinate of a data point by the appropriate factor given in each diagram.

Figure 20 Wave Height Decay
Normalized to Sensor 16
Shot 2 Radial 1

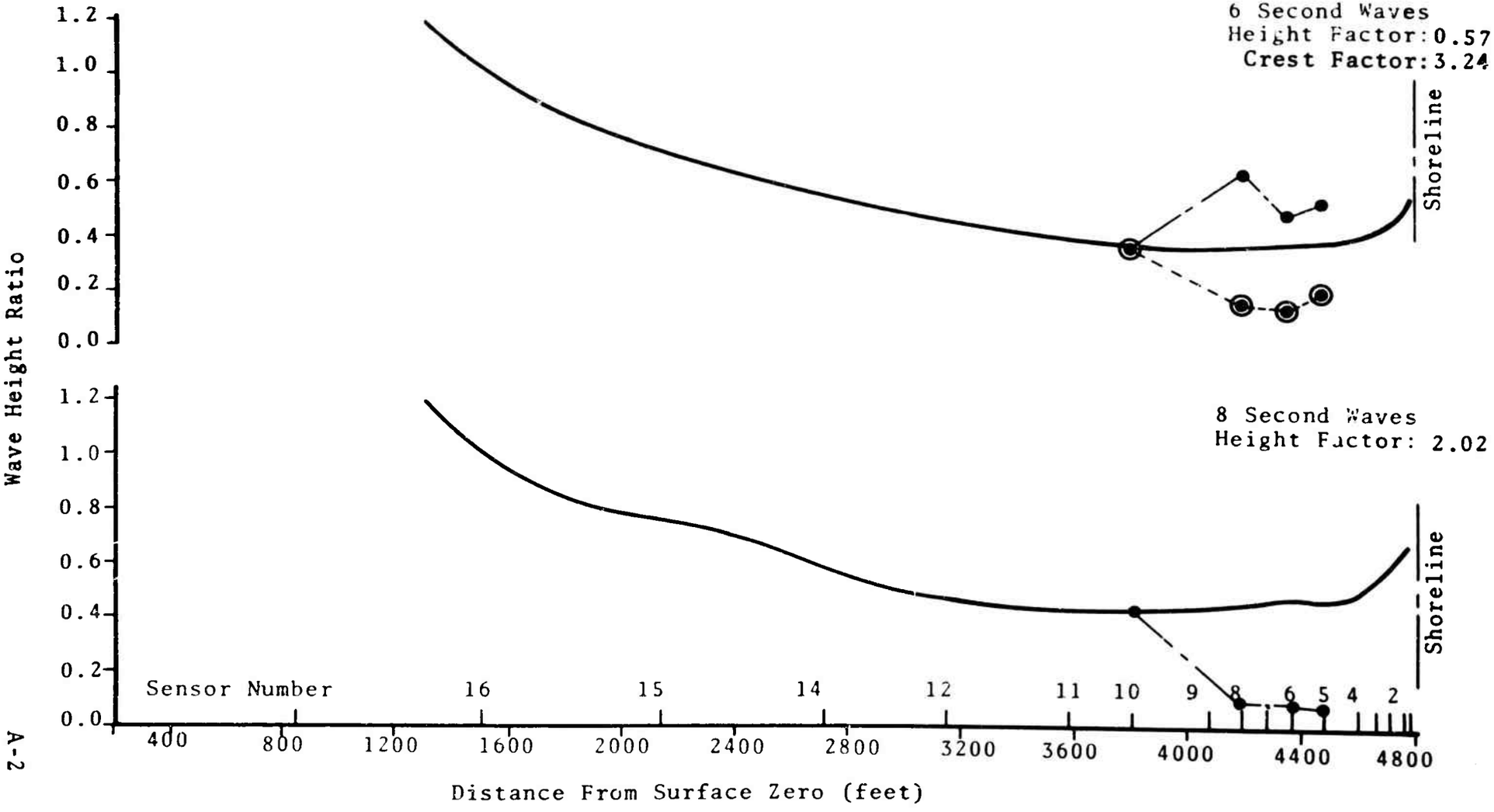

Figure 21 Wave Height Decay
Normalized to Sensor 16
Shot 3 Radial 1

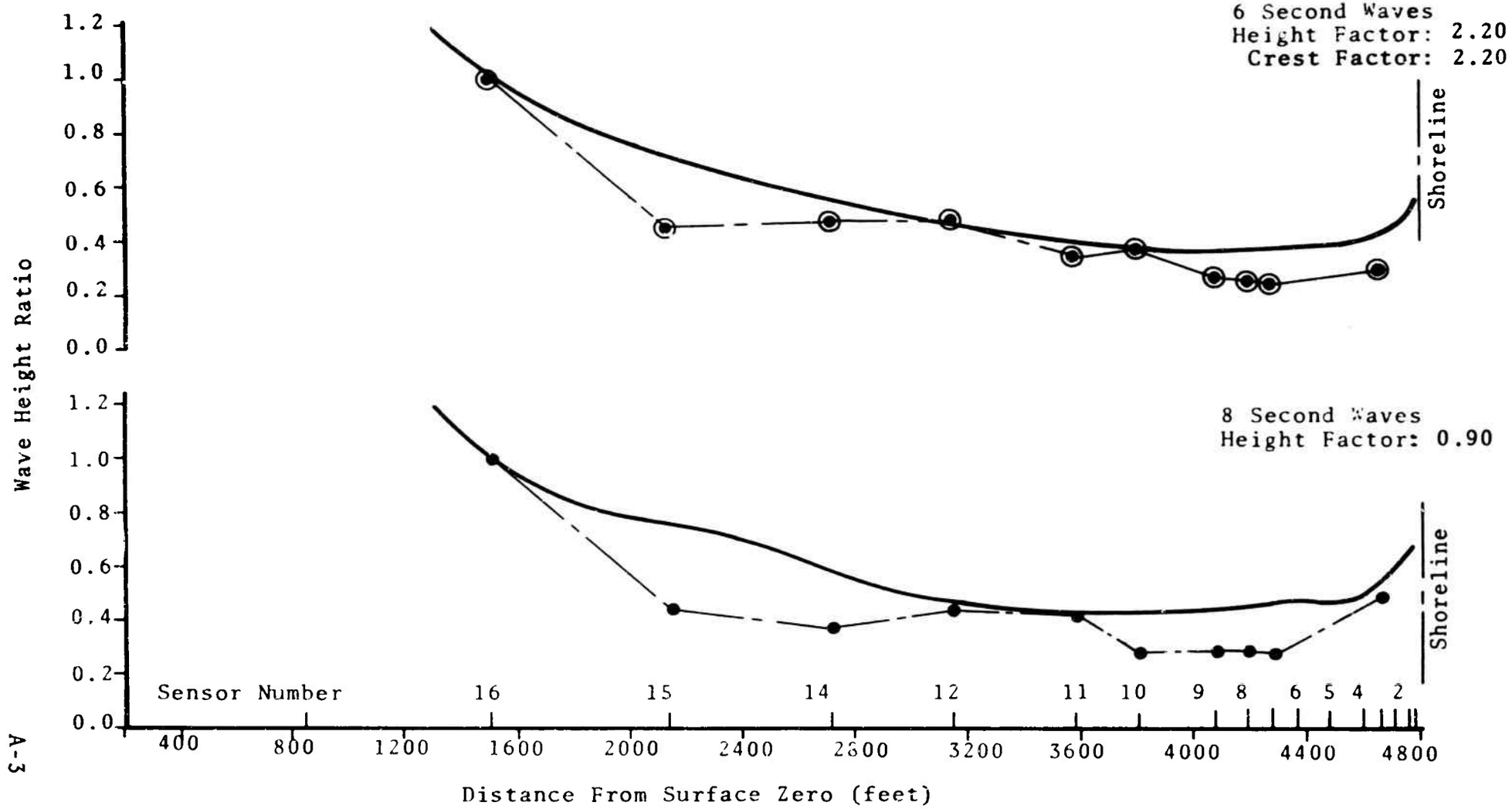

Figure 22 Wave Height Decay
Normalized to Sensor 16
Shot 4 Radial 1

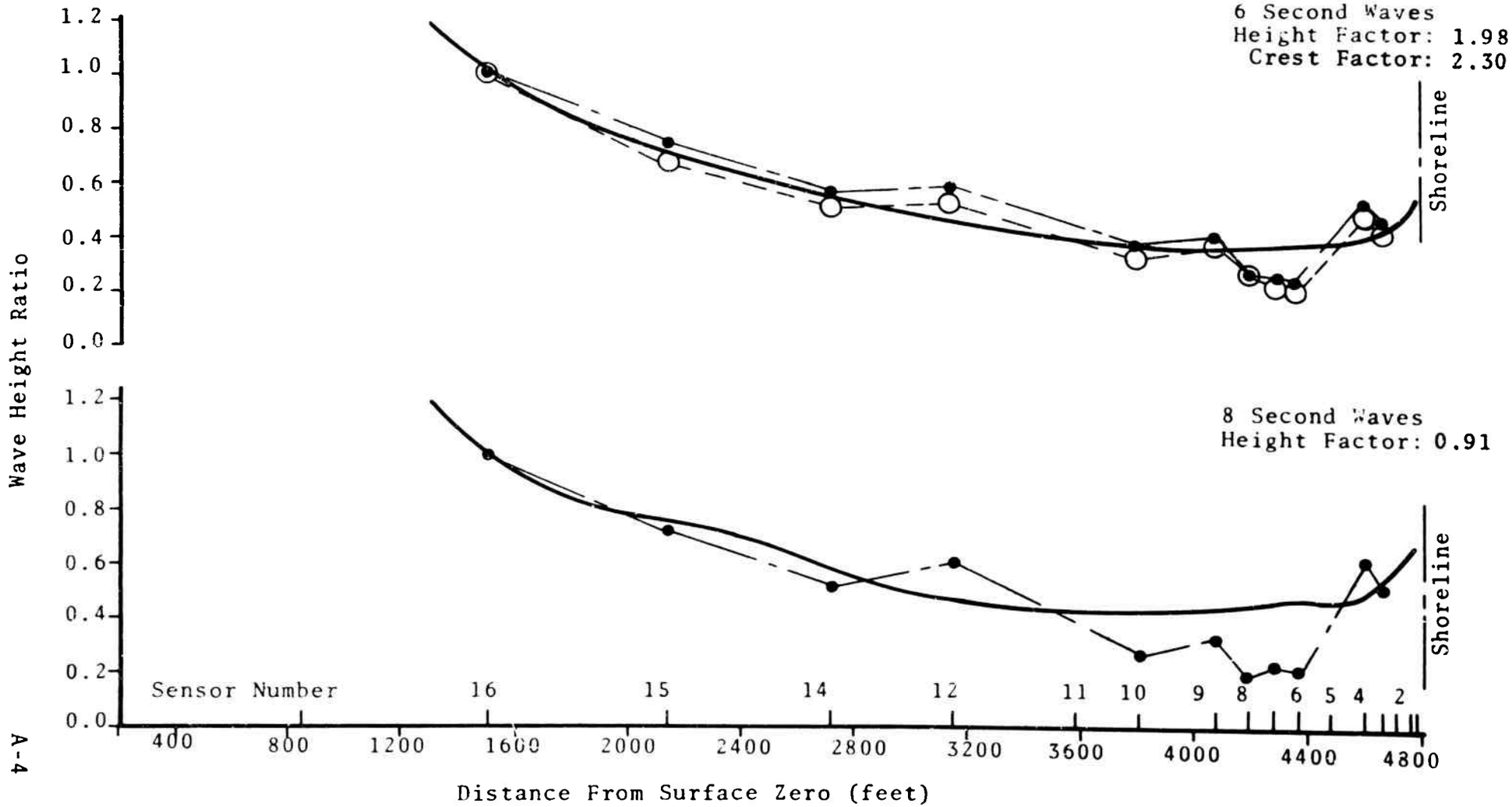

Figure 23 Wave Height Decay
Normalized to Sensor 16
Shot 5 Radial 1

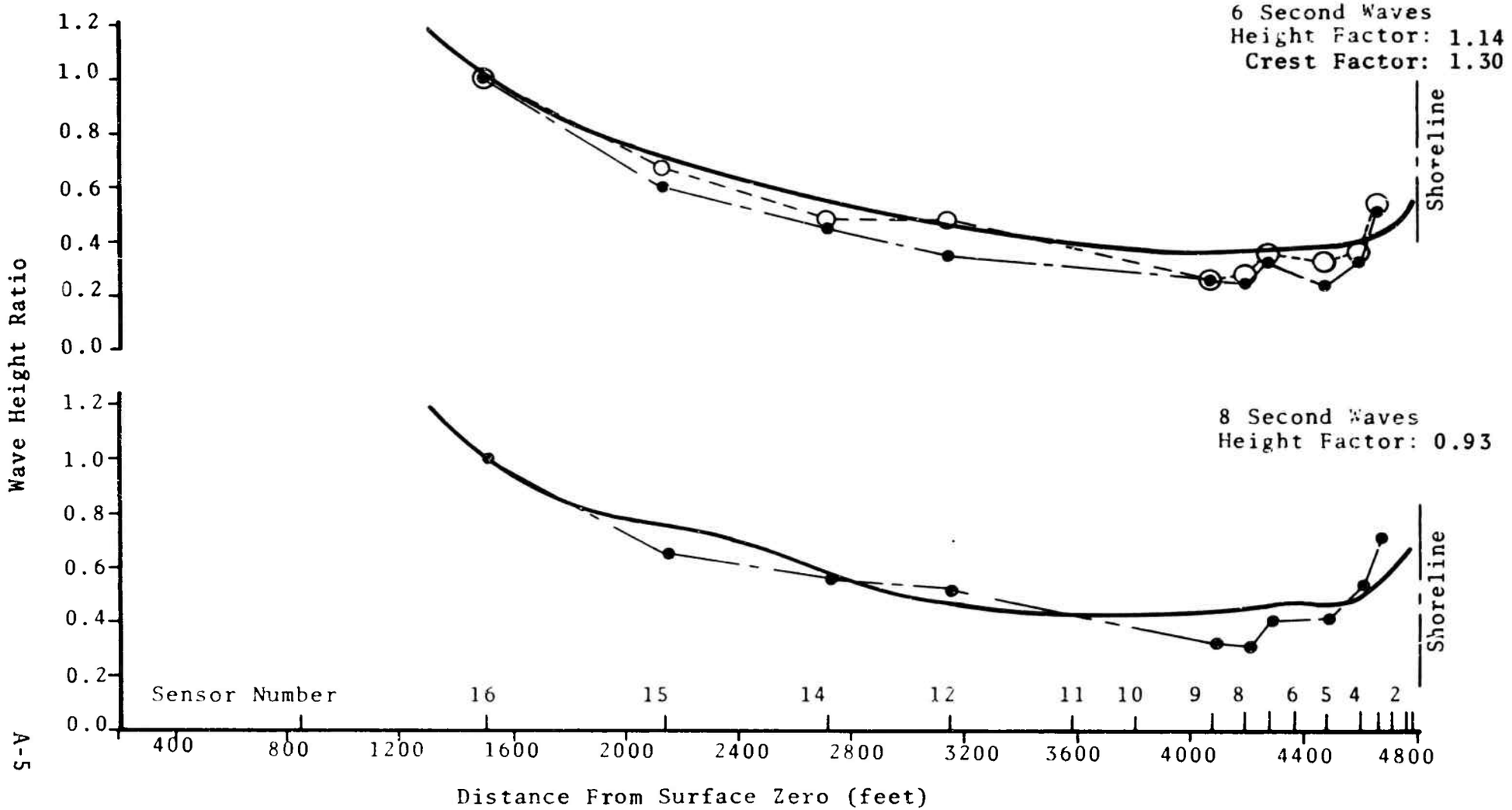

Figure 24 Wave Height Decay
Normalized to Sensor 16
Shot 6 Radial 1

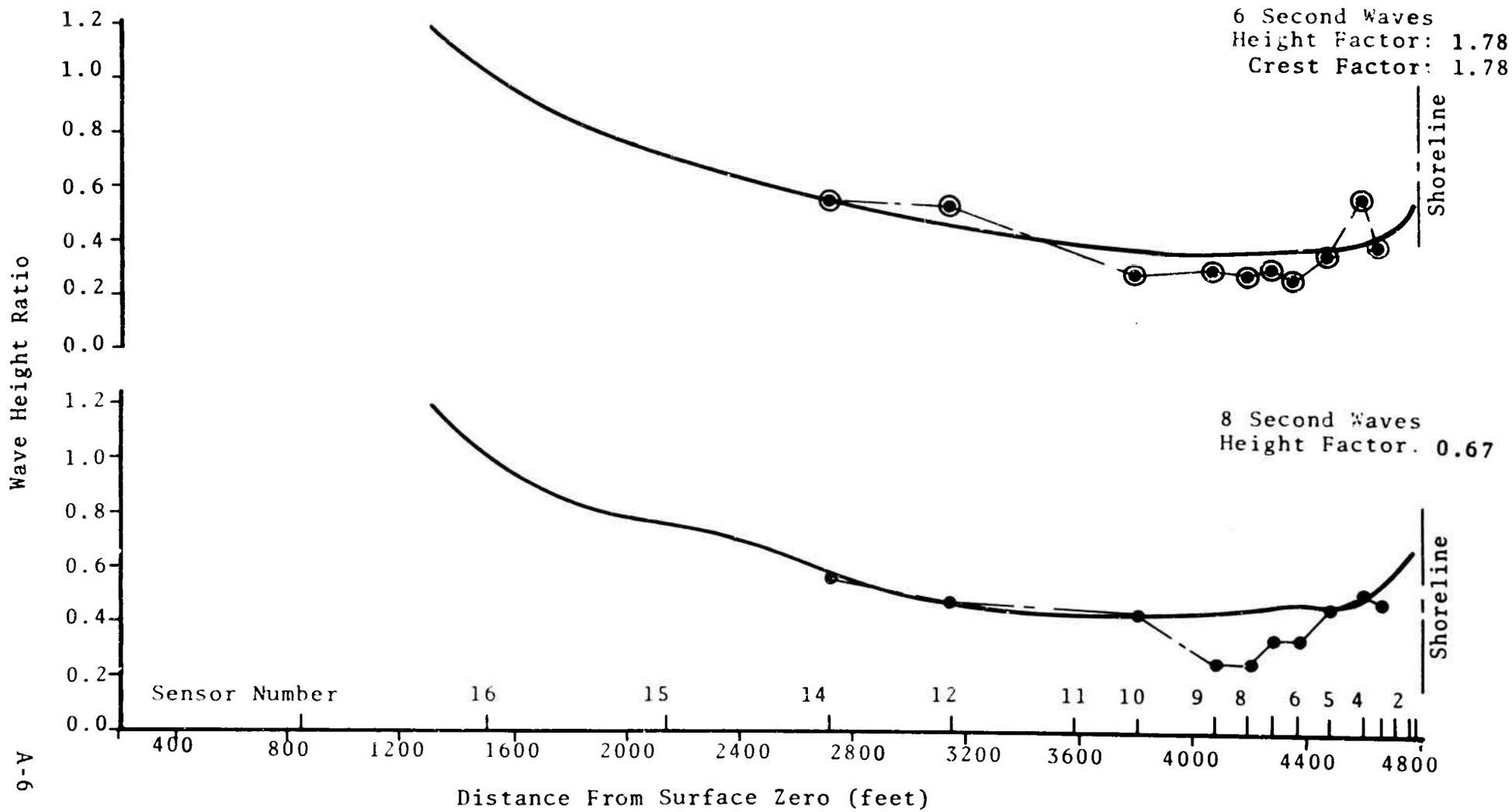

Figure 25 Wave Height Decay
Normalized to Sensor 16
Shot 7 Radial 1

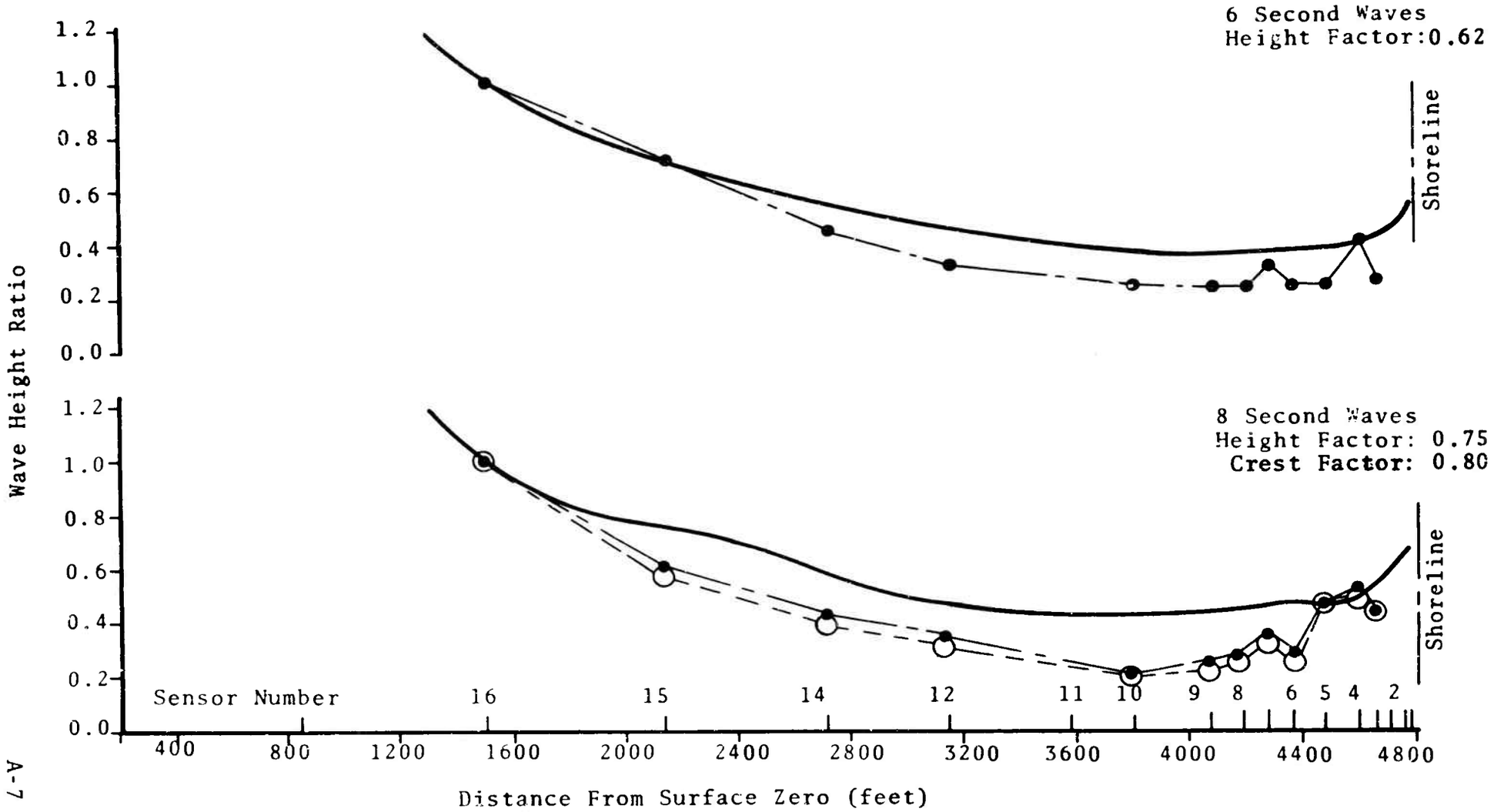

Figure 26 Wave Height Decay
Normalized to Sensor 16
Shot 8 Radial 1

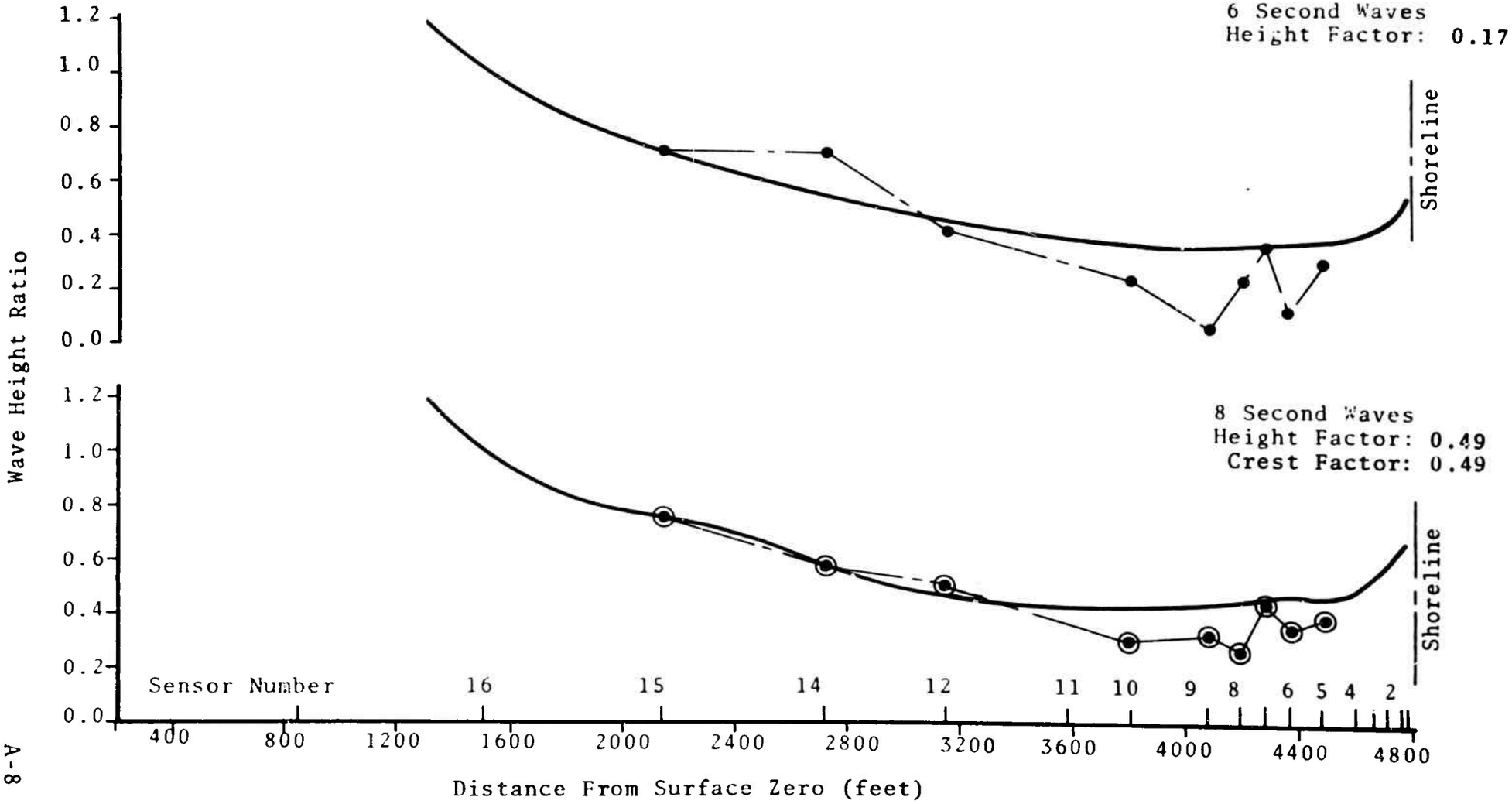

Figure 27 Wave Height Decay
Normalized to Sensor 16
Shot 9 Radial 1

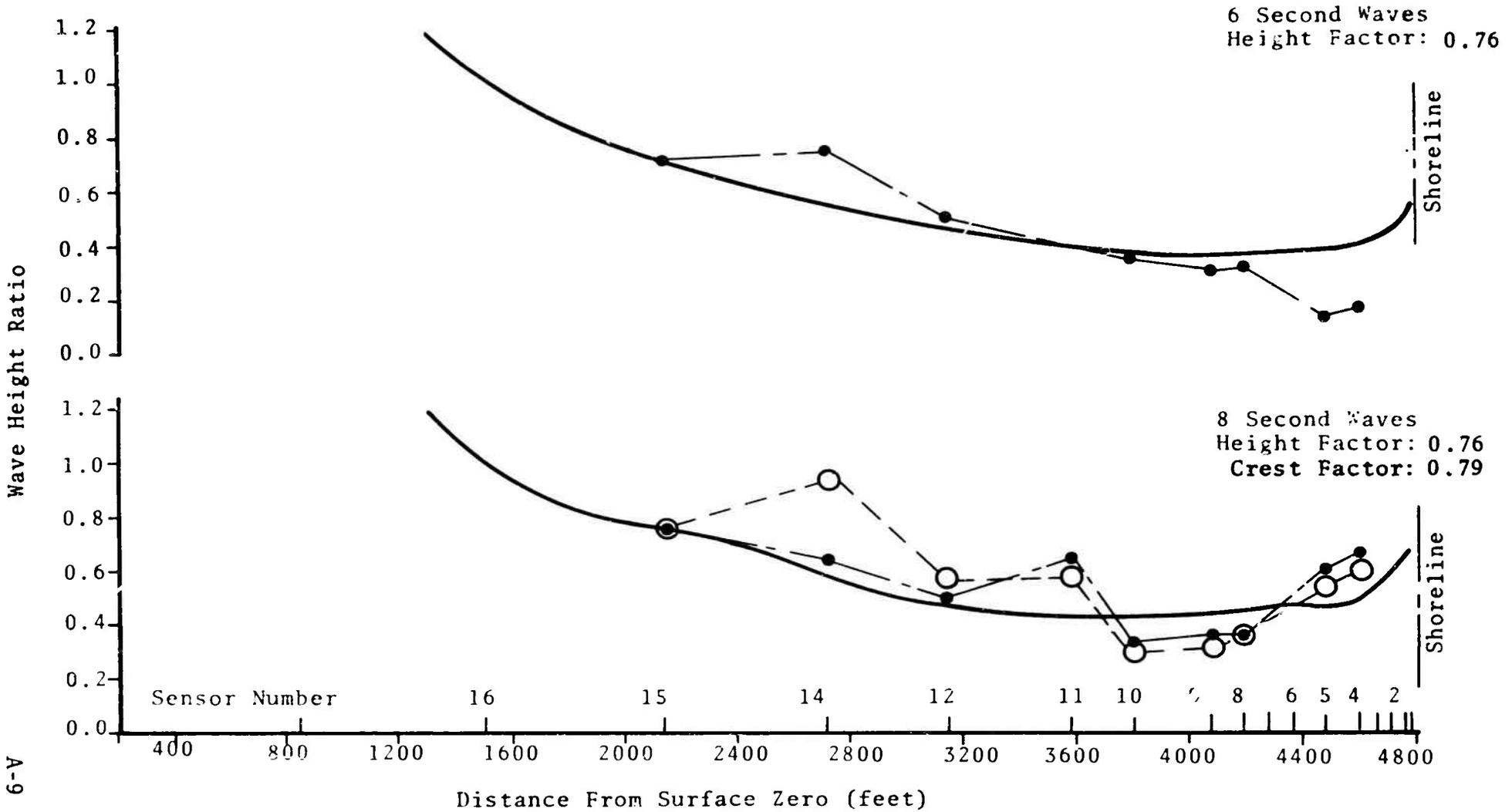

Figure 28 Wave Height Decay
Normalized to Sensor 12
Shot 2 Radial 2

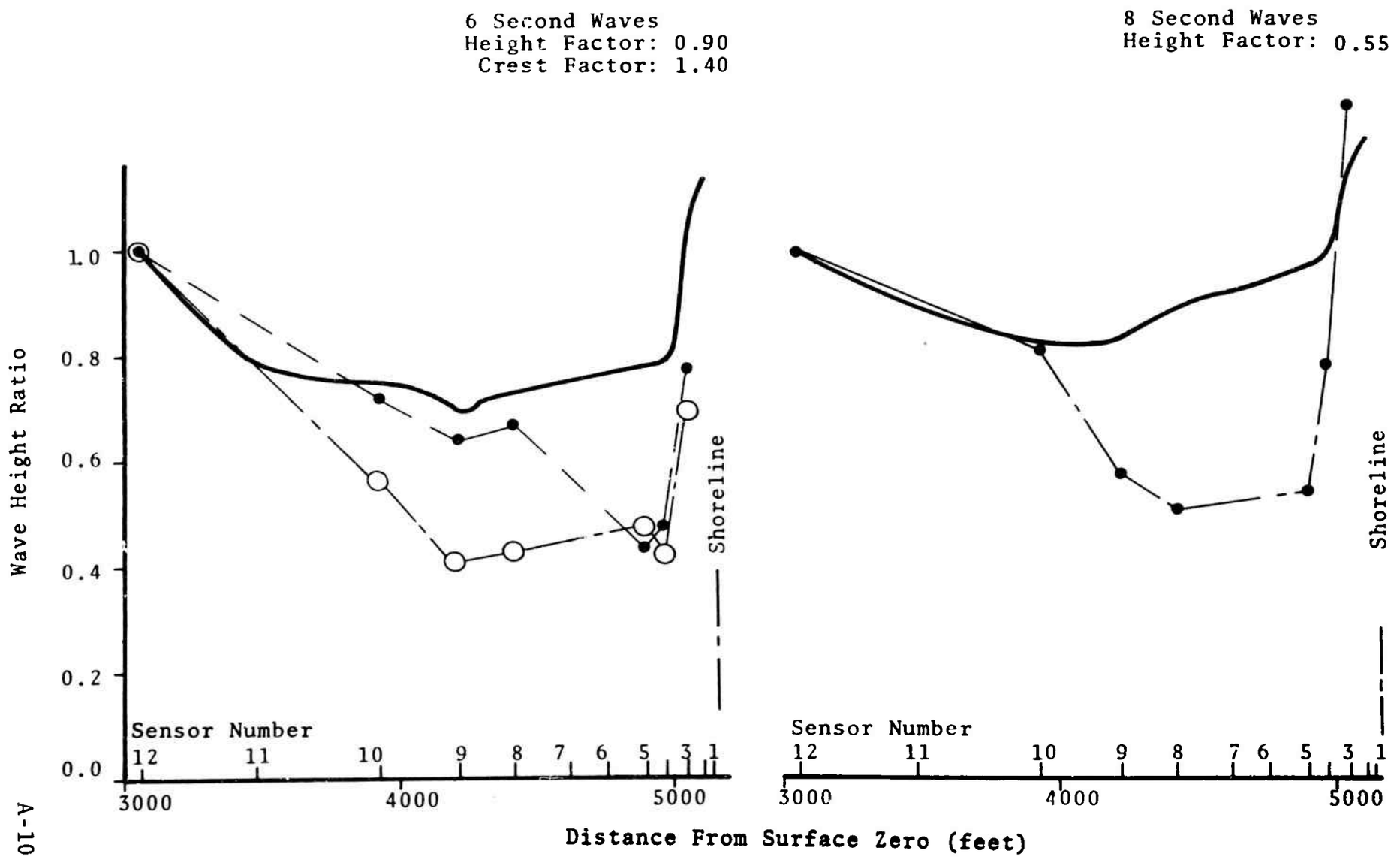

Figure 29 Wave Height Decay
Normalized to Sensor 12
Shot 3 Radial 2

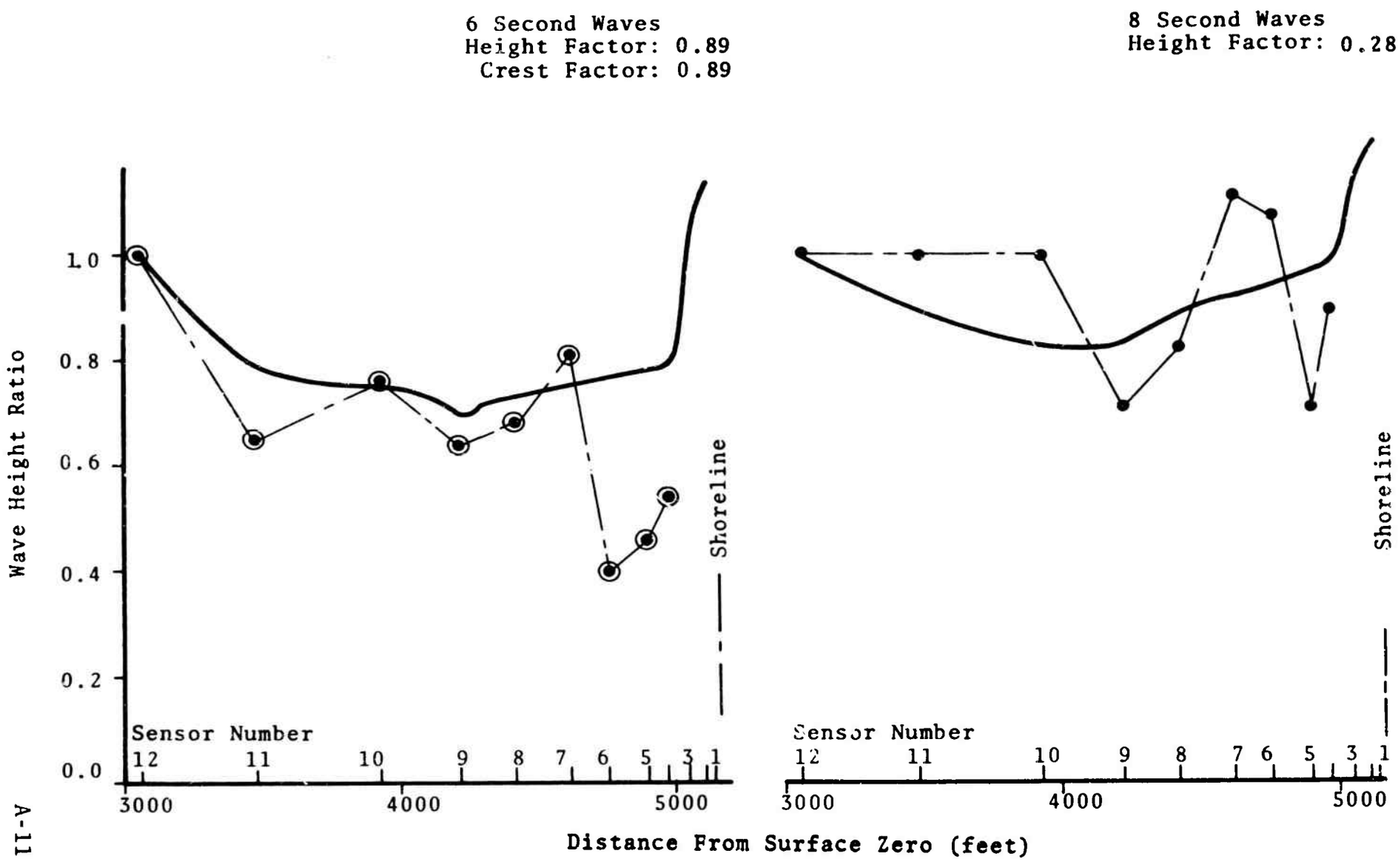

Figure 30 Wave Height Decay
Normalized to Sensor 12
Shot 4 Radial 2

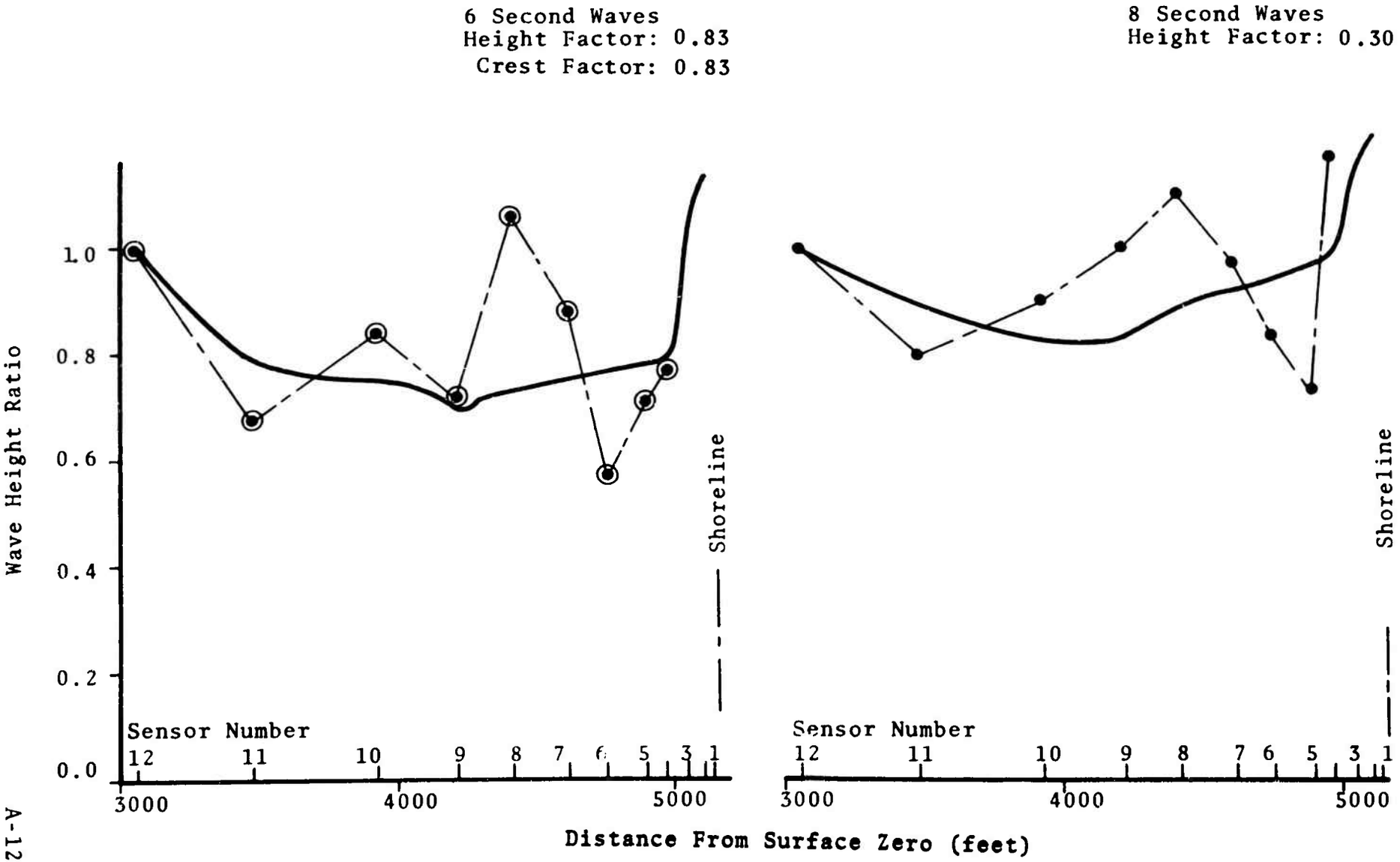

Figure 31 Wave Height Decay
Normalized to Sensor 12
Shot 5 Radial 2

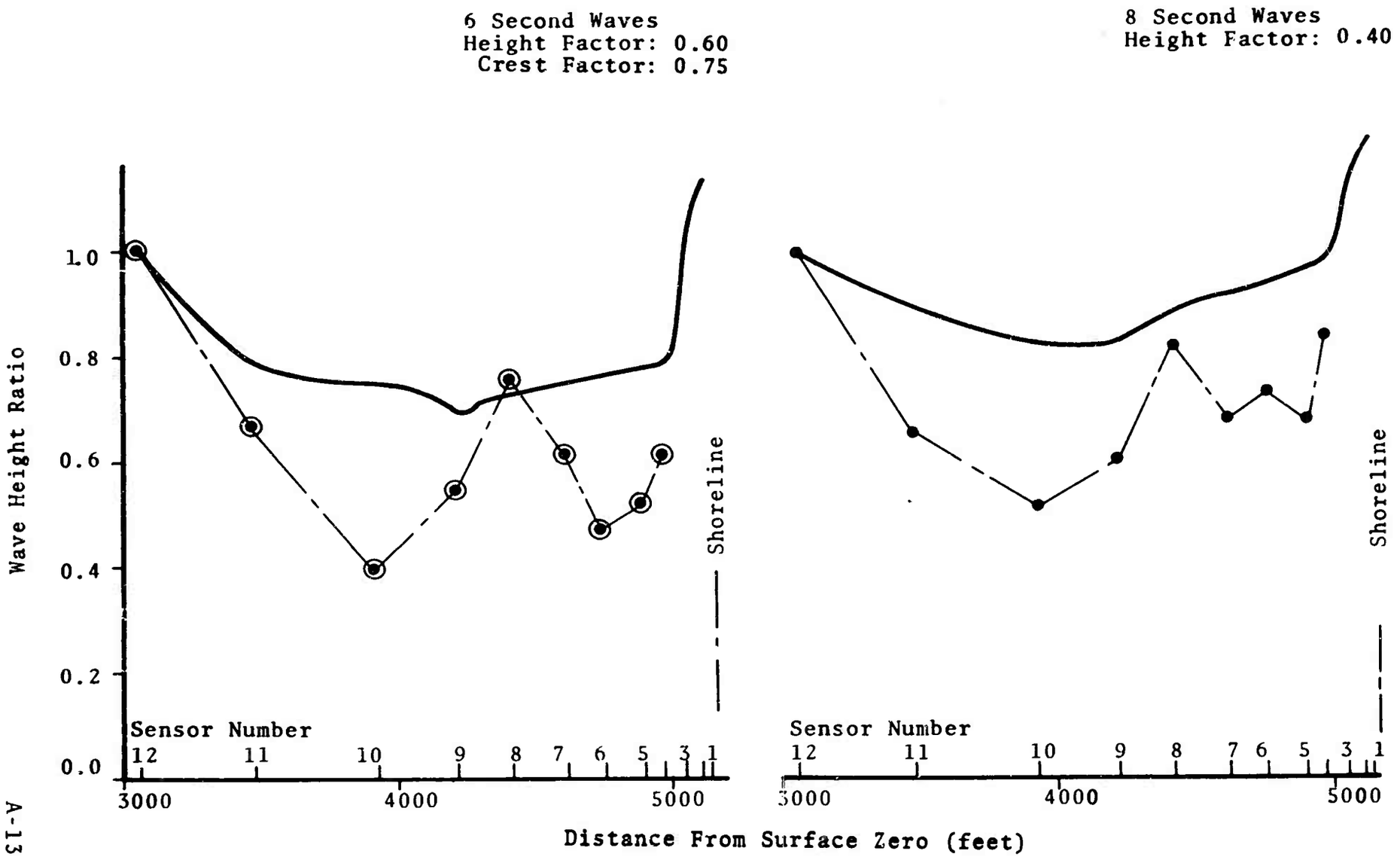

Figure 32 Wave Height Decay
Normalized to Sensor 12
Shot 6 Radial 2

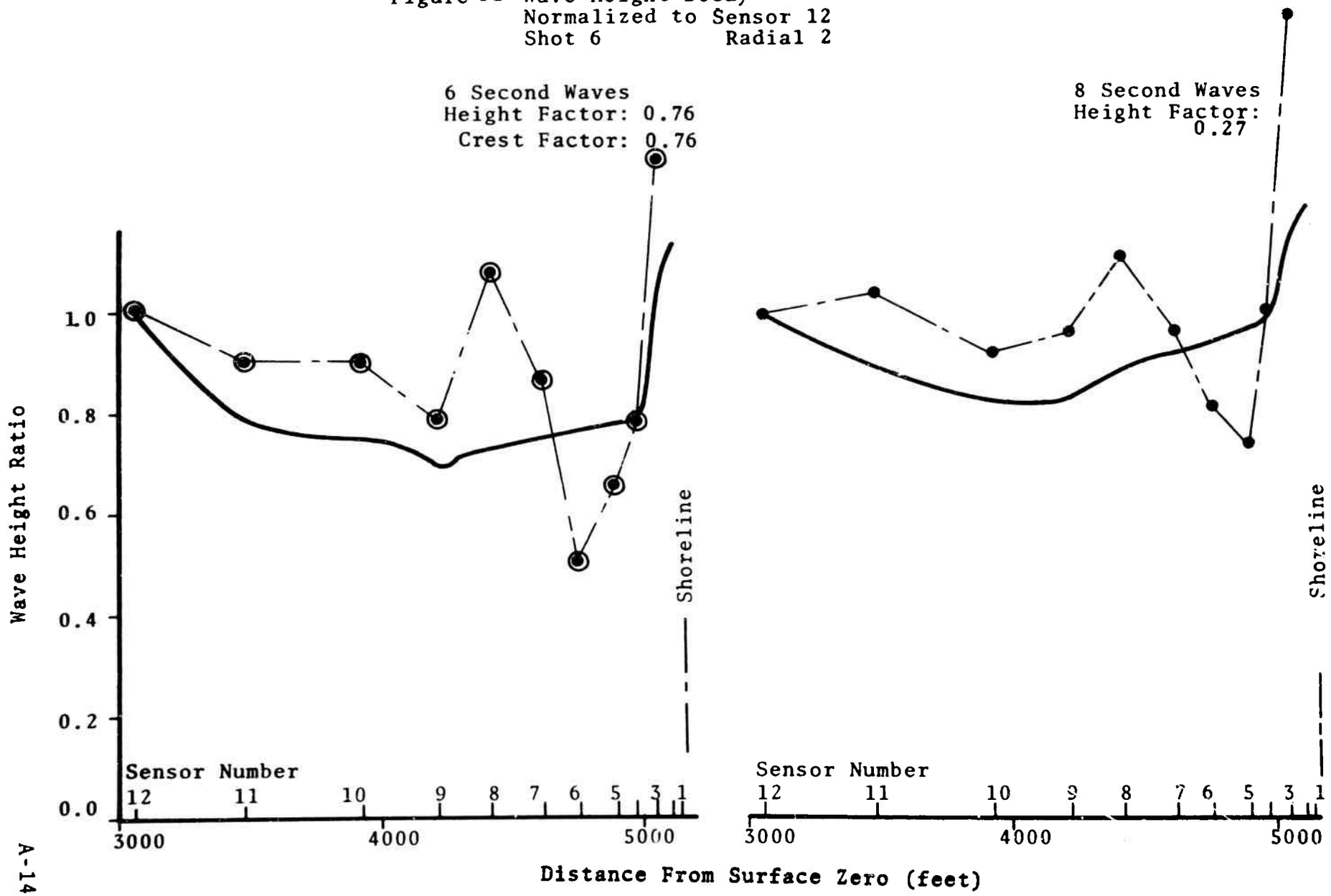

Figure 33 Wave Height Decay
Normalized to Sensor 12
Shot 7 Radial 2

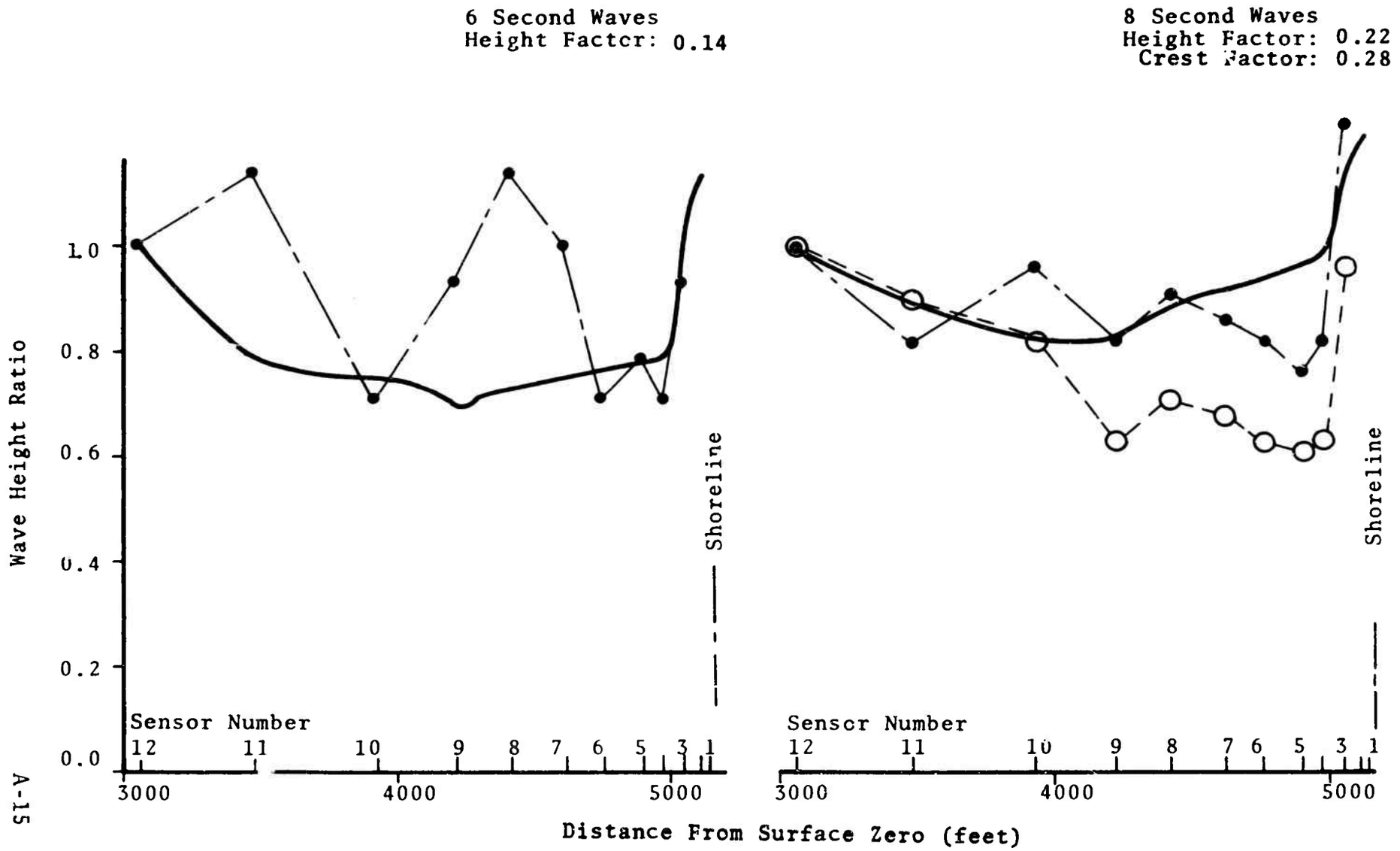

Figure 34 Wave Height Decay
Normalized to Sensor 12
Shot 8 Radial 2

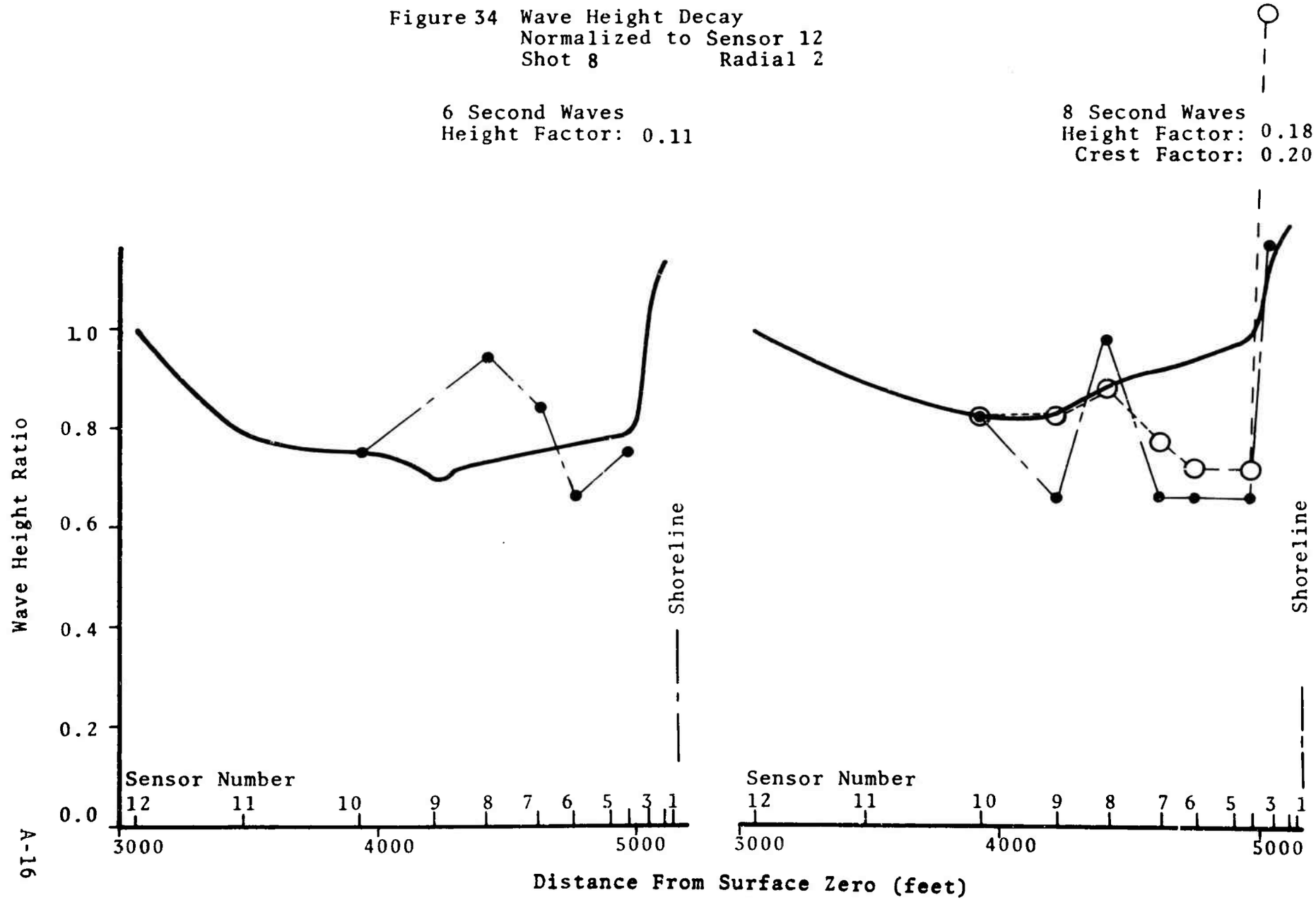

Figure 35 Wave Height Decay
Normalized to Sensor 12
Shot 9 Radial 2

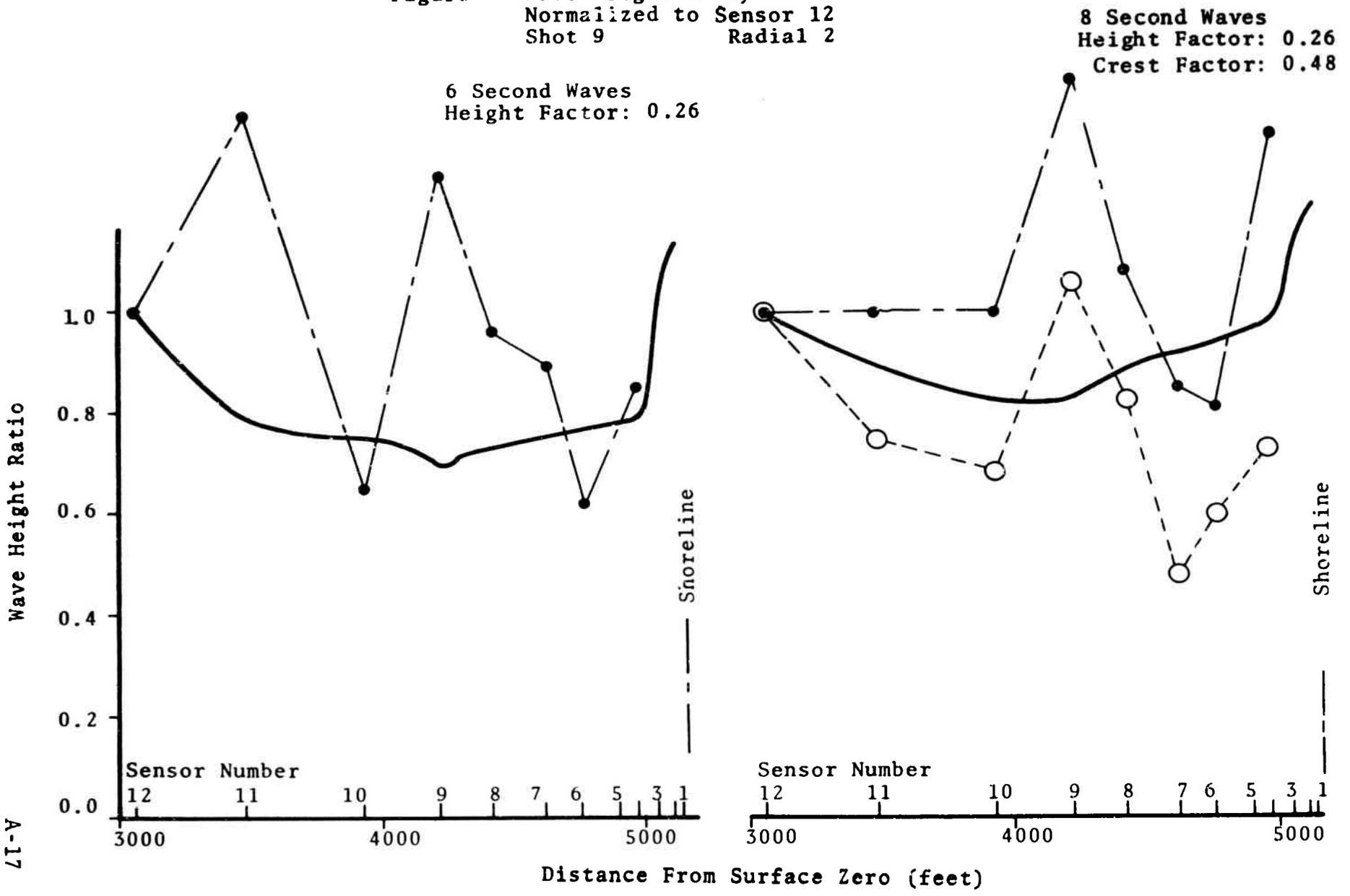

Figure 36 Wave Height Decay
Normalized to Sensor 12
Shot 10 Radial 2

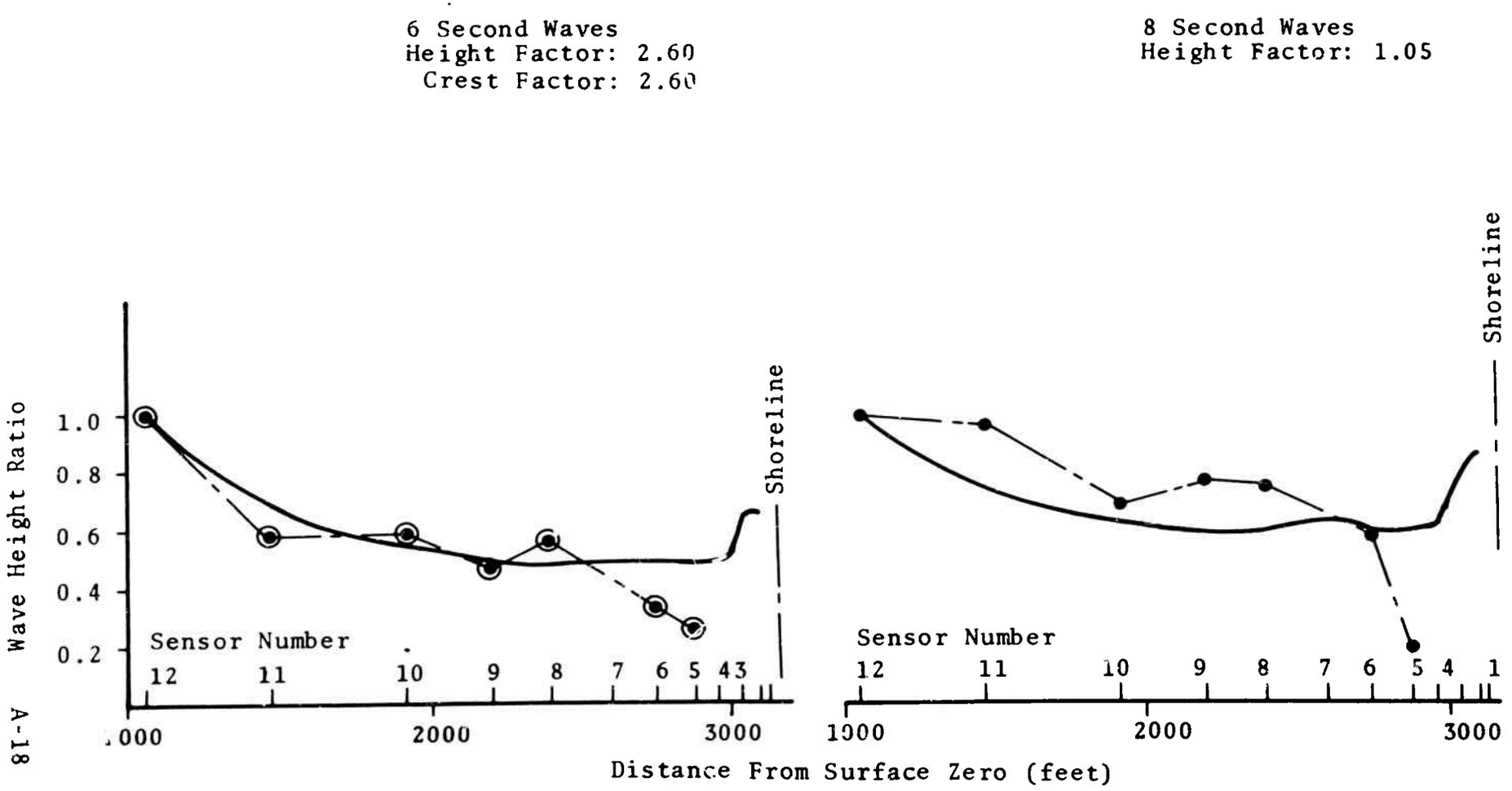

Figure 37 Wave Height Decay
Normalized to Sensor 14
Shot 2 Radial 3

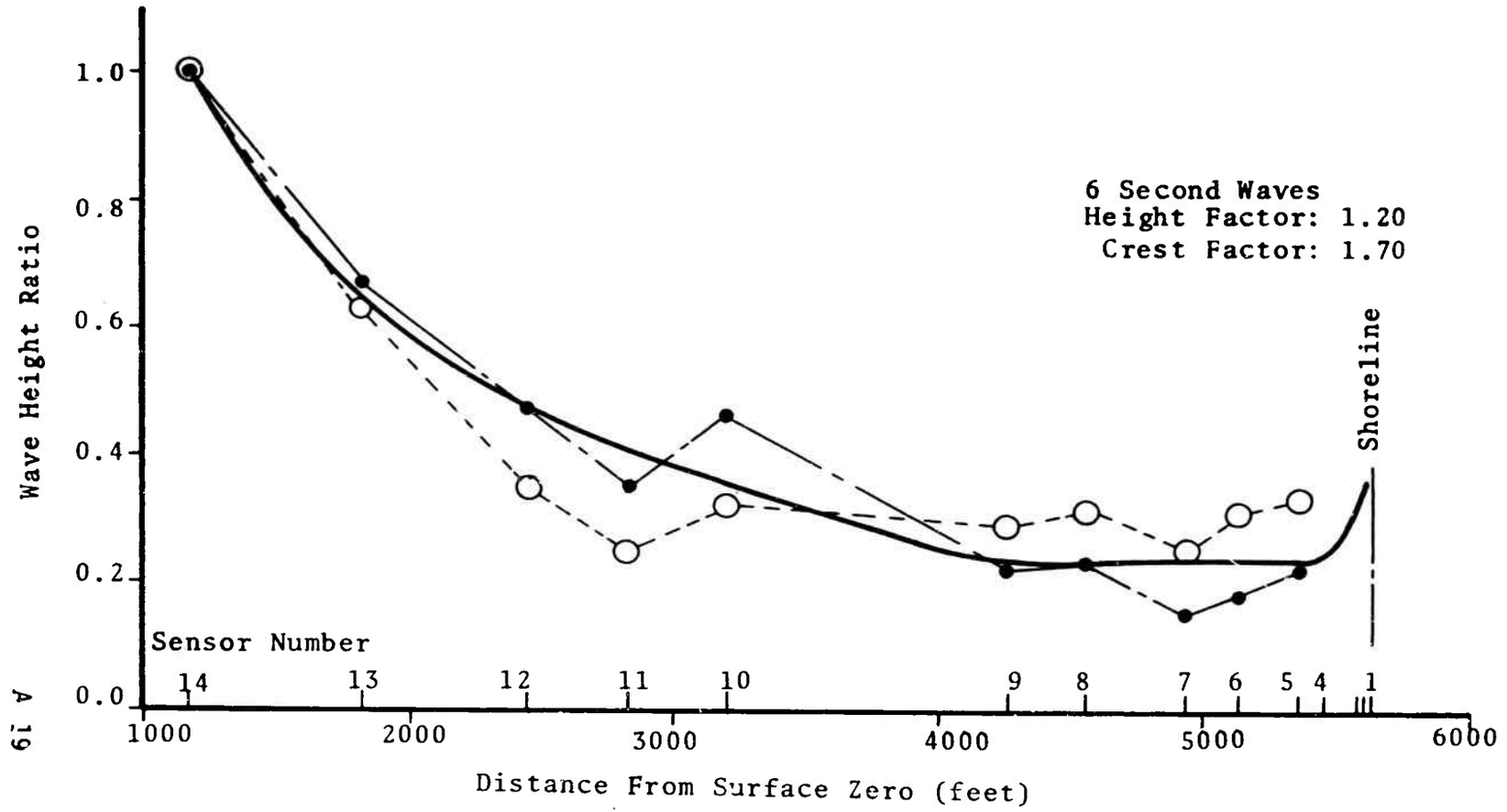

Figure 38 Wave Height Decay
Normalized to Sensor 14
Shot 2 Radial 3

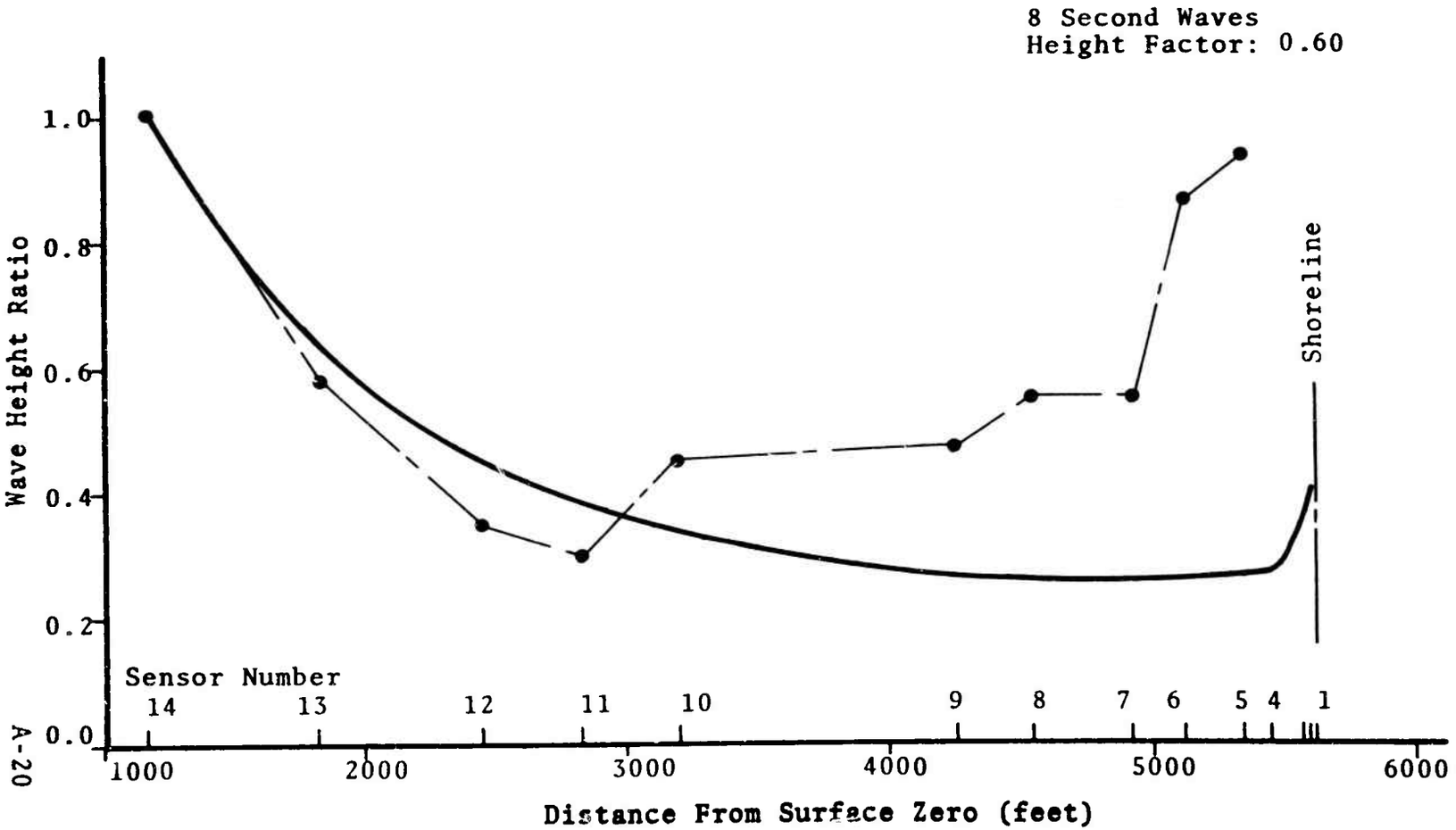

Figure 39 Wave Height Decay
Normalized to Sensor 14
Shot 3 Radial 3

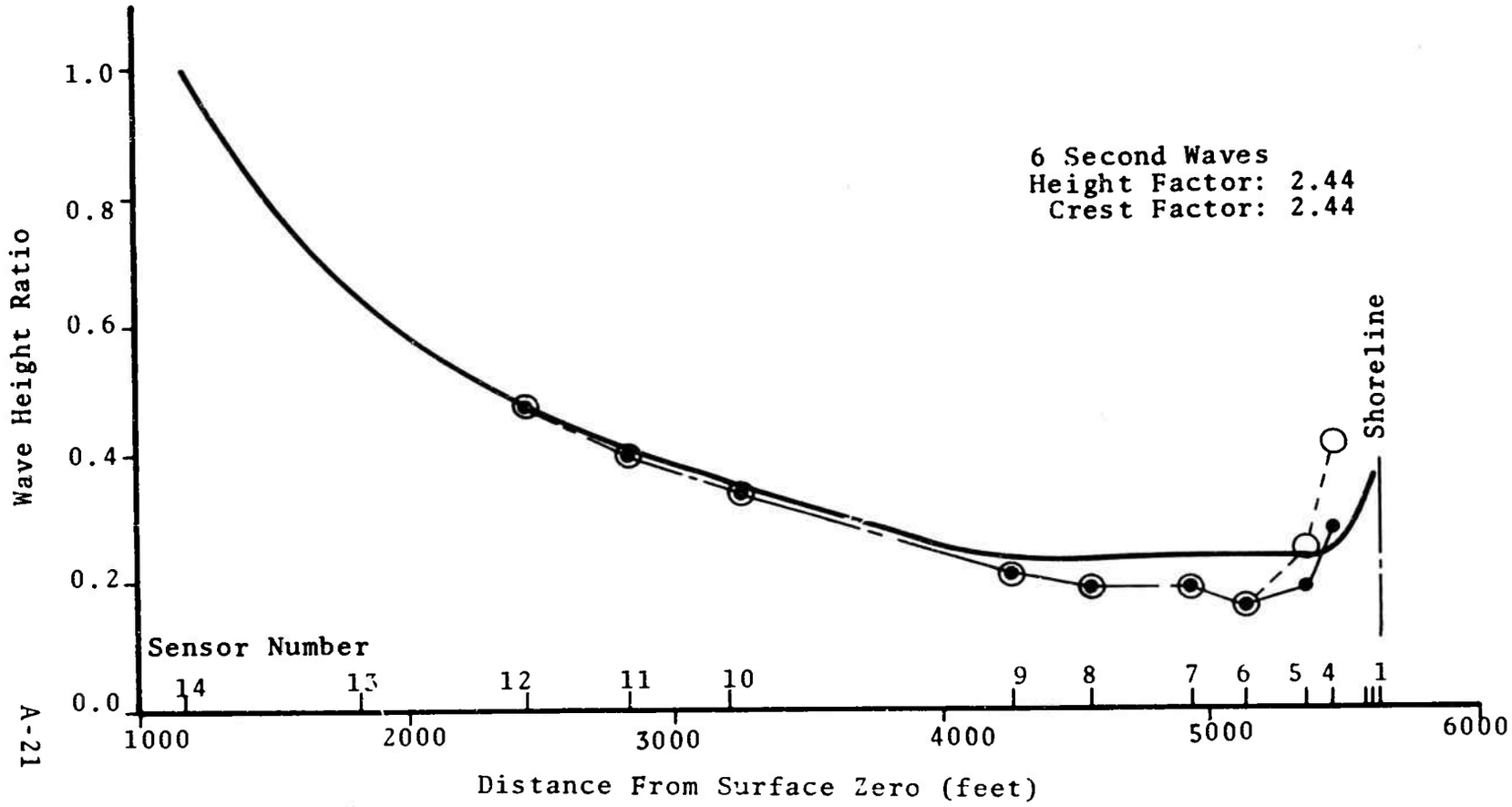

Figure 40 Wave Height Decay
Normalized to Sensor 14
Shot 3 Radial 3

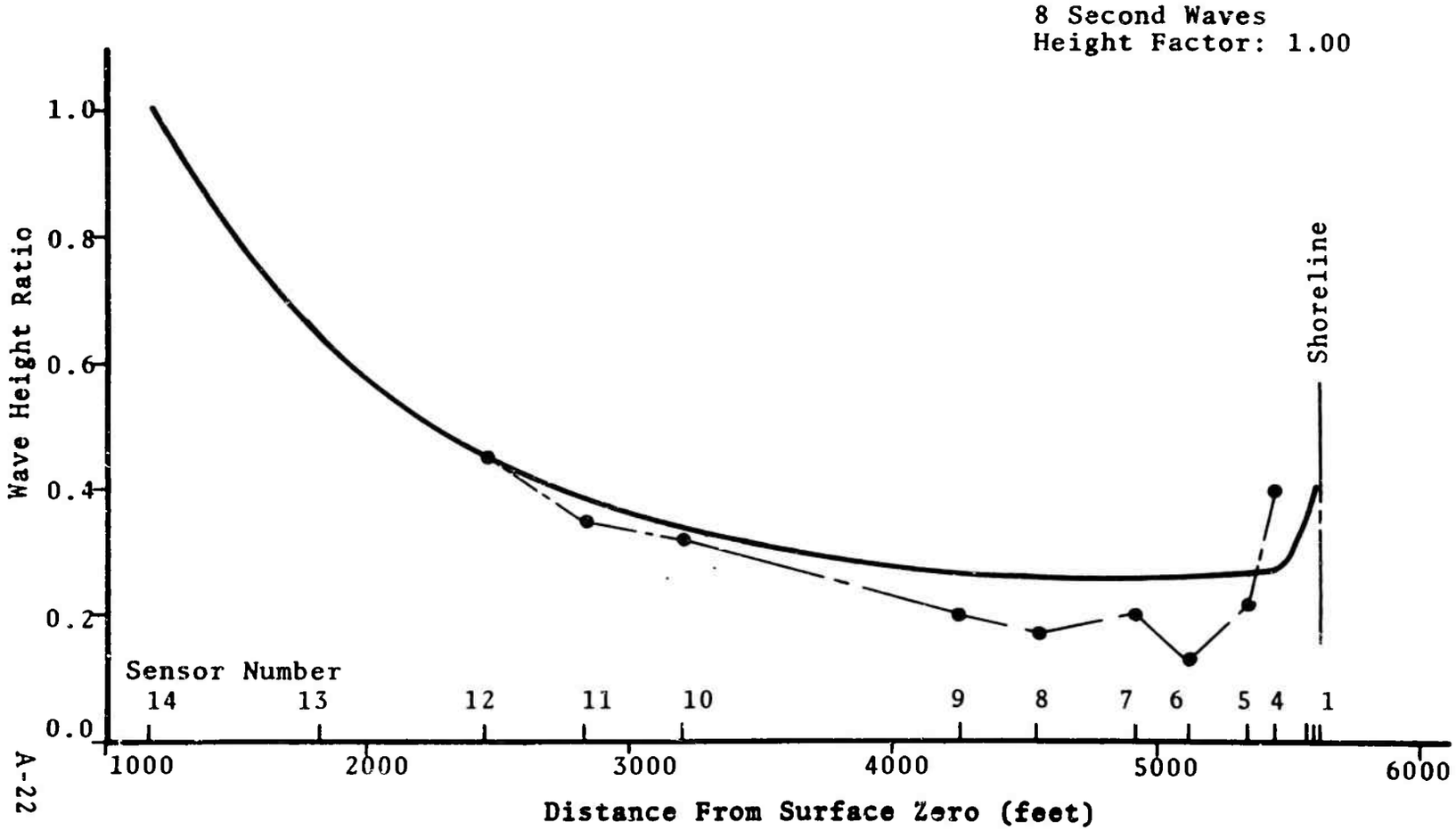

Figure 41 Wave Height Decay
Normalized to Sensor 14
Shot 4 Radial 3

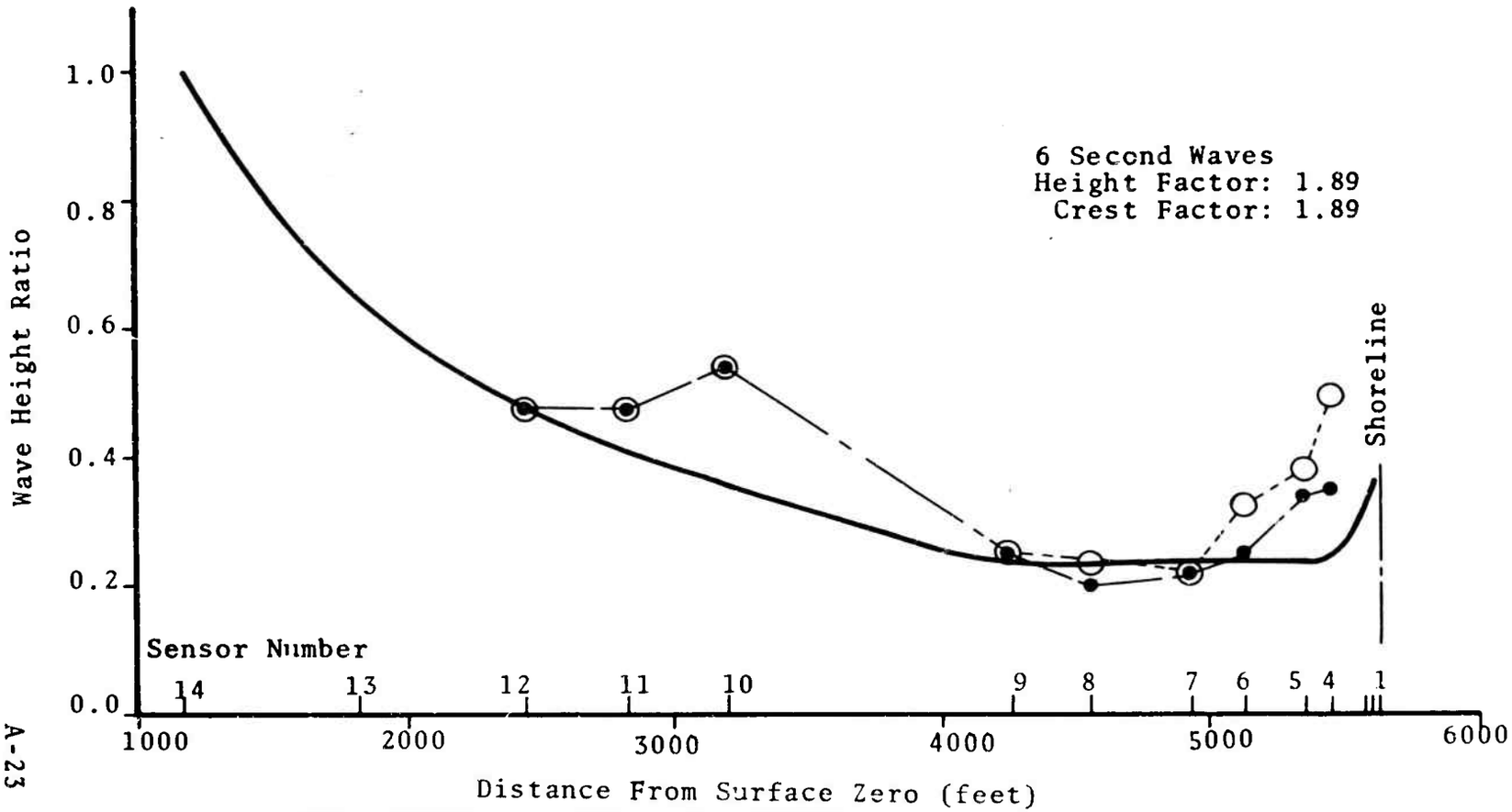

Figure 42 Wave Height Decay
Normalized to Sensor 14
Shot 4 Radial 3

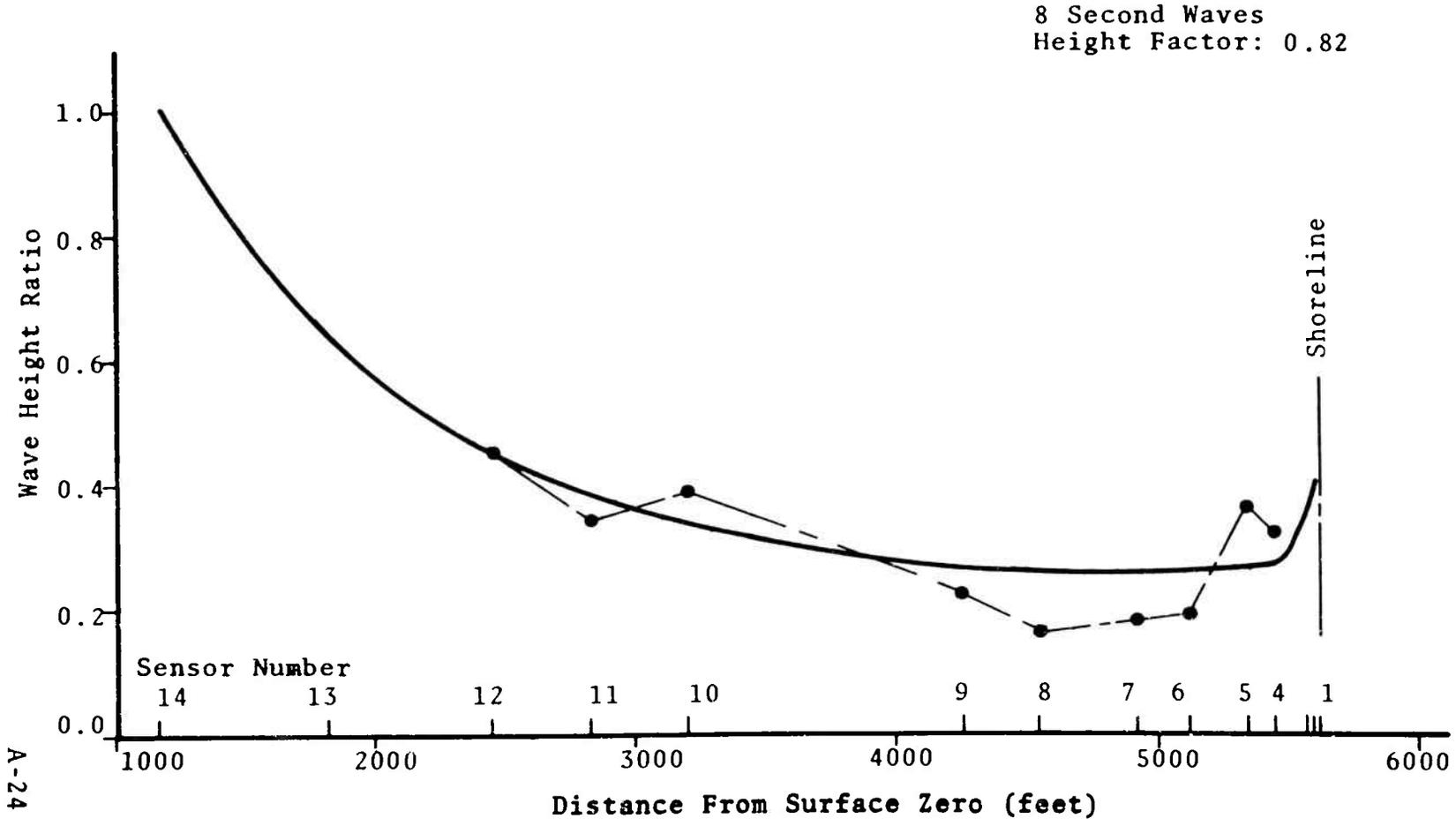

Figure 43 Wave Height Decay
Normalized to Sensor 14
Shot 5 Radial 3

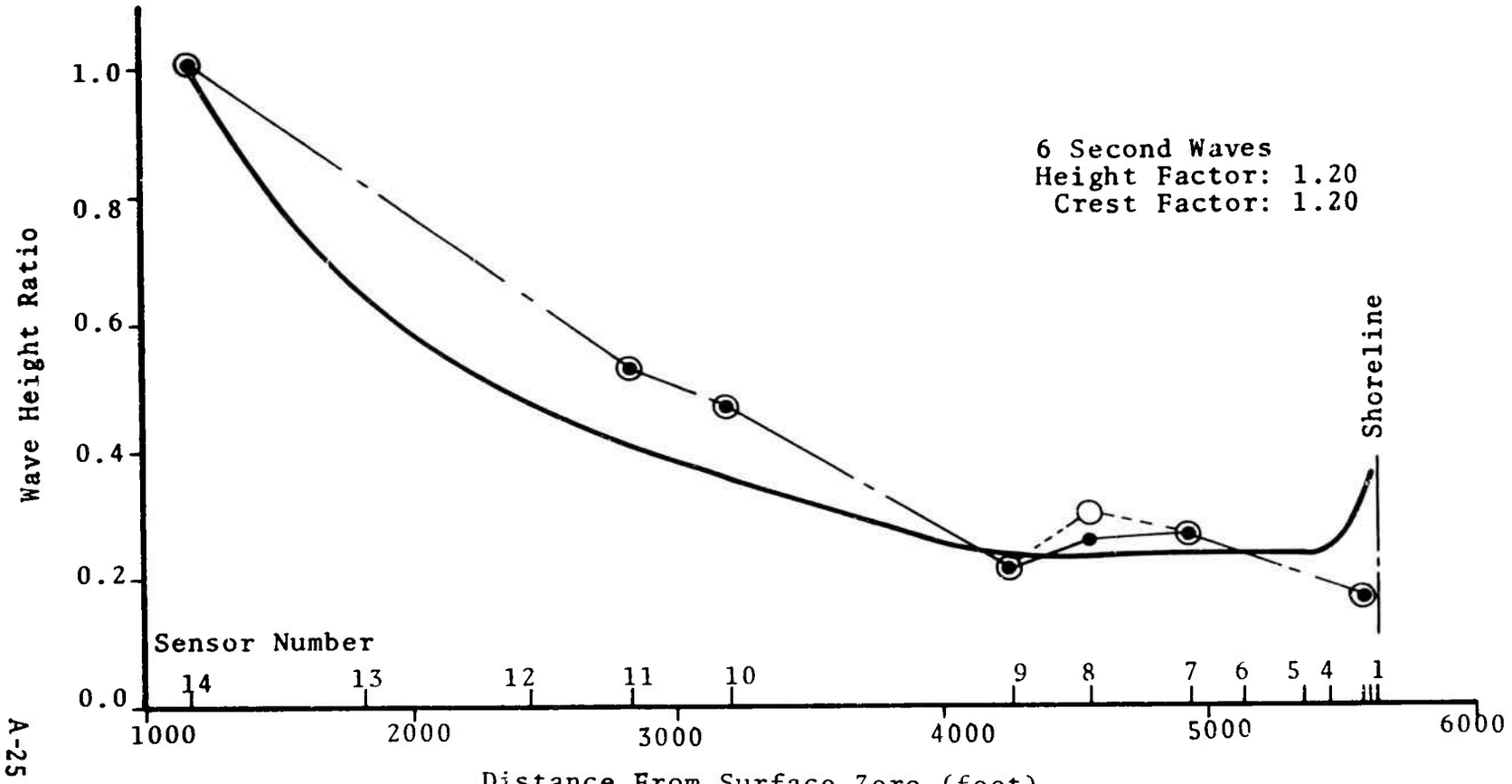

Figure 44 Wave Height Decay
Normalized to Sensor 14
Shot 5 Radial 3

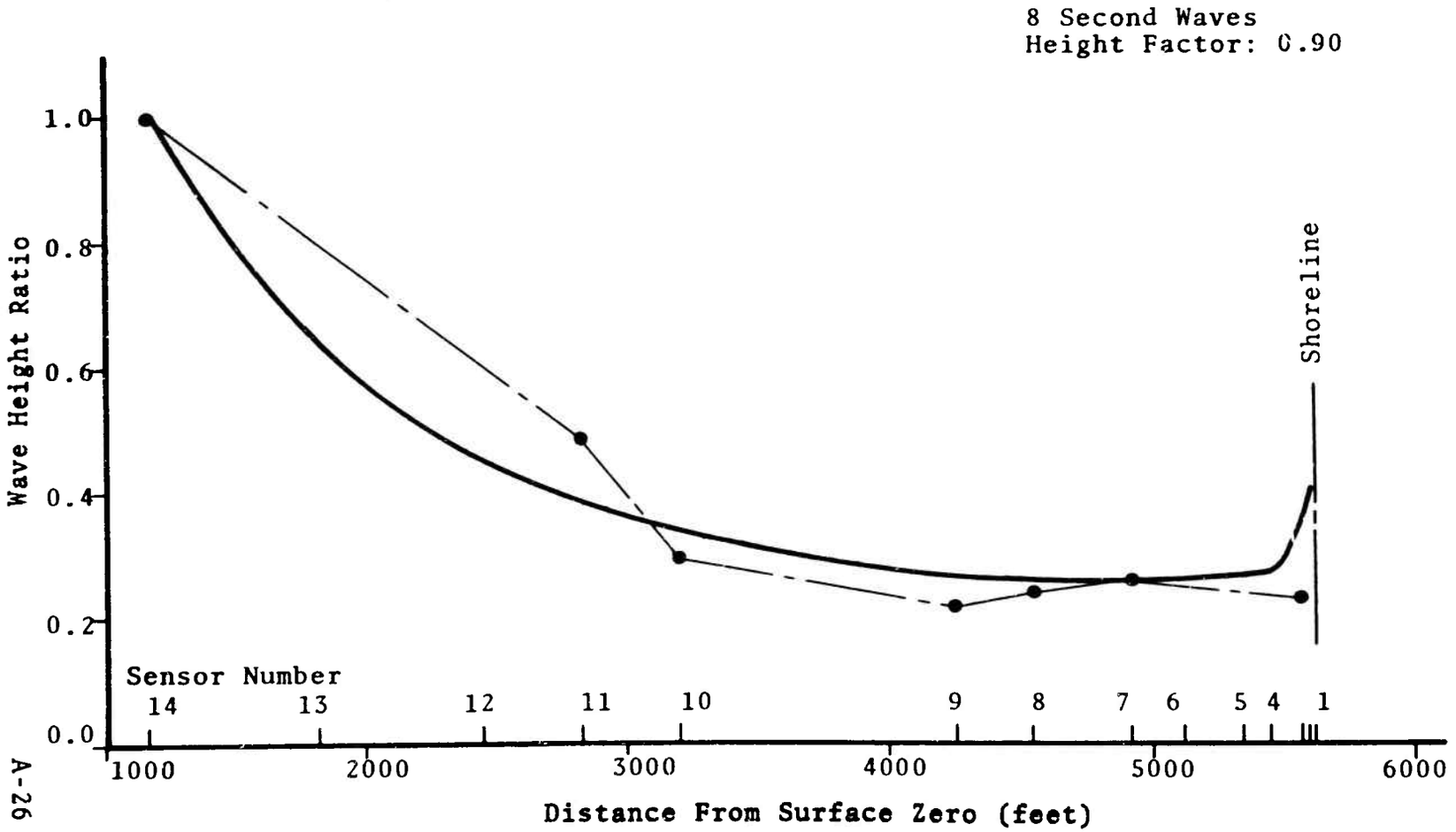

Figure 45 Wave Height Decay
Normalized to Sensor 14
Shot 6 Radial 3

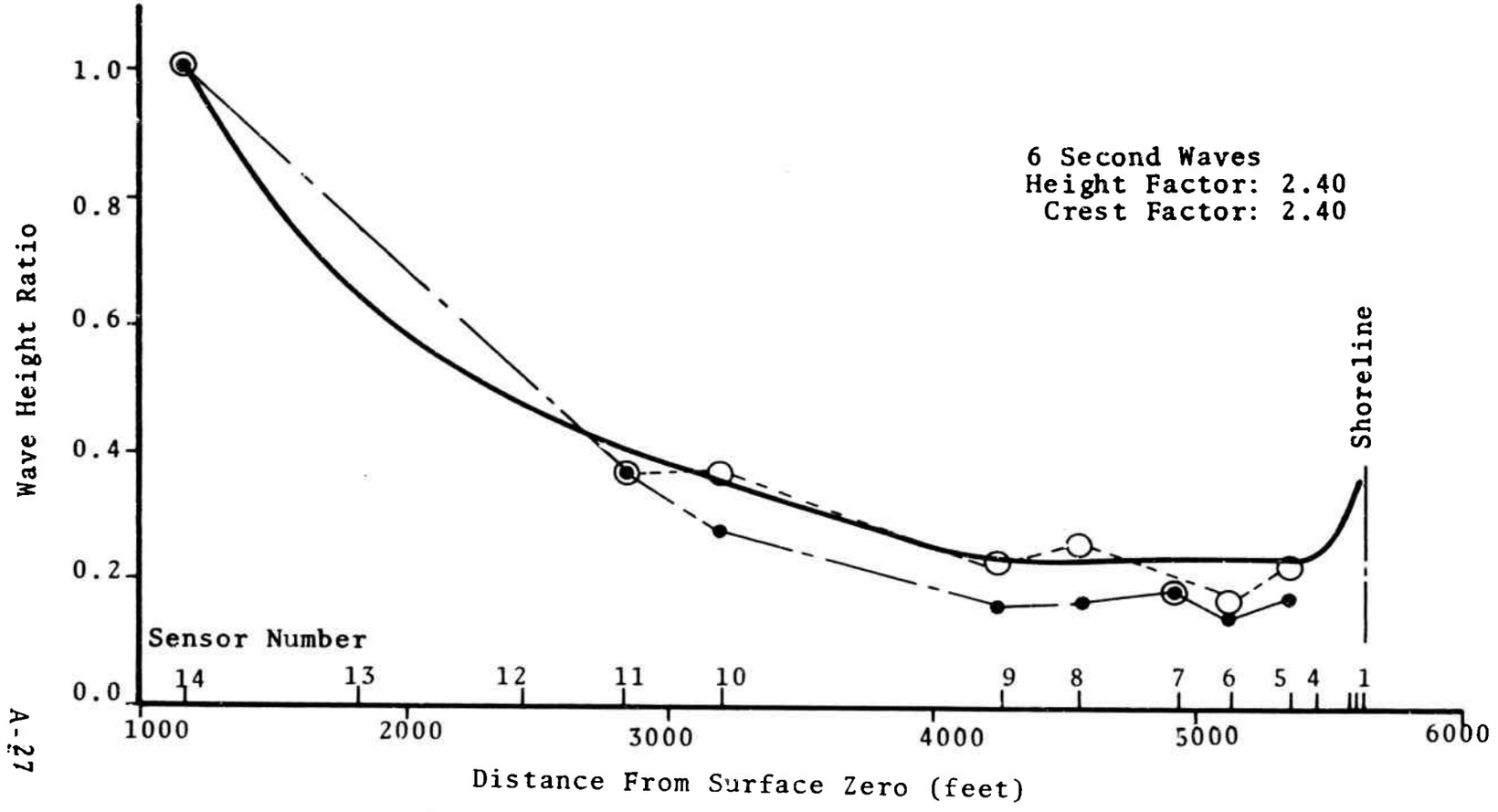

Figure 46 Wave Height Decay
Normalized to Sensor 14
Shot 6 Radial 3

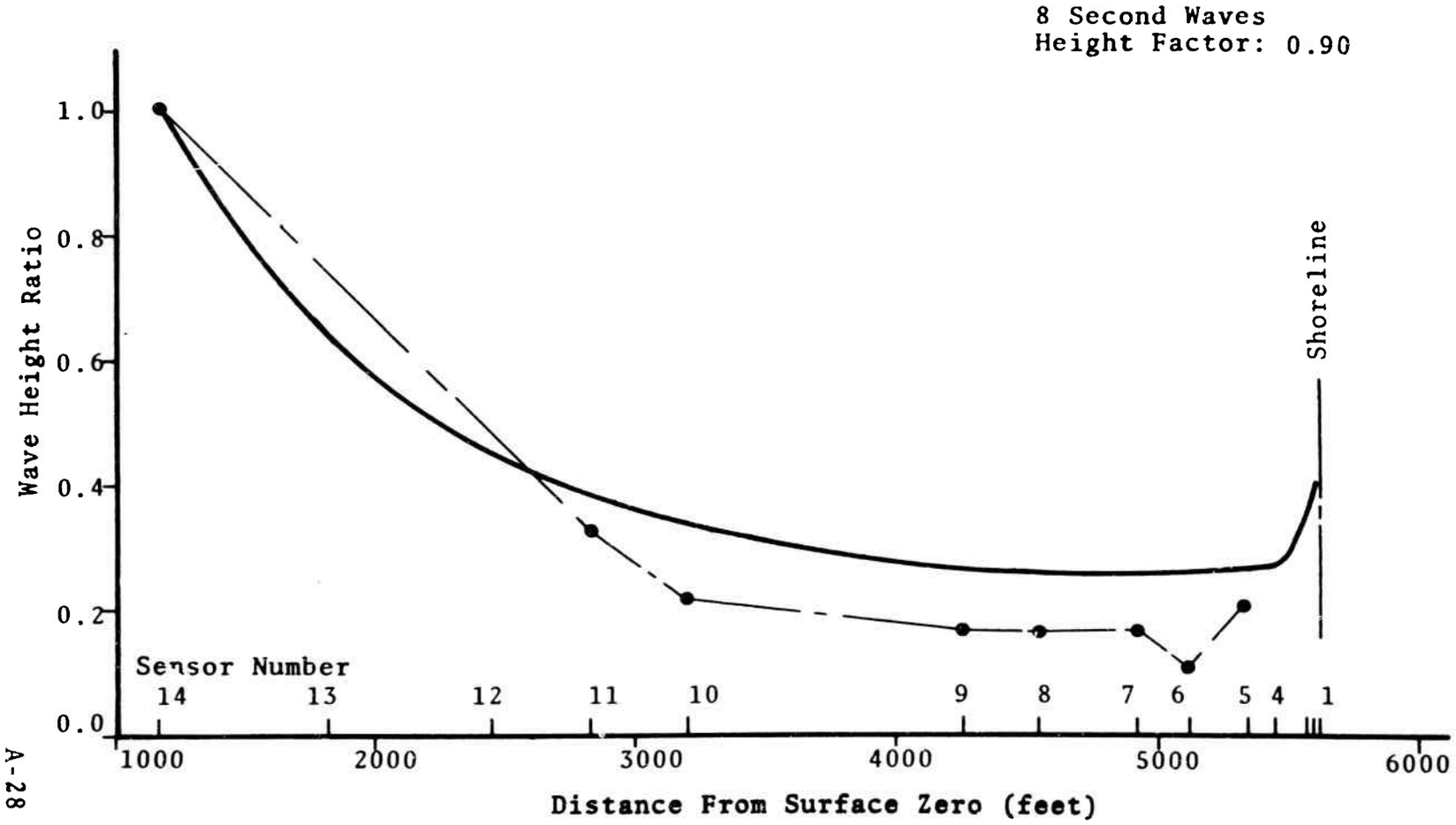

Figure 47 Wave Height Decay
Normalized to Sensor 14
Shot 7 Radial 3

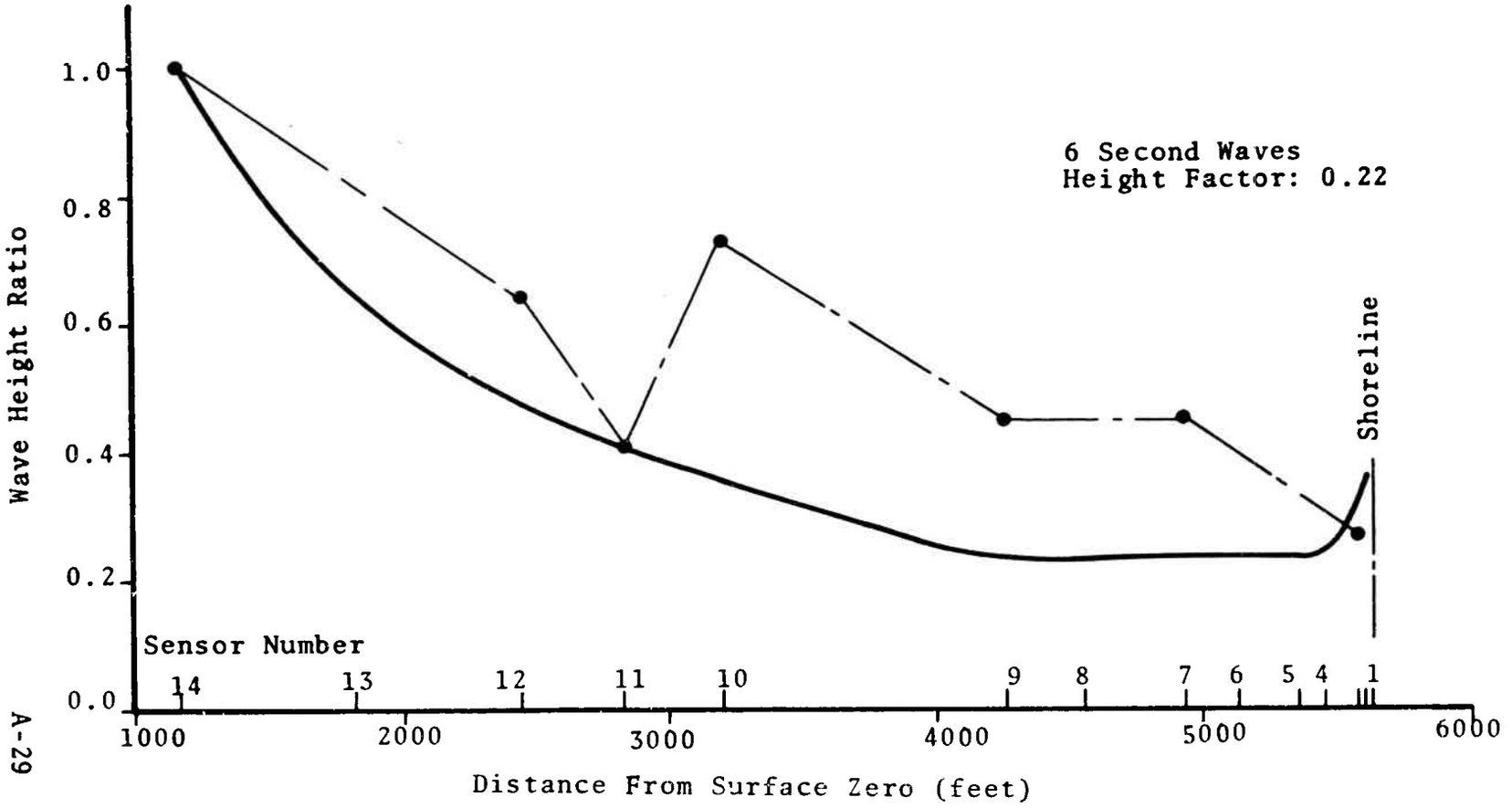

Figure 48 Wave Height Decay
Normalized to Sensor 14
Shot 7 Radial 3

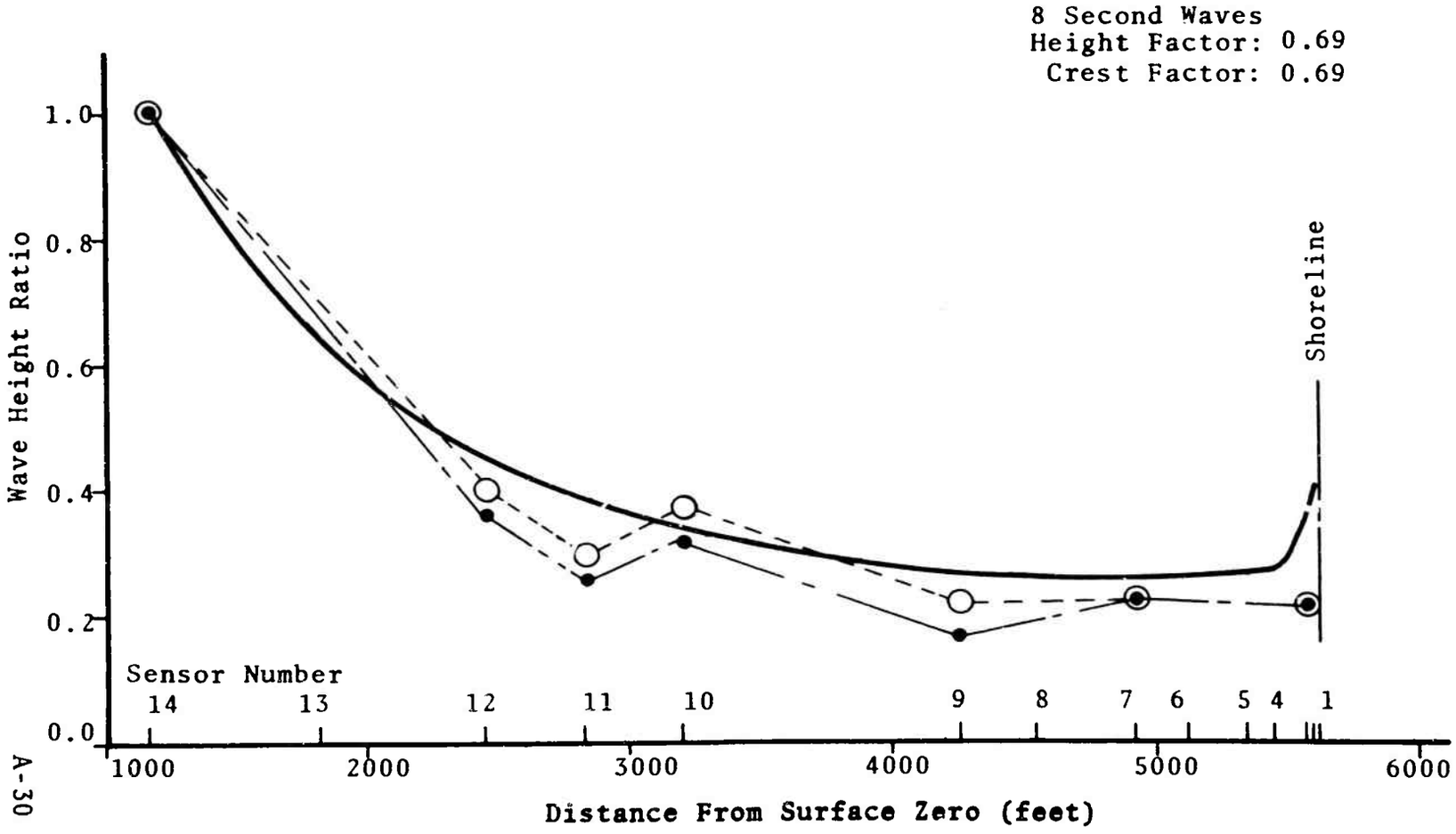

Figure 49 Wave Height Decay
Normalized to Sensor 14
Shot 8 Radial 3

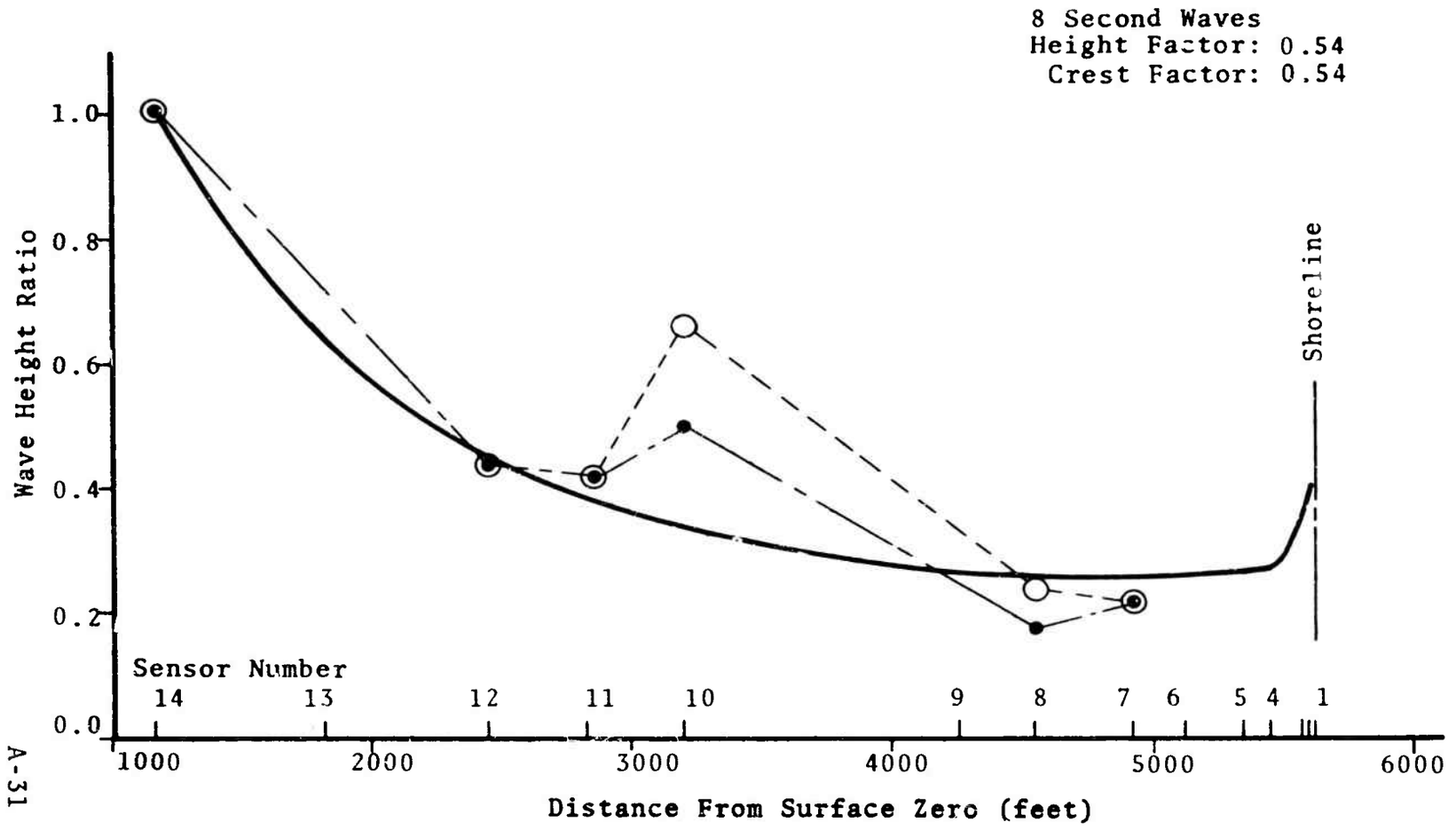

Figure 50 Wave Height Decay
Normalized to Sensor 14
Shot 9 Radial 3

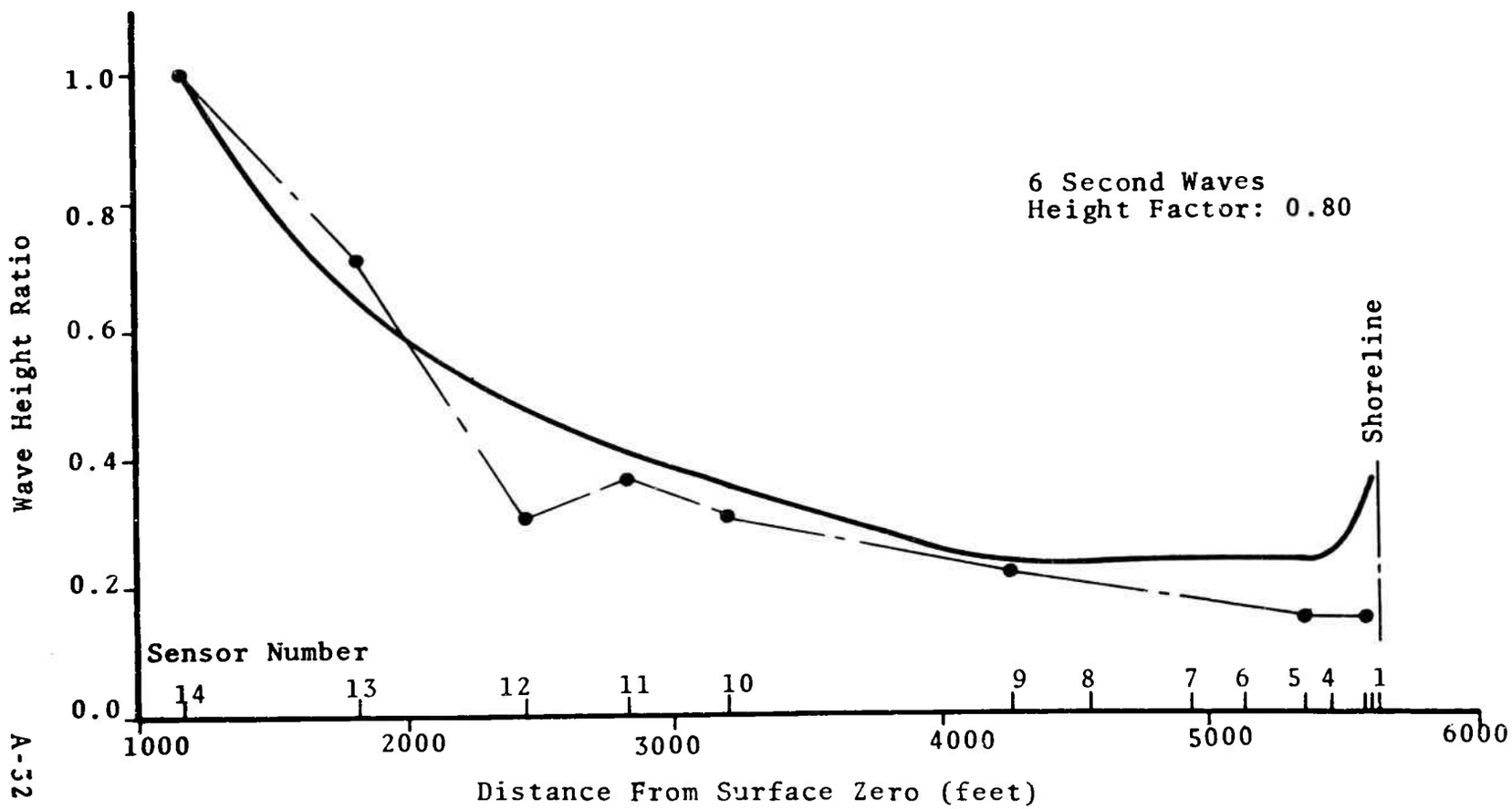

Figure 51 Wave Height Decay
Normalized to Sensor 14
Shot 9 Radial 3

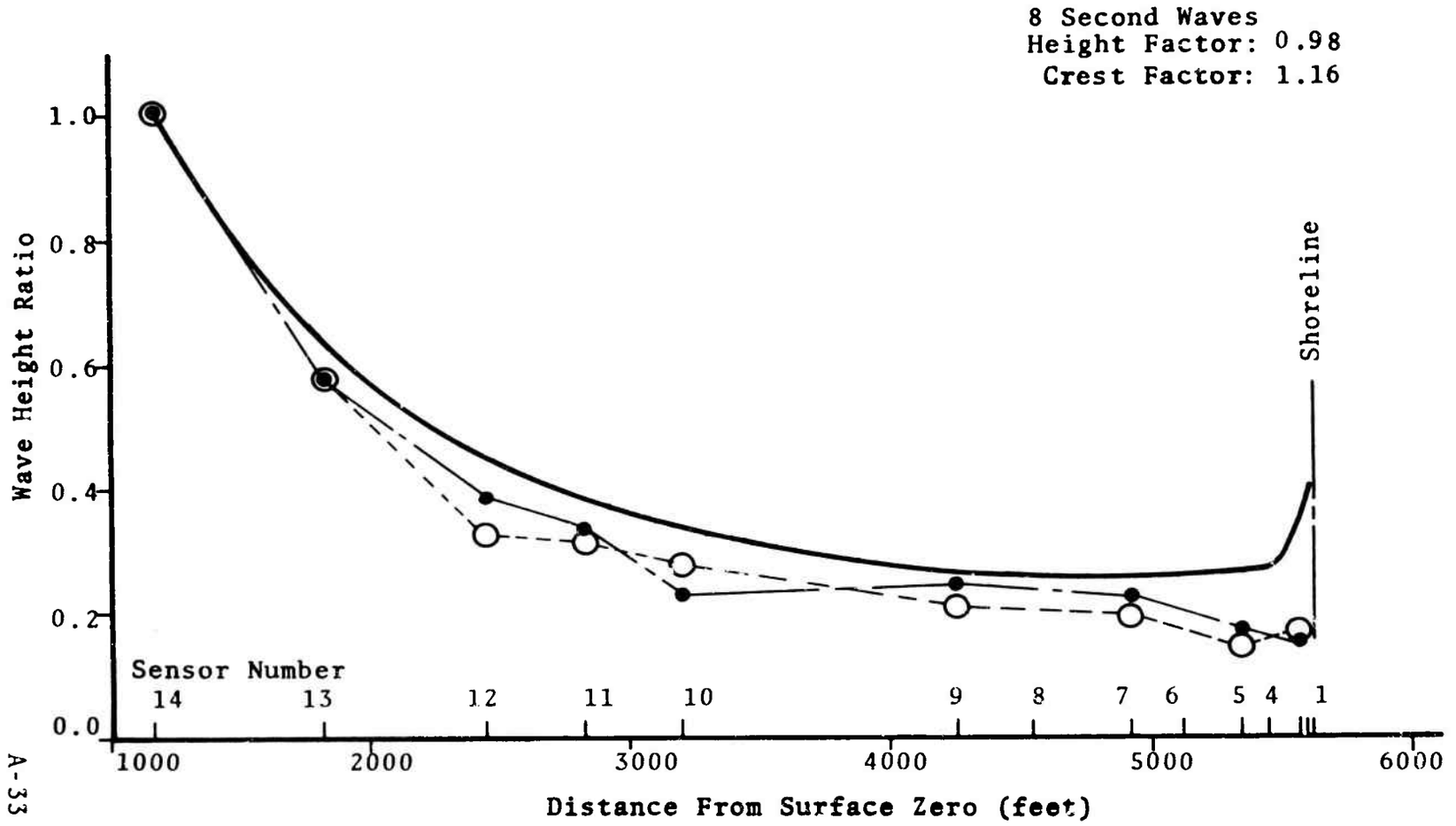

Unclassified

Security Classification

DOCUMENT CONTROL DATA - R&D

(Security classification of title, body of abstract and indexing annotation must be entered when the overall report is classified)

1 ORIGINATING ACTIVITY (Corporate author)

Oceanographic Services, Inc.
5375 Overpass Road
Santa Barbara, California 93105

2a REPORT SECURITY CLASSIFICATION: Unclassified

2b GROUP:

3 REPORT TITLE

Explosion-Generated Waves
1965 Mono Lake Test Series

4 DESCRIPTIVE NOTES (Type of report and inclusive dates)

Final Report

5 AUTHOR(S) (Last name, first name, initial)

N. R. Wallace and C. W. Baird

6 REPORT DATE	7a TOTAL NO OF PAGES	7b NO OF REFS
10 December 1968	114	11

8a CONTRACT OR GRANT NO.	9a ORIGINATOR'S REPORT NUMBER(S)
Nonr 4904(00) - NR 087-159	OSI#102-2
b PROJECT NO.	
c	9b OTHER REPORT NO(S) (Any other numbers that may be assigned this report)
d	

10 AVAILABILITY/LIMITATION NOTICES

This document has been approved for public release and sale; its distribution is unlimited

11 SUPPLEMENTARY NOTES	12 SPONSORING MILITARY ACTIVITY
	Office of Naval Research, Code 418 Washington, D. C. 20360

13 ABSTRACT

In the summer of 1965, 10 spherical TNT charges, each weighing about 9,200 pounds were detonated in Mono Lake, California. This report treats the analysis and comparison of wave data collected during the tests. Generation, propagation, and runup of the explosion-generated waves are discussed and the results are examined in relation to current methods of predicting these properties.

DD FORM 1 JAN 64 1473

Unclassified

Security Classification

Unclassified

Security Classification

14 KEY WORDS	LINK A		LINK B		LINK C	
	ROLE	WT	ROLE	WT	ROLE	WT
wave runup						
wave propagation						

INSTRUCTIONS

1. ORIGINATING ACTIVITY: Enter the name and address of the contractor, subcontractor, grantee, Department of Defense activity or other organization *(corporate author)* issuing the report.

2a. REPORT SECURITY CLASSIFICATION: Enter the overall security classification of the report. Indicate whether "Restricted Data" is included. Marking is to be in accordance with appropriate security regulations.

2b. GROUP: Automatic downgrading is specified in DoD Directive 5200.10 and Armed Forces Industrial Manual. Enter the group number. Also, when applicable, show that optional markings have been used for Group 3 and Group 4 as authorized.

3. REPORT TITLE: Enter the complete report title in all capital letters. Titles in all cases should be unclassified. If a meaningful title cannot be selected without classification, show title classification in all capitals in parenthesis immediately following the title.

4. DESCRIPTIVE NOTES: If appropriate, enter the type of report, e.g., interim, progress, summary, annual, or final. Give the inclusive dates when a specific reporting period is covered.

5. AUTHOR(S): Enter the name(s) of author(s) as shown on or in the report. Enter last name, first name, middle initial. If military, show rank and branch of service. The name of the principal author is an absolute minimum requirement.

6. REPORT DATE: Enter the date of the report as day, month, year; or month, year. If more than one date appears on the report, use date of publication.

7a. TOTAL NUMBER OF PAGES: The total page count should follow normal pagination procedures, i.e., enter the number of pages containing information.

7b. NUMBER OF REFERENCES: Enter the total number of references cited in the report.

8a. CONTRACT OR GRANT NUMBER: If appropriate, enter the applicable number of the contract or grant under which the report was written.

8b, &, & 8d. PROJECT NUMBER: Enter the appropriate military department identification, such as project number, subproject number, system numbers, task number, etc.

9a. ORIGINATOR'S REPORT NUMBER(S): Enter the official report number by which the document will be identified and controlled by the originating activity. This number must be unique to this report.

9b. OTHER REPORT NUMBER(S): If the report has been assigned any other report numbers *(either by the originator or by the sponsor)*, also enter this number(s).

10. AVAILABILITY/LIMITATION NOTICES: Enter any limitations on further dissemination of the report, other than those imposed by security classification, using standard statements such as:

(1) "Qualified requesters may obtain copies of this report from DDC."

(2) "Foreign announcement and dissemination of this report by DDC is not authorized."

(3) "U. S. Government agencies may obtain copies of this report directly from DDC. Other qualified DDC users shall request through _____."

(4) "U. S. military agencies may obtain copies of this report directly from DDC. Other qualified users shall request through _____."

(5) "All distribution of this report is controlled. Qualified DDC users shall request through _____."

If the report has been furnished to the Office of Technical Services, Department of Commerce, for sale to the public, indicate this fact and enter the price, if known.

11. SUPPLEMENTARY NOTES: Use for additional explanatory notes.

12. SPONSORING MILITARY ACTIVITY: Enter the name of the departmental project office or laboratory sponsoring *(paying for)* the research and development. Include address.

13 ABSTRACT: Enter an abstract giving a brief and factual summary of the document indicative of the report, even though it may also appear elsewhere in the body of the technical report. If additional space is required, a continuation sheet shall be attached.

It is highly desirable that the abstract of classified reports be unclassified. Each paragraph of the abstract shall end with an indication of the military security classification of the information in the paragraph, represented as *(TS)*, *(S)*, *(C)*, or *(U)*

There is no limitation on the length of the abstract. However, the suggested length is from 150 to 225 words.

14 KEY WORDS. Key words are technically meaningful terms or short phrases that characterize a report and may be used as index entries for cataloging the report. Key words must be selected so that no security classification is required. Identifiers, such as equipment model designation, trade name, military project code name, geographic location, may be used as key words but will be followed by an indication of technical context. The assignment of links, rules, and weights is optional.

Unclassified

Security Classification